AD-A096 723 FRAUNHOFER-GESELLSCHAFT GARMISCH-PARTENKIRCHEN (GERMA--ETC F/G 4/1
SLANT PATH LOW VISIBILITY ATMOSPHERIC CONDITIONS.(U)
SEP 80 R REITER, W CARNUTH, R SLADKOVIC DA-ERO-77-G-064

UNCLASSIFIED NL

1 OF 2
AD A 096723

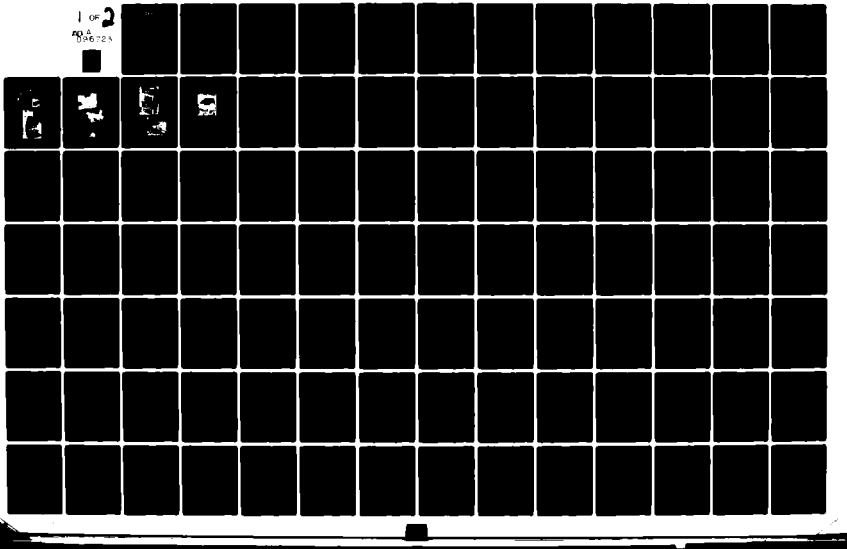

LEVEL II

AD

SLANT PATH LOW VISIBILITY ATMOSPHERIC CONDITIONS

FINAL TECHNICAL REPORT

BY

Reinhold Reiter

Walter Carnuth

Rudolf Sladkovic

and

Werner Funk

September 1980

EUROPEAN RESEARCH OFFICE
United States Army
London England

Grant Number DA-ERO-77-G-064

Fraunhofer Institut für Atmosphärische
Umweltforschung
Kreuzeckbahnstraße 19
D-8100 Garmisch-Partenkirchen

Approved for Public Release; distribution unlimited

AD A096723

DTIC FILE COPY

DTIC
MAR 24 1981
F

81 3 24 061

UNCLASSIFIED

SECURITY CLASSIFICATION OF THIS PAGE (When Data Entered)

REPORT DOCUMENTATION PAGE

READ INSTRUCTIONS BEFORE COMPLETING FORM

1. REPORT NUMBER

2. GOVT ACCESSION NO. AD-A096 723

3. RECIPIENT'S CATALOG NUMBER

4. TITLE (and Subtitle)
Slant Path Low Visibility Atmospheric Conditions

Short Title "Light Transmission"

5. TYPE OF REPORT & PERIOD COVERED
Final Report, July 1977 - June 1980

6. PERFORMING ORG. REPORT NUMBER

7. AUTHOR(s)
Reinhold Reiter, Walter Carnuth, Rudolf Sladkovic and Werner Funk

8. CONTRACT OR GRANT NUMBER(s)
DAERO-77-G-064

9. PERFORMING ORGANIZATION NAME AND ADDRESS
Institute for Atmospheric Environmental Research
Director: Dr. R. Reiter
D-8100 Garmisch-Partenkirchen, W-Germany

10. PROGRAM ELEMENT, PROJECT, TASK AREA & WORK UNIT NUMBERS
IT161102BG57-01

11. CONTROLLING OFFICE NAME AND ADDRESS
USARDSG-UK
Box 65, FPO New York, NY 09510

12. REPORT DATE
September 1980

13. NUMBER OF PAGES
54

14. MONITORING AGENCY NAME & ADDRESS (if different from Controlling Office)

15. SECURITY CLASS. (of this report)
Unclassified

15a. DECLASSIFICATION/DOWNGRADING SCHEDULE

16. DISTRIBUTION STATEMENT (of this Report)

This document has been approved for public release and sale; its distribution is unlimited.

17. DISTRIBUTION STATEMENT (of the abstract entered in Block 20, if different from Report)

Approved for public release; Distribution unlimited

18. SUPPLEMENTARY NOTES

19. KEY WORDS (Continue on reverse side if necessary and identify by block number)
Slant path transmissivity; fog; precipitation rate; humidity; aerosol concentration; particle spectrum; local aerosol inhomogeneities; air mass type; LOWTRAN

20. ABSTRACT: A slant path for measuring light transmission in two windows: 0.35-0.90 μm and 1.25-12.75 has been installed. Transmitters are at 1650 m ASL on a mountain peak, receivers at the valley institute. (Lower limit <0,1% transmission). Distance 2,7 km, inclination 19°. Recorded at both stations: Precip. rate, temp., hum., aerosol particle spectrum 0.4-0.20 μm Ø, visibility. Temp. and hum. profiles are recorded by sondes on a cable car or radiosondes. Aerosol backscatter between valley and mountain station is recorded by a multi-frequency slant lidar. This system serves to study depedence of light transmiss. on the met. situation (fog, precipit., hum.) and aerosol cond. during strong haze/mist, and on air mass type in cases of verttical inhomogeneity. Acquired data are intercorrelated and used for improved LOWTRAN.

DD FORM 1 JAN 73 1473 EDITION OF 1 NOV 65 IS OBSOLETE

Unclassified

SECURITY CLASSIFICATION OF THIS PAGE (When Data Entered)

282 650

AD_____

SLANT PATH LOW VISIBILITY ATMOSPHERIC CONDITIONS

Final Technical Report

by

REINHOLD REITER, WALTER CARNUTH, RUDOLF SLADKOVIC
and
WERNER FUNK

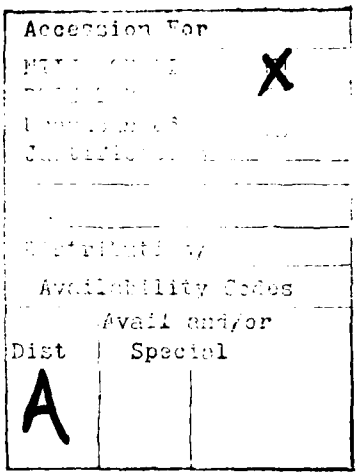

September 1980

European Research Office
United States Army
London England

GRANT NUMBER DA-ERO-77-G-064

Fraunhofer Institut für Atmosphärische
Umweltforschung
Kreuzeckbahnstrasse 19
D-8100 Garmisch-Partenkirchen

Approved for Public Release; distribution unlimited

Table of contents

Abstract

A slant transmission path for measuring the quality of light transmission in the visible (0.35 to 0.90 µm) and thermal (1.25 to 12.75 µm) window has been installed. Transmitters are located at 1650 m a.s.l. on a mountain peak, receivers at the valley institute where the signals (lower limit <0,1% transmission) are processed. Direct distance is 2.7 km, inclination of the path against horizon 19°. The following quantities are recorded at the mountain and also at the valley station: Precipitation rate, temperature, humidity, aerosol particle spectrum from 0.4 to 20 µm Ø, and visibility. Profiles of temperature and humidity are recorded by sondes on one of the gondolas of a nearby cable car or by small radiosondes. Aerosol backscatter between valley and mountain station is recorded by a multi-frequency slant lidar (347 nm, 530 nm, and 694 nm, in near future also 1060 nm).

This system serves to study in the course of measuring campaigns the dependence of light transmission on the meteorological situation (fog, precipitation, humidity) and on aerosol conditions mainly during moderate to strong haze or mist, as well as generally on the air mass type, particlarly in cases of vertical inhomogeneity (layer structures).

The acquired data are intercorrelated and applied later on in the sense of an improved LOWTRAN.

Keywords

Slant path transmissivity / influence of fog, precipitation rate, humidity / influence of aerosol concentration, particle spectrum, and local aerosol inhomogeneities / influence of air mass type / improvement of LOWTRAN.

1. Objectives and Background

The objective of the research work described in Chapter 2. differs indeed significantly from our former works under US Army contracts; nevertheless it is based on all experiences and data on atmospheric aerosols gathered at our Institute till today, further on the existence of mountains in the immediate vicinity of the Institute, as well as on the use of institute-operated mountain observatories including cable cars and - last not least - on the development of lidar systems for remote aerosol sensing and evaluation and interpretation of the data obtained therewith. Thus, the project newly to be tackled is consciously a matter of applied research founded on all hitherto gained experiences. The subject is to study the dependence of light transmission in the visible and thermal window on the aerosol structure and meteorological quantities (fog, precipitation), air mass characteristics, and others. That means, that in view of these controlling factors in the geographical mesoscale environment of the Institute, the mentioned parameters must undergo considerable variations and that - with the aid of appropriate measuring techniques - their influence on light transmission can be studied. Our meteorological and physico-chemical studies carried out over decades ensure that the necessary requirements are met, especially with regard to conditions of very low light transmission.

2. Subject Posed, Feasibility

In compliance with our proposal of 25 October 1976 - which has been discussed in detail with scientists of ASL - and an experimental plan set up by Mr. James D. Lindberg on 20 January 1977, the objective of the research work may be described as follows:

i. The fog/haze optical propagation models for different light wavelengths, known and temporarily used so far, shall become verifiable through the data to be gathered by ASL under realistic conditions as they do frequently occur in Europe. Special value is attached to slant path measurements because such have not yet been made on larger scale under an adequate, concomitant meteorological-physical measurement program. This will result in further development of models and scaling laws to make them applicable to air to ground optical paths.

ii. The resulting new optical data base will include better meteorological support data than has been available previously, making it possible to begin modeling the relationships between more routine meteorological measurements and haze/fog/precipitation optical propagation conditions. Thus, the second objective is to attempt development techniques for predicting optical propagation conditions for low visibility slant paths from meteorological data forecasts.

In the following a brief description be given of the experimental plan and its feasibility in the environment of the Institute as agreed with ASL. Accomplishment of the objectives discussed above requires intercoordination of several elements in a field test situation.

a) An optical propagation slant test path, of a length over which infrared transmissometer measurements can be made that are in a magnitude range permitting accurate measurements under the low visibility conditions of interest must be chosen. A path which is too short will produce transmission measurements which are close to 100% and therefore do not accurately relate to absolute transmissivity. A path which is too long will result in transmission measurements which are very low, and are signal to noise limited during low visibility cases.

The direct distance of 2.7 km between valley and Kreuzeck peak station and an elevation angle of 19^{o} appears to be optimal.

b) The inhomogeneous nature of the optical slant path must be known during the time the absolute integrated transmissometer measurements are made. Therefore, it is essential that a multi-frequency lidar be operated along the path, together with the transmissometer and a Knollenberg particle spectrometer at each end of the path.

c) The prevailing meteorological and aerosol conditions in the general area must be precisely measured during the test period, so that all atmospheric data which might reasonably be expected to correlate in some way with the optical measurements are recorded and documented. The climatological history of the site should be known and well understood micro-meteorologically, so that the relationships between meteorological and optical data can be recognized and properly interpreted.

In the Garmisch valley the Institute operates a unique system of direct meteorological and aerosol sensing instrumentation on the valley floor, on two mountain peaks, and on two cable cars that connect the mountain peaks with the valley floor. In addition, radiosonde measurements are routinely made. A two frequency (ruby and doubled) lidar operates on a routine basis at the Institute, giving a vertical profile of aerosol backscatter cross section. The valley station, at the main institute building, is at an elevation of 740 m above sea level. The two mountain top stations (Wank and Zugspitze) are at elevations of about 1780 and 2960 m, respectively. All the resulting data, including the lidar returns, are fed directly to computerized data processing equipment, partly

via telemetry links. This highly sophisticated met/aerosol system which has been in operation for a number of years, provides an excellent picture of the micrometeorological conditions that prevail at any time in the atmosphere above the Institute. This system does satisfy requirement c. above to an extent never before attained by a propagation experiment of this kind.

In addition to the two-frequency lidar operating from the institute building, a second three-frequency (ruby, doubled ruby, and doubled neodymium) lidar which can operate on a slant path is available for measurement of backscatter cross section along the chosen transmissometer path.

3. Rough Cross Cut of the Works under Contract in Brief Outline

It goes without saying that the whole complex of parallel and simultaneous measurements to be performed during the measuring campaigns of 6 - 10 hrs duration each (current measurements over still longer intervals or even days have not yet been possible for obvious reasons including the limited number of skilled staff and related costs) had first to be "trained". Table 3.1. shows the total extent of simultaneous measurements and recordings. Sampling and evaluation of all acquired data had just as well to be coordinated, organized, and optimized with regard to expenditure of time and effort and preparatory works for scientific interpretation.

After delivery of the Barnes system (Table 3.1., 1a and 1b) it was essential to mount the receiver as stably as possible at a suitable place at the back wall of the Kreuzeck cable car entrance room which consists of concrete with extreme carrying capacity (see Fig. 3.1., protecting cover removed). Inside the

Table 3.1.

1a. Barnes transmissometer recording, infrared 7.25 - 12.75 µm
1b. Barnes transmissometer recording, visible range, 0.35-0,90 µm
2a. Lidar backscatter profiles, vertical, 694 and 347 nm
2b. Lidar backscatter profiles, slant : between valley and Kreuzeck, 694, 530, and 347 nm (1060 in preparation)
3. Precipitation - if any, recorded by ombrometers at Kreuzeck and the valley station
4a. Knollenberg particle spectra, valley station
4b. Knollenberg particle spectra, Wank station
4c. Knollenberg particle spectra, Kreuzeck station
5. Small balloon-borne radiosondes
6. Small radiosondes on the cable car of the Osterfelderbahn near Kreuzeck (temp. and rel. humidity versus altitude)
7. Recording of meteorological data and visibility (valley and Wank) - on Kreuzeck in preparation
8. Cloud and visibility observations with the naked eye
9. Cloud photographs
10. Zugspitze cable car telemetry data (temperature and humidity profiles)
11. Temperature and relative humidity at all stations, including Kreuzeck

protective housing a constant temperature of +10°C is maintained. The outlet for the coaxially directed beam of visible and infrared light is closed when inoperative, and is mechanic- automatically opened when the Barnes system is switched on. Power supply is in a closed room of the building and just so the data processing system for Knollenberg spectra, temperature, humidity, precipitation, and lateron visibility. The complete system can be turned on and off from the Institute via a telemetry signal. Sensors for the above mentioned measured values are mounted outside the building at an appropriate place. Until expiration of this contract, data have been stored on punch tape at the station Kreuzeck. At a later date these data will be telemetered to the valley institute. Fig. 3.2. shows the open view from the Barnes transmitter at the Kreuzeck to the Institute (circle), Fig. 3.3. conversely the view from the valley institute (Barnes receiver) to station Kreuzeck (circle). Fig. 3.4. illustrates the two parallel receivers for both wavelengths. They, as well as the tripod, are protected against insolation by a down-hanging umbrella and look at the transmitter only through a small aperture. Fig. 3.5. presents the electronic Barnes-units, recording happens through appropriate high resolution analog-recorders. Fig. 3.6. gives the three-frequency lidar (optical part) in position (electronic data processing and power supply is housed in the truck inside the building). Fig. 3.7. shows the Kreuzeck-oriented position of the lidar during the shots (Target: see circle), in the case of haze.

In the reporting period, until completion of the Barnes system, works to improve the lidar systems have been continued. In particular, it was attempted to utilize wavelength 1060 (non-doubled neodymium-glass laser beam). As described further below first attempts with a pin diode proved fruitless.
A photomultiplier which is supposed to be appropriate has been

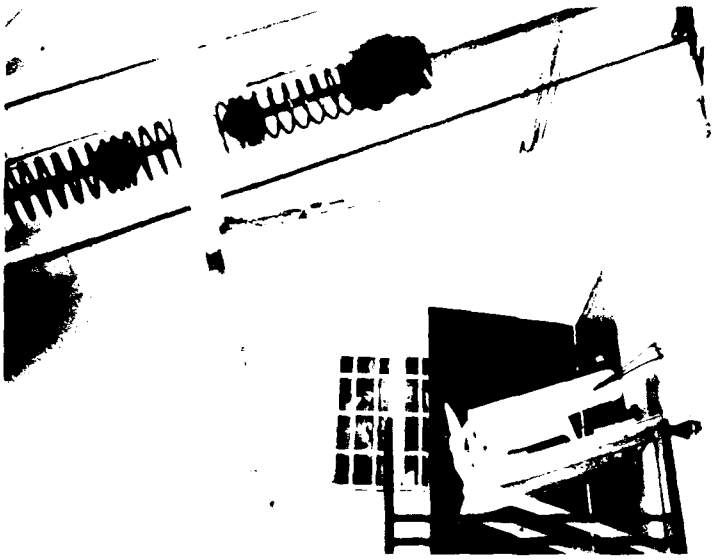

Fig. 3.1.

O Institute O

Fig. 3.2.

Fig. 3.3.

○ Barnes-Transmitter

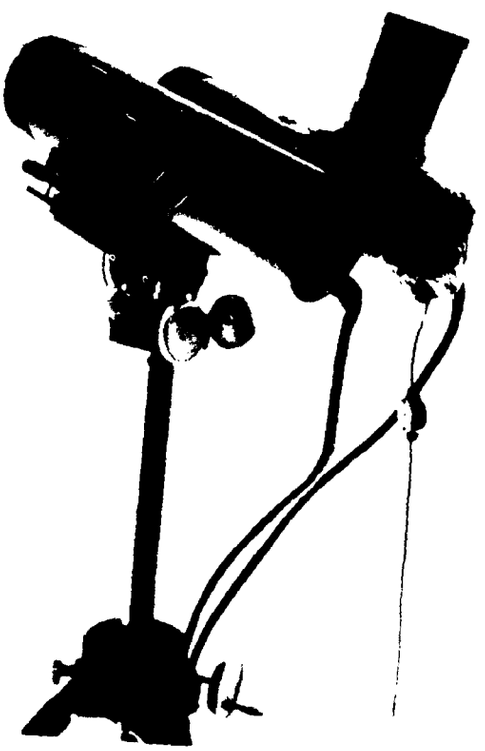

Fig. 3.4.

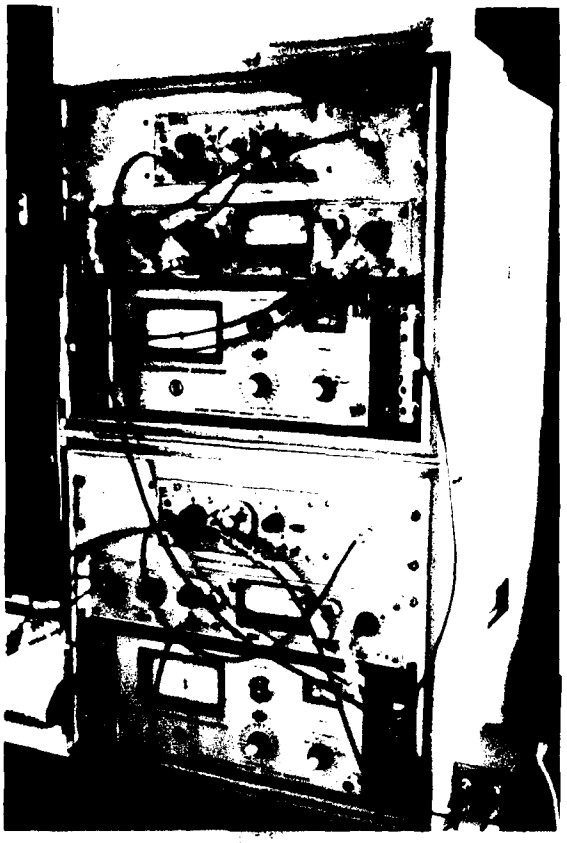

Fig. 3.5.

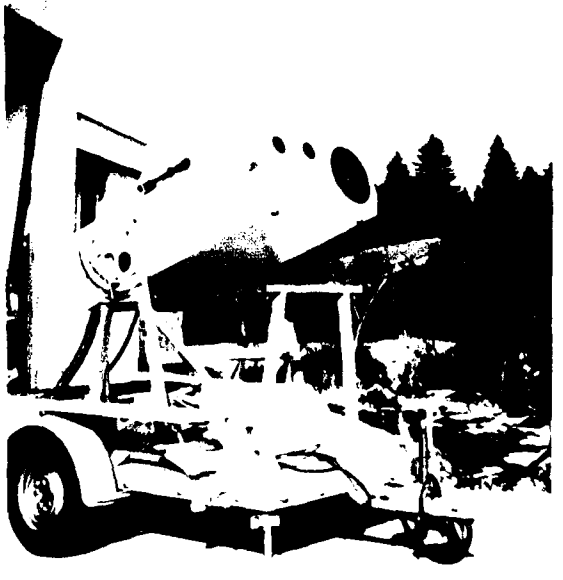

Fig. 3.6.

O O Barnes-Transmitter

Fig. 3.7.

ordered but was not as yet delivered. All other components (filter, telescope, etc.) are available and also electronic processing of signals is prepared. A photodiode for measuring the supplied energy/shot must still be installed.

Concerning capability of the Barnes instruments, the following can be said:

During a very thorough evaluation of the systems by scientists of ASL in fall 1979 it was found that up to this time the system was only capable of measuring transmission levels as low as 50% on account of the original phase lock system which used the chopper frequency of the transmitted signal. In the case of weak signals-and just then measurements are desired - the signal-to-noise ratio was too bad to control the lock-in amplifier reliably. In fall 1979 we constructed at first in haste a preamplifier permitting measurements as low as 12% transmission. At the same time, under a small independent parallel-contract with the US Army, a telemetry link was procured and incorporated in the Barnes system. This instrument supplies the chopper frequency of the transmitter independent of weather to the lock-in amplifier in the receiver. The result (see 4.3.) has surprised us very much indeed. We are now able to measure even under extremely low visibility conditions. However, this latest improvement will become effective only under the present Contract DAJA37-80-C-0345 since the telemetry system was ready for operation not until the middle of 1980. Resonably, the subsequent description of measurement results is restricted to the period in which we were able to measure reliably as low as 12% transmission. Under these transmissometer conditions numerous (80) effective measuring campaigns have been conducted in the first half-year 1980. All of the latest technical improvements are of advantage to the present, new contract.

In preparation is moreover the total on-line transmission of

data obtained on the Kreuzeck (transmitter station) such as aerosol spectra, temperature, humidity, precipitation, later visibility and other data to the valley via the existing telemetry link for the purpose of current checks on the performance of instruments and actual data processing.

4. Detailed Description of the Various Systems Used

4.1. Stationary lidar system

In the stationary lidar system a Q-switched ruby laser with 964 nm wavelength, 2 Joules maximum output energy, 20 nanoseconds pulse length and 1 Hz maximum pulse repetition frequency serves as transmitter. By shifting a KDP frequency doubler into the beam path the second wavelength, 347 nm, is generated. The beam of the horizontally mounted laser is directed vertical by one dielectric mirror for each wavelength. The energy of each laser pulse is measured by a photodiode with integration stage, peak digitizer and A/D converter with digital data output. The backscattered light is collected by a fixed vertical pointing 52 cm dia. Cassegrainian telescope and detected after passage of a field stop, an optical shutter, filter wheels containing neutral and narrow-band interference filters and a polarizer by a range-gated EMI 9816 photomultiplier tube. The polarizer can be turned for measurement of the depolarization ratio of the return signals. The electrical signals from the photodetector are recorded by a Biomation 8100 digital transient recorder with 8 bit amplitude resolution, 10 ns minimum sampling interval, and 2024 bytes memory capacity. Immediately after each signal record the data are transferred to an on-line minimcomputer with 16 k core memory, graphic display terminal and data output on floppy discs. By means of the computer the first steps of data processing are performed such as averaging several successive signals for improvement

of the signal to noise ratio, subtraction of the skylight background which is measured immediately before each laser shot, range correction by multiplication with the square of distance and energy normalization. The resulting normalized backscatter profiles are plotted together with range scale and house keeping data on the screen of the display terminal and copied by a hardcopy unit immediately after each measurement. These profiles are proportional to the total backscattering coefficient, F (sum of molecular and aerosol part), as function of distance, x, times the squared transmission factor, τ, along the light path between lidar and distance x. For further processing on the main computer the raw data are stored on floppy discs.

Special electronic circuits developed in our laboratory allow a completely automatic, computer controlled operation of the whole system. Individual measuring series can be started at any time by a digital quartz clock.

The lidar system is calibrated absolutely by comparison with aerosol data (number concentration and size distribution) from five-stage impactors at the Institute and at 1800 and 3000 m altitude, and Knollenberg type optical aerosol spectrometers located at the Institute, the 1800 m mountain station and , more recently, at the site of the transmissometer source at 1650 m. For this purpose backscattering coefficients for both lidar wavelengths must be calculated from the aerosol spectra using the Mie theory. Since in principle this theory applies to spherical particles with known refractive index only, these calculations are always affected with some uncertainties. Especially useful for calibration purposes are atmospheric conditions with extremely low aerosol concentrations, occurring normally several days a year at the location of our Institute, when aerosol backscattering can be neglected compared with molecular backscattering. The calculation of the molecular

backscatter coefficients by the Rayleigh theory is much easier since they depend only on atmospheric pressure, temperature and water vapor content which all are measured by stationary instruments and different kinds of airborne and cable car sondes.

By these methods we were able to derive reliable values for the calibration factors for the two wavelengths of the stationary lidar system. With these factors known, it is first of all possible to calculate the above mentioned Fr^2-profiles in absolute units ($m^{-1}sterad^{-1}$). The next step, the derivation of aerosol data from these absolute profiles, is much more difficult, since the backscatter and extinction coefficients depend on many aerosol parameters such as concentration, size distribution, refractive index of the particles and so on. Using more than one transmitter wavelength, it is in principle possible to get information about the size distribution of the particles, if their refractive index is known or reliable assumptions can be made about it. For this purpose the particle size distribution function is to be approximated by a simplified model containing not more independent parameters than the number of different wavelengths used. We chose for the evaluation of our two-wavelength lidar data a two-parameter model consisting of two log-normal distributions with constant center diameters (.4 and 2.0 microns, respectively) and standard deviations (.3), but variable total number concentrations, N_1 and N_2. In this model we use a refractive index varying with relative humidity since for background aerosol far from emission sources the major changes of the index result from humidity-determined water content of the particles. Using this model, we developed a calculation scheme for the iterative solution of the lidar equation for the aerosol backscatter coefficients in both wavelengths as function of altitude and the derivation of the profiles of the aerosol parameters N_1 and N_2. The iterative method is required since the lidar equation, which relates the backscattered light intensity to distance, molecular and aerosol extinction and back-

scattering, and lidar system parameters, contains the transmissivity as an integral term.

4.2. Mobile lidar system

Whereas the stationary lidar system with its automatic operation capability serves, with regard to the transmission measurements, mainly as a monitor for the actual atmospheric situation, a second, mobile lidar system, which can be directed to any azimuth and elevation angle, is used for assessment of the aerosol distribution along the transmission path. It is equipped with two lasers: A ruby laser used with and without frequency doubling similar to the stationary system, and a frequency-doubled neodymium-glass laser, allowing measurements in 530 nm wavelength in addition to the 347 and 694 nm of the ruby laser. Again a Cassegrainian telescope collects the backscattered light, in this case only 30 cm in diameter, and an EMI 9816 photomultiplier tube is used as detector. The fundamental wavelength of the neodymium laser, 1060 nm, is not utilized up to now because of detector problems, but, since it is desirable to extend the wavelength range towards the infrared, we will try to use this wavelength also in the future. For this purpose we ordered a S1 photomultiplier tube, with a quantum efficiency of .05% at 1060 nm. A commercial pin diode/preamplifier combination did not give satisfactory results. All other optical equipment required for the 1060 nm wavelength such as fourth interference filter, and beam expanding telescope, has already been installed in the system.

The energy of each outgoing laser pulse is measured by an energy monitor of the same kind as in the stationary system. The lidar return signals are recorded by the same Biomation 8100 transient recorder as in the other system, and also transferred to an on-line minicomputer for further processing. The range-

corrected and energy-normalized backscatter profiles are plotted on a display tube and on an x-y recorder. The data are stored on magnetic tape cassettes in this case. The operation of the mobile system is only partly automated, mainly since the change of wavelength must be done manually.

For the evaluation of the data from the mobile lidar we use a calculation scheme similar to that for the stationary lidar data. The bimodal model for the particle size distribution is still used in this case because it did not seem useful to change the model for the intermediate wavelength, 530 nm, for example by introducing a third mode of particles. The problem of inversion of the three-wavelength lidar data into a trimodal size distribution model would be much more complicated and sensitive to measurement errors than in the bimodal case. Instead of that the 530 nm data are used to optimize the procedure, e.g. by changing the refractive index.

It is to be mentioned here that the evaluation of the lidar profiles along the transmission path is facilitated by the availability of Knollenberg particle spectra from both ends of it. The task of the lidar in this case is the interpolation between both these data.

4.3. Barnes transmissometer system

The transmissometer system, delivered by Barnes Engineering Co., Stamford, Connecticut, (USA), consists of two main parts, the radiation source for the visible and the infrared region, and the receivers for both channels together with data processing electronics. The radiation source assembly contains a blackbody source for emission of infrared radiation maintained precisely at a selected temperature in the vicinity of 1000^{o}C, and a tungsten iodide source maintained at about 3000 K for visible radiation. One common reflective collimator is used for both

sources to produce exact coaxial beams with a divergence of 5,5 milliradians. Also contained in the source assembly is a mechanical modulator that chops or interrupts source radiation at 1000 Hz to differentiate it from the background and other sources. The chopper wheel is equipped with a pickup that generates a pulse each time the radiation is interrupted. This pulse is used to transmit the chopper frequency to the receiver assembly for synchronization, via a telemetry link which is in operation since June 1980 and which is described below. The source assembly is mounted in a cable car station building on a mountain peak close to the Institute at 1650 m a.s.l., slant distance 2,7 km.

The receiver assembly, which is mounted at the Institute at the end of the transmission path, consists of one receiver system for each wavelength range. The receiver systems are identical except for the spectral sensitive photodetectors, and consist of a sensing head with optical telescope, detector and preamplifier, an electronic control unit, a selective amplifier, a lock-in amplifier and a strip-chart recorder. The telescopes are of Cassegrainian type with 10.8 cm aperture and 2.3 milliradians FOV. In the infrared (IR) receiver a liquid-nitrogen cooled mercury-cadmium-telluride detector is used, in the receiver for visible radiation a pin-diode detector. Filters limit the spectral ranges from 7.25 to 12.75 and .35 to .90 microns, respectively. A preamplifier amplifies the detector signals to a level and impedance suitable for transmission through a cable to the remote electronic control unit. In this unit the signals can be attenuated in 3 dB steps and are amplified by a general-purpose amplifier. Further amplification and noise reduction is accomplished by a selective amplifier with a 50 Hz bandpass filter centered at the chopper frequency. Because of the limited stability of this frequency a further reduction of bandwidth and improvement of signal-to-noise ratio can only be achieved by using a lock-in amplifier which is

synchronized to the chopper frequency and allows a precise measurement of the signal of interest in the presence of frequency drift and broad-band noise. This amplifier demodulates only those components of the incoming signal which are exactly in phase with a reference frequency applied to a special input connector, and converts them to an amplitude-proportional dc-voltage with 1 volt full scale, which is recorded by a paper chart recorder. In the initial version of the system the measuring signal itself was used as reference. The reference signal, however, must fulfill some minimum requirements, first of all it must cross its mean only twice each cycle, and the minimum amplitude should be at least 100 mV pk-pk. The incoming signals from the sensing heads do not meet these requirements if the transmission is less than some ten percent, and the lock-in amplifier then gets unlocked and the output voltage goes to zero. Since the sensitivity of the receivers was unsufficient in this state, two diode clipped amplifiers were built in October 1979 in order to improve the signal from the selective amplifier for reference purposes. These amplifiers were connected between output of the selective and reference input of the respective lock-in amplifiers. By this method the lower limit of measurable signal amplitude was reduced to a value corresponding to a few percent transmission. The largest increase in sensitivity, however, was achieved by the telemetry link for the chopper frequency which becomes effective under the present new contract. Transmissivities down to .1% in the IR and .2% in the visible region can now be easily measured.

4.4. Exact alignment of the sensing heads

For exact alignment of the sensing heads with respect to the radiation source, one external sighting telescope with variable magnification is provided for each telescope for raw alignment allowing observation of the source without interruption of the

measurement. Furthermore, the images produced by the telescopes can be viewed parallax-free through auxiliary telescopes by shifting a deflecting mirror into the beam path. These telescopes can be used both for angular alignment and focusing of the receiving telescopes. The most precise method for alignment and focusing, however, is maximizing the detector signal. We found that in the visible detector the alignment state found by the auxiliary telescope is practically the same than that found by signal maximation, but not in the IR detector, where the alignment telescope (or the detector itself) is obviously both out of focus and off-axis.

5. Evaluation of Data from the Knollenber Particle Spectrometer (Classical Type)

5.1. Different exposure times for individual ranges

Reasonably, we have a short exposure time for small particles and a long exposure time for large particles.

Since we use an electronic auxiliary unit constructed by ourselves, the different exposure times are as follows:

Range 0	13 minutes	2.00 to 20.00 microns
Range 1	4 minutes	1.00 to 12,25 "
Range 2	2 minutes	0.50 to 2.75 "
Range 3	1 minute	0,320 to 0,755 "

Thus, a complete measuring cycle comes up to 20 minutes, beginning with range 0 and always at the full hour. In future, the total length of this measuring cycle will be reduced by factor 2 - 3 but the intervals between exposure times in the single ranges will be retained. The flow rate through the measuring volume is 0,11 cm^3/sec.

5.2. Combination of the channels to one spectrum

In the former evaluation the complete measuring range (65 channels) from 0.32 to 20 µm diameter has been bridged by 9 mean particles sizes which subdivide the existing measuring range equidistant (in logarithmic scale). Later on we departed a little from this original subdivision (strongly equidistant) because dependence between relative scatter intensity and particle size according to Mie's theory was not evident. This concerned particles sizes between 0.80 and 2.00 microns (range 2, channels 3 - 10).

Initially we combined:

Channels 3 to 5 with mean diameter 1.00 microns

Channels 6 to 10 with mean diameter 1.55 microns

On account of the above mentioned Mie theory we combined later channels 3 - 10 which corresponds to a mean diameter of 1.25 µm. For program-technical reasons we combined in the evaluation additionally channels 9 - 10 because in this size range we have again a clear dependence according to Mie theory (see Table 5.1.).

From Table 5.1. it can be seen that there is no overlapping of measuring ranges in the combination of channels (except for Y_3, Y_4) but quite on contrary we note small gaps between Y_2 and Y_3, or Y_5 and Y_6 (caused by the transition from one range to the other). The spectrum was built up more by the particle number of fine particles in the channels per range.

From the paper of J. Abele[+]) it follows that a rather clear dependence between relative scatter intensity and particle

[+]) J. Abele: Report F fo 1980/62, Tübingen, (Forschungsinstitut für Optik)

size must be expected for the natural aerosol. For this reason we wish in future to base the aerosol particle spectrum on 12 particle sizes (Y_1 - Y_{12} in Table 5.2.).

In this combination overlapping of measuring ranges will be used (during transition from one range to another: From Y_2 to Y_3, from Y_5 to Y_6, and from Y_7 to Y_8). Hence, we rely then on the particle number of the more coarse particles in the channels per range.

For control purposes (check on the counting in overlapping areas in the different ranges) we will calculate in addition another partial spectrum with mean particle size from 0.570 µm = K_3 and 8.367 µm = K_{11} (see Table 5.2., bottom part).

If the Knollenberg spectrometer can be considered as functioning properly, no great difference may exist between the spectrum from Y_1 - Y_{12} (solid line in Fig. 5.1.) and the spectrum from K_3 - K_{11} (dashed line in Fig. 5.1.) or, respectively, reality must be intermediate between these two partial results. First outcomes show fairly good agreement (see Fig. 5.1.).

Table 5.1.

	Used combination of individual channels for one spectrum							Originally planned				
	Range	Channel	from	to	Mean Ø	Width of interval	Length of exp.	Channel	from	to	Mean Ø	Width
			[µm]	[µm]	[µm]	[µm]	[min]		[µm]	[µm]	[µm]	[µm]
Y_1	3	1-7	0,320	0,523	0,41	0,203	1					
Y_2	3	8-15	0,523	0,755	0,63	0,232	1					
Y_3	2	3-10	0,80	2,00	1,26	1,20	2	3-5	0,80	1,25	1,00	0,45
Y_4	2	9-10	1,70	2,00	1,84	0,30	2	6-10	1,25	2,00	1,58	0,75
Y_5	2	11-15	2,00	2,75	2,34	0,75	2					
Y_6	1	4-6	3,25	5,50	4,23	2,25	4					
Y_7	1	7-10	5,50	8,50	6,84	3,00	4					
Y_8	1	11-15	8,50	12,25	10,20	3,75	4					
Y_9	0	10-15	12,80	20,00	16,00	7,20	15					

Table 5.2.

Evaluation
Planned in Future

Particle size [µm]							
	Range	Sum of channels	from	to	Mean ⌀	Width of interval	Length of exposure
			[µm]	[µm]	[µm]	[µm]	[min]
Y_1	3	1-4	0,320	0,436	[illegible]	0,116	1
Y_2	3	5-9	0,436	0,581	[illegible]	,145	1
Y_3	3	7-12	0,494	0,668	0,574	0,174	1
Y_4	3	13-15	0,668	[illegible]	0,710	0,087	1
Y_5	2	3-5	0,80	1,25	[illegible]	0,45	2
Y_6	2	4-9	0,95	1,85	1,326	0,90	2
Y_7	2	9-14	1,75	2,65	2,102	0,90	2
Y_8	1	2-4	1,70	4,00	2,646	2,25	4
Y_9	1	4-5	3,25	4,75	3,929	1,50	4
Y_{10}	0	3-4	4,40	6,80	5,47	2,4	13
Y_{11}	0	5-7	6,80	10,40	8,409	3,6	13
Y_{12}	0	8-15	10,40	20,00	14,422	9,6	13
K_3	2	1	0,50	0,65	0,570	0,15	2
K_4	2	2	0,65	0,80	0,721	0,15	2
K_6	1	1	1,00	1,75	1,323	0,75	4
K_7	1	2	1,75	2,50	2,092	0,75	4
K_8	0	1	2,00	3,20	2,53	1,2	13
K_9	0	2	3,20	4,40	3,75	1,2	13
K_{10}	1	5-8	4,00	7,00	5,292	3,0	4
K_{11}	1	9-12	7,00	10,00	8,367	3,0	4

FIG. 5.1

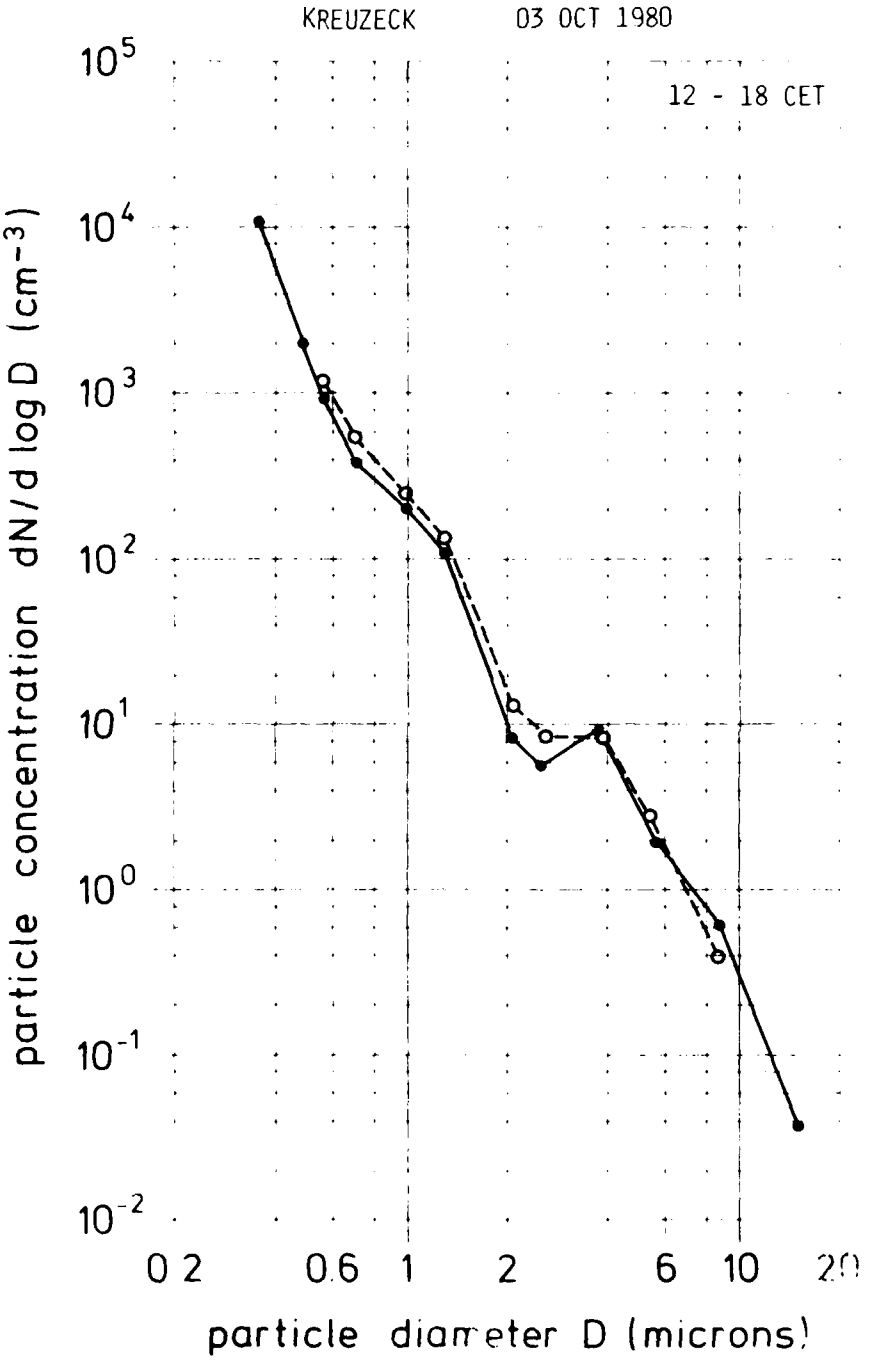
KREUZECK
03 OCT 1980
12 - 18 CET
10^5
10^4
10^3
10^2
10^1
10^0
10^{-1}
10^{-2}
particle concentration dN/d log D (cm^{-3})
0.2
0.6
1
2
6
10
20
particle diameter D (microns)

6. Brief Description of Details Regarding Data Sampling at Station Kreuzeck and Institute (Garmisch) in the Valley, Telemetric Transmissions

6.1. Switching on- and off of systems at station Kreuzeck

Until about a year back, the transmissometer system at station Kreuzeck including sampling of aerosol spectra and meteorological data as well as storage on punch tape was turned on and off upon telephone call by operators of the Kreuzeck cable car. This, however, was only possible during normal duty hours of the personnel. Hence, measurements before the first and after the last run and also during shutdown of the cable car in fall were excluded.

Therefore, a telemetric connection was established using a pair of radiotelephones. Upon transmission of the respective code signal, the whole complex of systems or only parts of it can be turned on- and off by radio.

Coding of the signals prevents an "extraneous release" by R/F traffic in the same frequency band and other radio installations.

6.2. Transmission of the chopper frequency from the Barnes transmitter at the Kreuzeck to the valley station

Thanks to an additional US Army Contract (DAJA37-80-C-0256) a telemetry link was installed which transmits the chopper frequency of the Barnes transmitter to the valley and feeds it into the lock-in amplifier.

Technical data:

i. Transmitter: Transmission frequency 2.45 GHz / output energy 1 watt

Manner of modulation : Helical antanna (directional antenna)

ii. Receiver: Sensitivity: about 20 microvolts
Image frequency attenuation: 40 dB
Antenna: analogous to transmitter

6.3. Data sampling at station Kreuzeck till June 1980

i. Knollenberg particle spectrum (0.35 - 20 µm Ø):
1 cycle over all 4 ranges per 20 minutes

ii. Air temperature,
rel. humidity (humidity sensor, lithium-chloride principle)
precipitation (ombrometer),
all values obtained over 5 minutes and then output

iii. Storage:
All data i - ii., along with date and time, are stored on punch tape at station Kreuzeck. Punch tapes have been brought down to the valley by a staff member after the end of the measuring campaigns.

6.4. Works on improving 6.4. (i. and ii.) and the telemetric data transmission

i. Time resolution will be increased, i.e.:
Detection of 3 cycles (4 ranges) of the Knollenberg particle spectrum every 20 minutes;
for the time being, still storage on punch tape.

ii. In preparation:

Current temperature measurements in the blackbody radiator to control its stability;

visibility measurements by Ruppersberg visibility meter additionally installed at Kreuzeck.

iii. Telemetric transmission:

Work is in progress to transmit the data as per 6.4.i. and ii. by the system described in Chapter 6.2. on-line to the valley institute where they are stored - as intermediate stage - equally on punch tape. This enables, however, immediate checks (e.g. fault identification) and evaluation of data.

iv. Data storage and on-line utilization in a separate computer. The ultimate goal (to be expected about early 1981) is to feed the Kreuzeck data and relevant valley data directly into a separate on-line computer at the Insitute, to store them there and make them currently visible by call-off on an optical terminal. Storage happens for safety reasons simultaneously on punch tape (for permanent reference) and on floppy discs for immediate further processing with the larger computer system.

7. Representation of Data Resulting from Measuring Campaigns Conducted from the End of 1979 until June 1980

First some preliminary remarks:

As mentioned in the beginning, we discuss here exclusively transmission measurements without telemetry link, i.e. those during which in case of transmission lower than about 12% reliable data could not be obtained any more.

After presenting selection criteria as to appropriate days for the conduct of measuring campaigns, a detailed description is given of each campaign that has been run effectively. Some had to be stopped prematurely due to unforeseen deterioration of weather conditions.

The description of each campaign begins with a presentation

of the general and special meteorological conditions on the respective day and proceeds to a discussion of the profiles detected by the slant path lidar in all three wavelengths (for manner of presentation see 7.1.ii.). For interpretation of the lidar backscatter profiles we provide diagrams of the radiosonde profiles (temperature (T), relative humidity (RH), and absolute humidity (AH). Knollenberg particle spectra, for the most part hourly-averaged, are also added.

Quantitative results of transmission measurements are supplied in tabular form and contain transmission factors τ and extinction coefficients σ.

In addition to these data which are obtained with the Barnes transmissometers, the time correlated, relevant meteorological data are given in the same table.

For calculating the absolute values of transmission factor τ we used as 100% values the highest signal amplitudes measured on haze-free calibration days ("Rayleigh days").

Further, mean extinction coefficients σ are indicated. These are calculated by dividing the negative natural logarithm of transmission factor τ by the length of the measuring path. The extinction coefficients are additively composed of the portions caused by the individual scattering elements (aerosol particles, fog droplets) so that arithmetic averaging is physically meaningful only for σ but not for τ. Only in case of minor variations in the single values both averaging methods do lead to an analogous result.

All figures belonging to this chapter can be found in the ANNEX, the tables are given at the respective passage in the text.

The figures are preceeded by a comparative scale (Fig. 1)

which enables the reader to relate the slant distance scale - given in km - (point 0 = lidar transmitter; end point = rock face close to the Kreuzeck mountain station, distance between the two points 2.7 km) to the radiosonde ascents whose height scale is plotted in m above sea level.

We would explicitly point out that the present report does not yet include a closer discussion of transmissometer results in connection with meteorological or lidar data because the hitherto available material is still too poor for an assessment of the relationships. Preconceived conclusions which possibly must be corrected later shall thus be avoided.

7.1. Preliminary remarks concerning selection of measuring campaigns

i. Two main criteria were always determinant in making a decision as to the start of measuring campaigns, namely, whether transmission values as low as possible or values as high as possible had to be expected. Low transmission conditions are of interest relative to practical application, especially for military purposes. On the other hand, data obtained during high transmission levels are needed for calibrating the system, i.e. for determining that level of the measured values which corresponds to completely unimpeded light transmission and 100% transmission, respectively. Even if conditions of 100% transmission can only approximately be reached in practice, the residual extinction can be determined the more reliable the smaller it is. In the visible range even a completely aerosol-free atmosphere has yet about 3% extinction due to Rayleigh scattering while in the range of the thermal infrared Rayleigh scatter can be neglected but line absorption through water vapor and trace gases such as ozone, CO_2, etc. must be considered.

Although the manufacturer supplied together with the system calibration data for both wavelength ranges obtained through measurements at the smallest possible distance from the radiation source and receiver, these can only be used as guiding data because the influence of the extremely varying geometries can probably not be calculated with sufficient accuracy, and moreover, long-term variations, e.g., through deteriorating quality of the optical components cannot be ruled out.

Days with low transmission in which measuring campaigns have been conducted will henceforth be briefly denoted as "measurement days" in contrast to "calibration days", i.e. days in which transmission was high. The decision as to whether a day was considered as"measurement day" or "calibration day" was made in the morning according to obvious visibility conditions and experiences available over many years concerning the development to be expected in the course of the day; further on the basis of recordings as, for instance, visibility, and above all on the basis of data from the stationary vertical lidar which on "promising" days is turned on as early as possible and is running during the transmission measurement concurrently as monitor in automatic operation where every half hour backscatter profiles from the lower 6 km of the atmosphere in the two wavelengths 347 and 694 nm are being detected and stored as well as output as hardcopy diagram.

In the measurement examples discussed below, transmissometer recordings are mainly described by the slant-lidar profiles which give a particularly illustrative picture not only of the aerosol distribution along the path but also of condensation processes, position of the actually existing clouds, and mainly of precipitation - if any - where it must be

emphasized that the detection limit for precipitation, especially for snow, lies for the lidar far below that of all the other conventional measuring instruments.

ii. In order not to delay formulation of the present report, the slant profiles have not been prepared on the main computer system; the raw data have been read without exchange right from the magnetic tape cassette into the computer of the mobile lidar. From that, the normalized backscatter profiles have been calculated and plotted by the X-Y recorder. For this reason the profiles are of somewhat "provisional" character. Plotted in the diagram are for the three wavelengths of the slant lidar (347, 530, 694 nm) the profiles of value $Fτ^2$ above the slant distance where F denotes the total backscatter coefficient (molecular plus aerosol part) and τ the two-way transmission factor which is the product of molecular and aerosol part and where in the slant distance zero can be defined as being equal to 1. Since the slant lidar is calibrated absolutely, F can be calculated in absolute units (m^{-1} $sterad^{-1}$), see tables and preliminary remarks to Chapter 7.

7.2. Description of the measuring campaigns

7.2.1. Calibration day 3 December 1979

This day, the weather situation was characterized by a stable anticyclone over the alpine area and the station was in the influence of mild, extremely clean subtropical air from southwesterly direction. Apart from some cirrus no cloudiness was observed. In the course of the day occurred in the height above 2000 m an influx of Saharan dust which is however negligible in this connection. The largely aerosol-free condition of air is documented in Fig. 2 by the slant lidar profiles which show in all three wavelengths a completely shapeless course at

very low level, practically caused only by Rayleigh scatter. The intense peak at 2500 m slant distance indicates here, and also in most of the profiles following, reflection from a rock face close to the Kreuzeck. The lidar was oriented to this fixed target in order to avoid DC loading of the detector by skylight background radiation which is often most intensive at low sun. A finite signal amplitude, possibly still present after the fixed target peak is caused by overload effects through extremely strong fixed-target reflection, especially under high visibility conditions.

Transmissometer data of this day may be regarded as tentative calibration and 100% values, respectively, in the infrared with reservation as to a possible residual extinction through absorption of atmospheric gas components which are difficult to calculate from the data records and require the use of LOWTRAN. For the visible range we measured a level of 990 millivolt at 6 dB attenuation, i.e., 1.98 V at 0 dB. The infrared signal was at 700 mV/6 dB, or, respectively, 1.39 V for 0 dB. Here, a residual level of 50 mV/0dB still existing also in the absence of an input signal is already deducted.

7.2.2. Measurement day 14 January 1980

This day, a typical wintertime,almost cloudless high pressure situation prevailed with slight geostrophic wind speeds and strong subsidence. In plain terrain forms under such conditions normally a flat, groundbased cold air layer below a temperature inversion which is more and more enriched with humidity, aerosols and other air pollutants. In the mountain valley, however, which is open to the plain and where our Institute is located, a pronounced mountain-valley-wind system prevails mostly during radiation weather and under its influence the cold surface air is carried off the valley at night. During the day the aerosol-rich cold air is transported again to the measuring site through

the valley wind, as a rule with increasing vertical thickness. According to our experiences this process was to be expected also for the measurement day but the upper boundary of the inflowing hazy air remained throughout the day below 1000 m a.s.l. and 350 m above ground, respectively.

A temperature inversion subsiding with time existed all over the day(Figs. 3 and 4). In the valley we had before noon $-9^{\circ}C$ and in the afternoon $-5^{\circ}C$ while above 1200 - 1000 m temperatures were around freezing level all through the day. In the valley 75% and 90% humidity have been recorded, above 1200 - 1000 m just 40%. In the forenoon of 14 January 1980 only slight haze was present at all altitudes, visibility conditions in the valley were about 30 km. This is evident from the slant lidar profiles (example Fig. 5) which remained unchanged all over the forenoon. The valley wind, with shift from SSW to NNE developed relatively late, i.e., between 13.00 and 14.00 and brought in first a very flat haze layer as apparent from the lidar profiles in Fig. 6. The "nose" caused by the aerosol layer is just dissolved in the short-range of the profiles. But one recognizes the already rather marked extinction through this layer by the reduction of the profile amplitudes above it as contrasted to the profiles in Fig. 5.
That the haze nose is pronounced strongest in the 530 nm profile is obviously due to the fact that just the begin of the haze advection has been detected since this profile was measured last of the three profiles (a complete measuring sequence in the three wavelengths takes 10 minutes). From the lidar profiles obtained in the following period till 13.30 (Figs. 7-12) it is evident that the haze layer increases in intensity and that its top - obviously fluctuating - rises from initially just 800 m a.s.l. (which corresponds to 200 m slant distance at 19.5^{0} inclination) slowly to 1000 m. (The structures in the upper half of the profiles are not real but due to uncertainties since with respect to non-overload detection of the short-range structures the lidar has been operated with very low

sensitivity). Visibility in the valley was reduced to 5 km in the haze layer. At times, cloud formation was observed at its upper boundary, mainly at the slopes, while a closed stratus sheet could be seen at the end of the valley.

It is well illustrated by Fig. 13 how the particle spectrum in the valley reflects from 12.00 - 14.00 only a weak increase in the particle number density. From 14.00 - 16.00 follows a marked enhancement of particles, mainly in the range of coarse particles which finally become identifiable up to 10 and 20 µm diameter. The inflowing layer with high aerosol concentration is thus - see lidar - documented.

Table 7.1 shows the effects of the near-ground layer, increasing from about 14.00 in thickness and aerosol load, on the slant transmission:

σ_{VIS} increases by factor 3.4, σ_{IR} only by factor 1.9; τ_{VIS} is reduced to 79,7%, τ_{IR} only to 89% The rather thin aerosol layer, maximum 100 m in thickness, has thus quite considerable effects along the 2,7 km slant optical path.

7.2.3. Measurement day 14 February 1980

In the early morning hours of this day our area was reached by an almost stationary, weakly pronounced air mass front which makes itself felt only at times through more intense cloudiness. From 08.00 on, the frontal clouds dissolve quickly and in the course of the forenoon slight convective clouding begins to form with its base lowering till afternoon from initially 2000 - 2500 m to 1500 m a.s.l., that is below Kreuzeck level. Between valley and Wank level there are no indications of a temperature inversion all through the day (see Fig. 14); humidity in the valley was between 60 and 75% and at the

Table 7.1. Transmission and Meteorological Data of 14.01.1980

Legend:

τ_{IR}, τ_{VIS} = Transmission factor in % in the infrared and visible range

σ_{IR}, σ_{VIS} = Extinction coefficient in km^{-1} in infrared and visible range, $\sigma = (-\ln\tau/100)/2,7$ km

t = Air temperature in degree Celsius (C)

RF = Relative humidity in %

e = Water vapor pressure in millibar

V = Visibility in km

CO_2 = Concentration of carbon dioxide in ppm

G = Insitute in the valley Garmisch-Partenkirchen, 720 m a.s.l.

W = Measuring site Wank (top), 1780 m a.s.l.

Time	τ_{IR}	σ_{IR}	τ_{VIS}	σ_{VIS}	t		RF		e		V		CO_2	
					G	W	G	W	G	W	G	W	G	W
12.30-13.30	94,1	0,0224	93,7	0,0241	-0,8	-1,0	80	40	4,6	2,3	25,9	57,4	334	334
13.30-14.30	96,3	0,0140	87,4	0,0498	-1,5	-1,1	72	41	4,0	2,3	8,6	58,6	372	334
14.30-15.30	93,0	0,0267	86,7	0,0528	-4,6	-1,0	74	46	3,2	2,6	6,3	56,6	375	33[illegible]
15.30-16.30	89,8	0,0400	86,7	0,0528	-6,7	-2,9	84	43	3,1	2,3	5,6	58,6	380	335
16.30-17.30	89,2	0,0422	79,7	0,0839	-7,2	-3,1	87	46	3,1	2,2	5,2	57,5	382	333

Kreuzeck near 80%. In the free atmosphere strong subsidence processes were recorded by the Zugspitze cable car sonde. The vertical lidar shows in the forenoon a strong markedly stratified haze layer with sharp upper boundary at 2400 m. In the course of the day the top of the haze layer becomes more and more faint due to convective processes.

The daily variation of the aerosol structure along the transmission path is shown by the slant lidar profiles Figs. 15 - 27. In the first hours of forenoon we observe also here a sharp stratification. Its most pronounced shape at 694 nm wavelength is suggestive of humidity structures as being the cause. Conspicuous is a gap in the haze layer at 900 m slant distance, corresponding to 1050 m a.s.l., which remains stable until 10.00 but is gone at 14.40. Towards noon, the backscatter profiles smooth more and more at slightly reduced mean level. With the valley wind, developing about noon, the dust concentration increases again; one observes a homogeneous, obviously well mixed ground haze layer whose upper boundary rises rapidly in the afternoon and reaches before the end of the measuring period at nearly 17.00 the Kreuzeck level where also clouds begin to form.

Figs. 28 (valley) and 29 (Kreuzeck) show the particle spectra. All over the day the particle number at Kreuzeck, ranging from 0.6 - 2 µm Ø is clearly lower than in the valley. The afternoon growth of the particle number by half an order of magnitude in the coarse particle range can be found at both stations. Interesting is the spectrum at the mountain station from 17.00 in fog with extremely high, almost constant particle number from 0.6 - 10 µm diameter.

Very informative are the transmissometer-results in Table 7.2. σ_{VIS} lies higher by about an order of magnitude than on 14 January (see Table 7.1.), τ_{VIS} decreases from 57,4% to 39%

Table 7.2.

Transmission and meteorological data of 14.02.1980

Legend:

τ_{IR}, τ_{VIS} = Transmission factor in % in infrared and visible range

σ_{IR}, σ_{VIS} = Extinction coefficient in km^{-1} in infrared and visible range, $\sigma = (-\ln\tau/100)/2{,}7$ km

t = air temperature in degree Celsius (C)

RF = Relative humidity in %

e = Water vapor pressure in millibar

V = Visibility in km

CO_2 = Concentration of carbon dioxide in ppm

G = Institute in the valley (Garmisch-Partenkichen), 750 m a.s.l.

W = Measuring site Wank peak, 1780 m a.s.l.

K = Measuring site Kreuzeck, 1650 m a.s.l.

Time	τ_{IR}	σ_{IR}	τ_{VIS}	σ_{VIS}	t		RF		e		V		CO_2	
					G	K	G	K	G	K	G	W	G	W
11.55-12.30	91,9	0,0311	57,4	0,206	+4,2	-1,9	65	94	5,4	5,0	19,5	10,1	347	338
12.30-13.30	88,7	0,0445	56,4	0,212	+5,2	-2,6	61	98	5,4	4,9	17,9	11,5	345	338
13.30-14.30	88,7	0,0445	52,4	0,239	+6,2	-2,6	59	96	5,6	4,8	15,8	11,4	346	340
14.30-15.30	89,8	0,0400	51,4	0,246	+6,1	-2,5	58	95	5,4	4,8	16,6	12,2	345	340
15.30-16.30	88,7	0,0445	39,1	0,348	+5,9	-3,4	58	98	5,4	4,7	14,1	11,2	347	338

(prior to fog formation). In contrast, σ_{IR} and τ_{IR} are just slightly affected by the high aerosol concentration in a thick layer: τ_{IR} (91,9 → 88,7%) and σ_{IR} (0,0311 → 0,0445) differ negligibly from the data in Table 1.

7.2.4. Calibration day 25 February 1980, only forenoon

This day, in calm and cloudless high pressure weather, very good visibility conditions prevailed in the forenoon being comparable to those of calibration day 3 December 1979. Only in the afternoon visibility was somewhat affected as a result of haze advection with developing valley wind. All over the day low humidity prevailed up to 2000 m a.s.l., inversions were absent (see Figs. 30, 31). Correspondingly, the slant lidar backscatter profiles show in the forenoon a low amplitude without any structure (Fig. 32).

From about 14.30 we had an aerosol influx from N into the valley with haze top rising towards evening above station Kreuzeck. This process can be well perceived in the particle spectrum from Kreuzeck (Fig. 33). In late afternoon the particle spectra from Kreuzeck and valley (Fig. 34) show very good agreement.

Table 7.3. gives again transmissometer data along with meteorological data. Until 13.30, τ_{IR} and τ_{VIS} were extremely high, σ_{IR} and σ_{VIS} very low. However, τ_{VIS} showed already slightly falling values and σ_{VIS} rising values (cf. decrease in horizontal visibility at Wank!). From 13.30, τ_{IR} decreased moderately, τ_{VIS} strongly, and σ_{IR} as well as σ_{VIS} increased considerably. In the same period, horizontal visibility in the valley and on the Wank decreased noticeably and the particle spectrum at the Kreuzeck shows a marked change.

Table 7.3. Transmission and meteorological data of 25.02.1980

Legend:

τ_{IR}, τ_{VIS} = Transmission factor in % in infrared and visible range

σ_{IR}, σ_{VIS} = Extinction coefficient in km^{-1} in infrared and visible range, $\sigma = (-\ln T/100)/2{,}7$ km

t = Air temperature in degree Celsius (C)
RF = Relative humidity in %
e = Water vapor pressure in millibar
V = Visibility in km
CO_2 = Concentration of carbon dioxide in ppm
G = Institute in the valley (Garmisch-Partenkirchen), 750 m a.s.l.
W = Measuring site Wank peak, 1780 m a.s.l.
K = Measuring site Kreuzeck, 1650 m a.s.l.

Time	τ_{IR}	σ_{IR}	τ_{VIS}	σ_{VIS}	t		RF		e		V		CO_2		
					G	K	G	K	G	K	G	W	G	W	
09.30-10.30	89,8	0,0400	89,0	0,0431	+7,3	+5,5	40	35	4,1	3,2	>40	67,6	335	338	CALIBRATION CONDITIONS
10.30-11.30	90,8	0,0355	88,5	0,0451	+7,3	+5,5	40	35	4,1	3,2	>40	67,6	335	338	
11.30-12.30	89,8	0,0400	86,5	0,0535	+10,6	+4,5	38	35	4,8	2,9	>40	65,4	334	338	
12.30-13.30	88,7	0,0445	83,1	0,0686	11,6	+3,6	28	37	3,8	2,9	>40	59,0	333	340	
13.30-14.30	83,2	0,0679	75,2	0,106	11,5	+3,4	32	38	4,4	3,0	>40	58,9	334	340	
14.30-15.30	76,7	0,0982	66,8	0,150	11,6	+3,1	34	40	4,7	3,0	27,0	54,3	335	340	INFLUX OF HAZE
15.30-16.30	71,3	0,125	55,9	0,216	11,1	+2,0	38	61	5,1	4,3	18,8	42,2	337	340	
16.30-17.30	70,2	0,131	53,9	0,229	10,2		40		5,0		20,0	23,5	339	344	

7.2.5. Measurement day 28 February 1980

This day, a high pressure ridge extended from the East Atlantic to the Ural and our area lay at the southern edge of the ridge in an air mass of continental origin (cPs) having very high aerosol concentration. Only medium-level clouds with strongly varying cloud cover have been observed. The aerosol structure developed very unusual this day which is rather impressively shown by the slant lidar profiles Figs. 35 - 49. Even in the early forenoon the structures show - mainly compared to 25 Feb - fairly high backscatter amplitudes with some structure along the transmission path. At 11.00 develops at 1500 m slant distance, corresponding to 1200 m a.s.l., a peak in the backscatter curves which is well pronounced at 694 nm and less defined - yet still clearly discernible - at 347 nm wavelength. Because of the intensive background skylight caused by the near sun it was temporarily impossible to measure at 530 nm. In the radiosonde profiles of 11.37 a small humidity maximum is indicated at this level, a temperature inversion, however, is but weakly pronounced or absent (weak T, RH effects also perceptible on Fig. 50). Somewhat more distinct is this inversion at 15.46 on Fig. 51.

About noon, extremely hazy air which increased in thickness was introduced by the prevailing valley wind and the measured visibility was reduced to 3 km in the valley and 6 km at the Wank which is absolutely unusual in our area in the case of dry aerosol (the limit of 70% humidity in which particles begin to grow due to water uptake was exceeded only for a short time in the afternoon). The noted aerosol concentrations, mainly at mean height levels, belong to the highest values ever measured here so that this day may be regarded as particularly interesting relative to transmissometer measurements. Figs. 52/53 and 54/55 indicate the systematic and drastic particle growth over the whole spectral range in the valley and at Kreuzeck where the concentrations increase however invariably with height.

The slant lidar profiles show even at about 14.00 very high backscatter values which continue to rise in the afternoon. It is remarkable that the aerosol layer shows largely homogeneous structure without stratification, at first up to 2 km slant range, later along the entire transmission path. This is also documented by conductivity profiles of the Zugspitze cable car sonde and is important in view of the future evaluations. Due to the homogeneity of the haze layer the slant lidar profiles assume the form of an exponential function whose decrease with increasing aerosol concentration becomes steeper and steeper (the steps and structures in the upper part are technically induced and not real). Through that, also the fixed-target peak (upper end of the lidar path = rock face) becomes smaller and smaller and vanishes even entirely at 347 nm.

Because of their exponential decay the lidar profiles can be easily extrapolated to distance zero without great arithmetical effort, i.e., the variable parameters of our bimodal model of particle size distribution used for the lidar measurements and consisting of two log-normal distributions with constant center diameter (0.4 and 2.0 µm) can be deduced.

These parameters are the partial concentrations N_1 and N_2 in the fine (around 0.4 µm) and coarse particle range. For 18.00 one obtains, for instance, $N_1 = 1{,}7 \times 10^9\ m^{-3}$ and $N_2 = 1{,}7 \times 10^6\ m^{-3}$. These values agree fairly well with the data from the Knollenberg particle spectrometer at the valley station, where for 0.4 µm concentrations $dN/d\ln D = 2{,}0 \times 10^9$, and for 2.0 µm $1{,}0 \times 10^7\ m^{-3}$ have been measured. The corresponding values from the spectrometer at the Kreuzeck are of about equal rate.

Independent of the particle partial concentrations, extinction coefficients can also be derived from the lidar profiles.

For the three wavelengths 347, 530, and 694 nm one obtains 1,88 x 10^{-3}, 1,36 x 10^{-3}, and 1,14 x 10^{-3} m^{-1}. From the value for wavelength 530 nm which lies almost in the center of the visible range, a standard optical range of 2,9 km may be deduced in reasonable agreement with a visibility range of about 3 km measured by the Ruppersberg instrument.

Transmissometer data and meteorological data are compiled in Table 7.4a (hourly means for τ, σ) and Table 7.4b, respectively, (half-hourly means for τ,σ): One recognizes immediately - as a result of the almost homogeneous aerosol (haze) layer extending from the valley floor beyond the Kreuzeck - the drastic difference in the behavior of τ_{IR} and σ_{IR} on the one hand (only slight changes with time) and τ_{VIS} and σ_{VIS} on the other. In the latter case τ_{VIS} decreases from 90,5% to 3,6%, or, resp., σ_{VIS} rises from 0,037 to 1,23. (Measurability of transmission was ensured because of the good optical chopper frequency transmission in the infrared). This measuring campaign yielded indeed extremely valuable data.

7.2.6. Measurement day 19 May 1980

The flow conditions in the lower and middle troposphere are rather different this day. At ground level an Azores high extends to our area but it lies at 500 mb at the north-western edge of a cut-off low over Italy and Yugoslavia with which cold polar air flows to the Mediterranean Sea. This leads to instability at high altitude and moderate to strong convection. In the early morning hours the sky was overcast, the cloud base at the mountain slopes reached down to 1000 m a.s.l., so that the radiation source at Kreuzeck was invisible. However, for the further course of the day improvement in visiblity conditions was expected which occurred indeed as the cloud base rose. From 10.00, station Kreuzeck was temporarily becoming clear and from 15.00 it was permanently free from clouds. Thus, extinction through thin clouds could be measured in both wavelength ranges.

Table 7.4a. Transmission and meteorological data of 20.02.1980

Legend:

τ_{IR}, τ_{VIS} = Transmission factor in % in infrared and visible range

σ_{IR}, σ_{VIS} = Extinction coefficient in km^{-1} in infrared and visible range, $\sigma = (-\ln\tau/100)/2{,}7$ km

t = Air temperature in degree Celsius (C)
RF = Relative humidity in %
e = Water vapor pressure in millibar
V = Visibility in km
CO_2 = Concentration of carbon dioxide in ppm
G = Institute in the valley (Garmisch-Partenkirchen), 750 m a.s.l.
W = Measuring site Wank peak, 1780 m a.s.l.
K = Measuring site Kreuzeck, 1650 m a.s.l.

Time	τ_{IR}	σ_{IR}	τ_{VIS}	σ_{VIS}	t		RF		e		V		CO_2	
					G	K	G	K	G	K	G	W	G	W
10.30-11.30	94,8	0,0198	75,4	0,105	+3,4	+1,3	54	48	4,2	3,2	19,0	36,0	348	*)
11.30-12.30	95,5	0,0171	51,1	0,249	+4,6	+0,9	50	47	4,3	3,1	10,0	27,9	349	
12.30-13.30	93,9	0,0233	32,6	0,414	4,6	+0,5	54	51	4,6	3,2	6,5	19,6	353	
13.30-14.30	92,9	0,0275	24,8	0,517	5,0	-0,7	52	61	4,5	3,5	6,1	14,6	353	
14.30-15.30	89,0	0,0433	10,6	0,833	4,8	-1,4	55	76	4,7	4,2	4,7	6,9	362	
15.30-16.30	85,9	0,0563	4,6	1,14	3,7	-2,0	60	86	4,8	4,6	3,7	4,4	372	
16.30-17.30	85,5	0,0580	4,1	1,18	1,9	-1,8	66	85	4,6	4,5	3,5	5,8	373	

*) from 10.00 defective; till this time, CO_2 at the Wank was about 15 - 20 ppm lower than in Garmisch-Partenkirchen

Table 7.4b. Transmission and meteorological data of 28.02.1980

Legend:

τ_{IR}, τ_{VIS} = Transmission factor in % in infrared and visible range

σ_{IR}, σ_{VIS} = Extinction coefficient in km^{-1} in infrared and visible range, $\sigma = (-\ln\tau/100)/2{,}7$ km

t = Air temperature in degree Celsius (C)
RF = Relative humidity in %
e = Water vapor pressure in millibar
V = Visibility in km

CO_2 = Concentration of carbon dioxide in ppm
G = Institute in the valley (Garmisch) 750 m a.s.l.
W = Measuring site Wank peak, 1780 m a.s.l.
K = Measuring site Kreuzeck, 1650 , a.s.l.

Time	τ_{IR}	σ_{IR}	τ_{VIS}	σ_{VIS}	t		RF		e		V		CO_2	
					G	K	G	K	G	K	G	W	G	W
10.30-11.00	95,8	0,0161	90,5	0,037	+3,4	+1,3	54	48	4,2	3,2	19,0	36,0	348	*)
11.00-11.30	93,8	0,0237	60,3	0,187										
11.30-12.00	95,2	0,0182	55,4	0,219	+4,6	+0,9	50	47	4,3	3,1	10,0	27,9	349	
12.00-12.30	95,8	0,0161	46,7	0,282										
12.30-13.00	93,7	0,0241	34,6	0,393	+4,6	+0,5	54	51	4,6	3,2	6,5	19,6	353	
13.00-13.30	94,1	0,0224	30,7	0,438										
13.30-14.00	94,1	0,0224	28,7	0,463	+5,0	-0,7	52	61	4,5	3,5	6,1	14,6	353	
14.00-14.30	91,6	0,0324	20,8	0,582										
14.30-15.00	89,8	0,0400	13,4	0,746	+4,8	-1,4	55	76	4,7	4,2	4,7	6,9	362	
15.00-15.30	88,1	0,0468	7,4	0,963										
15.30-16.00	86,2	0,0551	5,1	1,099	+3,7	-2,0	60	86	4,8	4,6	3,7	4,4	372	
16.00-16.30	85,6	0,0574	4,06	1,187										
16.30-17.00	85,4	0,0584	4,06	1,187	+1,9	-1,8	66	85	4,6	4,5	3,5	5,8	37:	
17.00-17.30	85,6	0,0574	4,15	1,178										
17.30-18.00	86,0	0,0560	3,6	1,23										

*) from 10.00 defective; till this time CO_2 at Wank was about 15-20 ppm lower than in Garmisch

By means of the series of slant lidar profiles shown in Figs. 56 - 66, the increase and later disintegration of clouds in the area of the transmission path can be well observed. In the morning, reflection from the cloud base at about 900 m slant distance can be perceived; below, long-wave backscatter indicates partial condensation in wet aerosol. At 10.00, the fixed-target reflection becomes visible for the first time with attenuated, yet still perceptible cloud signal. In the following period the cloud signals slowly increase with further attenuation and vanish at about 15.00 completely (Fig. 67). At the same time, the underlying aerosol layer loses rapidly its structure and the decline of the profile amplitudes signals a general slight haze diminution which is also evident from the visibility recordings. The aerological profiles are presented by two examples in Figs. 68 and 69.

Fig. 70 shows the uniform structure of the particle spectrum in the valley throughout the day. On Kreuzeck (Fig. 71), the particle spectrum is higher than in the valley at 10.30 and 16.10. The almost horizontal distributions at 11.10 and 14.30 are due to cloud droplets.
Thus, τ_{IR} and τ_{VIS} values in Table 5 fit well to each other. At 11.10 and 14.30 transmission breaks down altogether or is little before a breakdown but IR-transmission remains always essentially better than VIS-transmission.

Table 5 gives an example - from the time *before* chopper telemetry - of strongly varying transmission values due to temporarily existing clouds in the transmission path. But in this case only τ-values could be calculated and averaged. Calculation of extinction coefficients was not possible since the signal amplitude was frequently zero because of the lower detection limit which was then still too high (formation of logarithm then impossible). Time intervals were chosen such as to agree with the Knollenberg-measuring periods.

Table 7.5. Transmission and meteorological data of 19.05.1980

Legend:

τ_{IR}, τ_{VIS} = Transmission factor in % in infrared and visible range

$\sigma_{IR}, \sigma_{VIS}$ = Extinction coefficient in km^{-1} in infrared and visible range, $\sigma = (-\ln\tau/100)/2{,}7$ km

t = Air temperature in degree Celsius (C)

RF = Relative humidity in %

e = Water vapor pressure in millibar

V = Visibility in km

CO_2 = Concentration of carbon dioxide in ppm

G = Institute in the valley (Garmisch-Partenkirchen, 730 m a.s.l.

W = Measuring site Wank peak, 1780 m a.s.l.

K = Measuring site Kreuzeck, 1650 m a.s.l.

Time	τ_{IR}	τ_{VIS}	cloud thickness	t		RF		e		V		CO_2	
				G	K	G	K	G	K	G	W	G	W
10.20-10.40	27,0%	13,9%	changing dispersed cloudiness	+10,1	-0,7	71	100	8,8	6,4	18,9	5,8	336	338
11.00-11.20	0,7%	0,0%	1500 - 1650 m (detected by lidar, 150 m thick)	+11,2	+0,1	67	100	8,9	6,2	18,3	5,9	333	340
14.20-14.40	25,6%	4,2%	first 1[illegible] - 1[illegible] m, base quickly rising	+10,9	+0,5	69	100	9,0	6,3	12,4	6,1	338	338
16.00-16.20	85,2%	68,7%	[illegible] cloud	+12,0	+1,6	60	99	8,4	6,8	19,1	6,3	335	338

7.2.7. Measurement day 23 May 1980

Our area was this day influenced by a cut-off low over the northern Mediterranean Sea and a cold and very hazy air mass fills the whole valley. Under the impact of the valley wind the haze layer intensifies during the course of the day. While mean and high level clouds are almost absent, stratocumulus forms already in the forenoon at 1100 - 1500 m a.s.l. and develops during the afternoon into a closed Sc-sheet thus interrupting the view to the Kreuzeck for several hours entirely. Such a weather situation is normally found in fall and is rather uncommon for May. Station Kreuzeck was open again only at 14.00. During the period in between it was once more possible to detect at times the different extinction in the visual and IR range through dispersed cloudiness.

Fig. 72 gives the most inhomogeneous structure of the aerological parameters. In contrast, the spectral distribution of aerosol particles over the day and the height difference valley - mountain station (here Wank instead of Kreuzeck) remained uniform as evident from Figs. 73 and 74.

Table 6 shows the transmission data. Due to the interruption of light transmission through cloud remnants, τ_{IR} was weakly, τ_{VIS} strongly reduced, for σ_{IR} and σ_{VIS} holds the reverse. Compare also the horizontal visibility conditions in the valley and at the Wank.

Table 7.5. Transmission and meteorological data of 23.05.1980

Legend:

τ_{IR}, τ_{VIS} = Transmission factor in % in infrared and visible range

σ_{IR}, σ_{VIS} = Extinction coefficient in km^{-1} in infrared and visible range, $\sigma = (-\ln\tau/100)/2{,}7$ km

t = Air temperature in degree Celsius (C)

RF = Relative humidity in %

e = Water vapor pressure in millibar

V = Visibility in km

CO_2 = Concentration of carbon dioxide in ppm

W = Measuring site Wank peak, 1780 m a.s.l.

G = Institute in the valley (Garmisch-Partenkirchen), 750 m a.s.l.

Time	τ_{IR}	σ_{IR}	τ_{VIS}	σ_{VIS}	t		RF		e		V		CO_2	
					G	W	G	W	G	W	G	W	G	W
14.30-15.30	78,6	0,0892	28,8	0,461	11,3	6,0	68	86	9,1	8,0	10,1	6,6	330	335
15.30-16.30	79,4	0,0854	23,2	0,376	12,3	5,6	64	80	9,2	7,3	11,4	9,1	327	336

8. Measurement of Length of Laser Pulses Reflected from a Rock Face

If a short laser pulse propagates through mist or fog with sufficient optical thickness for occurrence of multiple scattering, the length of the pulse is known to be stretched up to several microseconds. Since this phenomenon is of considerable practical importance, we measured on request of ASL the width of laser pulses reflected from a rock face close to the location of the transmitter source (Kreuzeck) under different visibility conditions. An as vertical as possible portion of the rock face has been chosen for the measurements in order to keep pulse stretching by distance variances of the reflector across the laser beam small. Table 8.7. presents widths of reflected 347 and 530 nm laser pulses during low (No. 1 - 14), high (No. 15 - 24), and extremely low aerosol concentration (No. 25 - 26) but with no fog or clouds present. The pulse FWHM (full width of half maximum) is between 30 and 40 nanoseconds in most cases, and the observed variations are - as Table 8.7. shows - not correlated with the aerosol concentration. It is interesting to compare these results with theoretical calculations.

Weinman and Shipley[+]) calculated the shape of an initially infinitely short laser pulse after passage of a cloud with extinction coefficient σ and optical thickness x. They got a pulse FWHM $\delta t \cong .11x^2/\sigma\lambda c$, where c is the velocity of light and λ a number which is related to the asymmetry of the scattering phase function and which is, e.g., 1 for isotropic Rayleigh scatterers and about 8 for most clouds and hazes.

In our extreme case, February 28, 1980, we measured in 530 nm

---

[+]) Weinman and Shipley, J. Geophys. Res. 77, 7123 (1972)

an extinction coefficient of 1.36 km^{-1}, resulting in an optical thickness x of the air mass along the transmission path equal to 3.67. For $\lambda = 8$, we get $\delta t = .45$ μsec, a value which is at least ten times as high than our data. This difference can only partially accounted for by assuming a smaller value for λ.

Table 8.7.

Measured Widths (FWHM) of Laser Pulses Reflected from a Rock Face

No.	Date (1980)	Wavelength (nm)	FWHM (nsec)	Aerosol Concentration
1	5-29	530	35	low
2	5-29	530	37	"
3	5-29	530	38	"
4	5-29	530	32	"
5	5-29	530	37	"
6	5-29	530	35	"
7	7-22	530	30	"
8	7-22	530	30	"
9	7-22	530	24	"
10	7-22	530	22	"
11	7-22	530	30	"
12	7-22	347	42	"
13	7-22	347	38	"
14	7-22	347	38	"
15	5-23	530	40	high
16	5-23	530	35	"
17	5-23	530	30	"
18	5-23	530	35	"
19	5-23	530	40	"
20	5-23	530	35	"
21	5-23	347	38	"
22	5-23	347	40	"
23	5-23	347	38	"
24	5-23	347	41	"
25	2-28	530	30	extremely high
26	2-28	530	23	" "

9. Future Plans

Improvements still to be made are mentioned in Chapters 1 - 6 at different passages.

They concern modification of the mobile lidar for the use of the 1060 nm wavelength, completion of computerized data telemetry from the Kreuzeck to the valley - on-line operation - and improvement of the visible light source (halogen lamp) to secure a longer lamp life.

Connection of the computer to data sampling for the transmissivity project requires still some programming work.

Apart from that, use will be made of all weather conditions relevant to the objective of our research work in order to ensure through measuring campaigns systematic sampling of specific, useful data. More importance is now attached also to measurements during precipitation of various type.

The final data are stored and scientifically processed and on request they will be supplied to ASL.

ANNEX WITH FIGURES

belonging to Chapter 7

F I G U R E S 1 - 74

Fig. 1

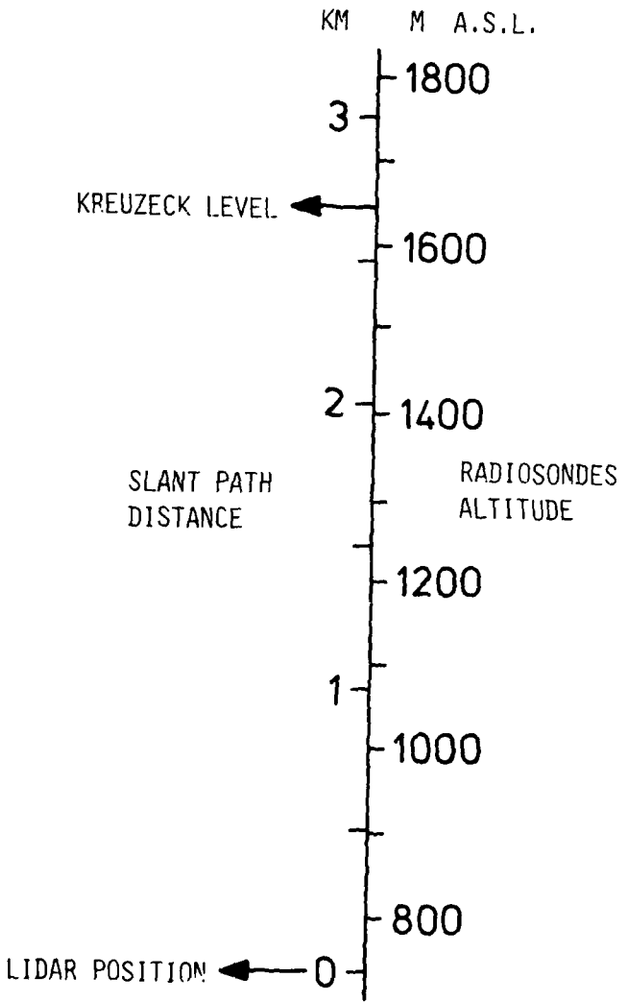
KM
M A.S.L.
1800
3
KREUZECK LEVEL
1600
2
1400
SLANT PATH
DISTANCE
RADIOSONDES
ALTITUDE
1200
1
1000
800
LIDAR POSITION
0

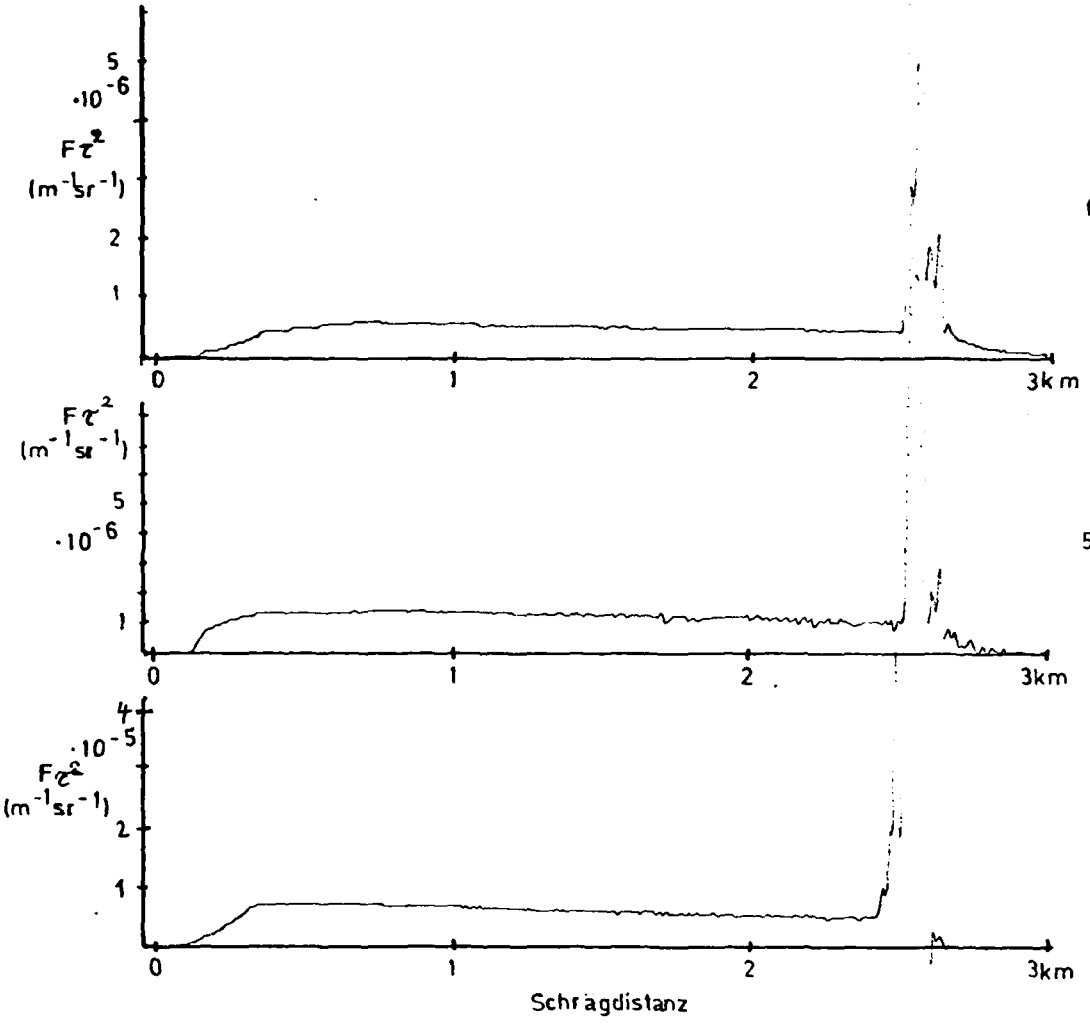

Datum:

3. Dez. 1979

Uhrzeit:

0930 MEZ

Fig. 2

Fig. 3

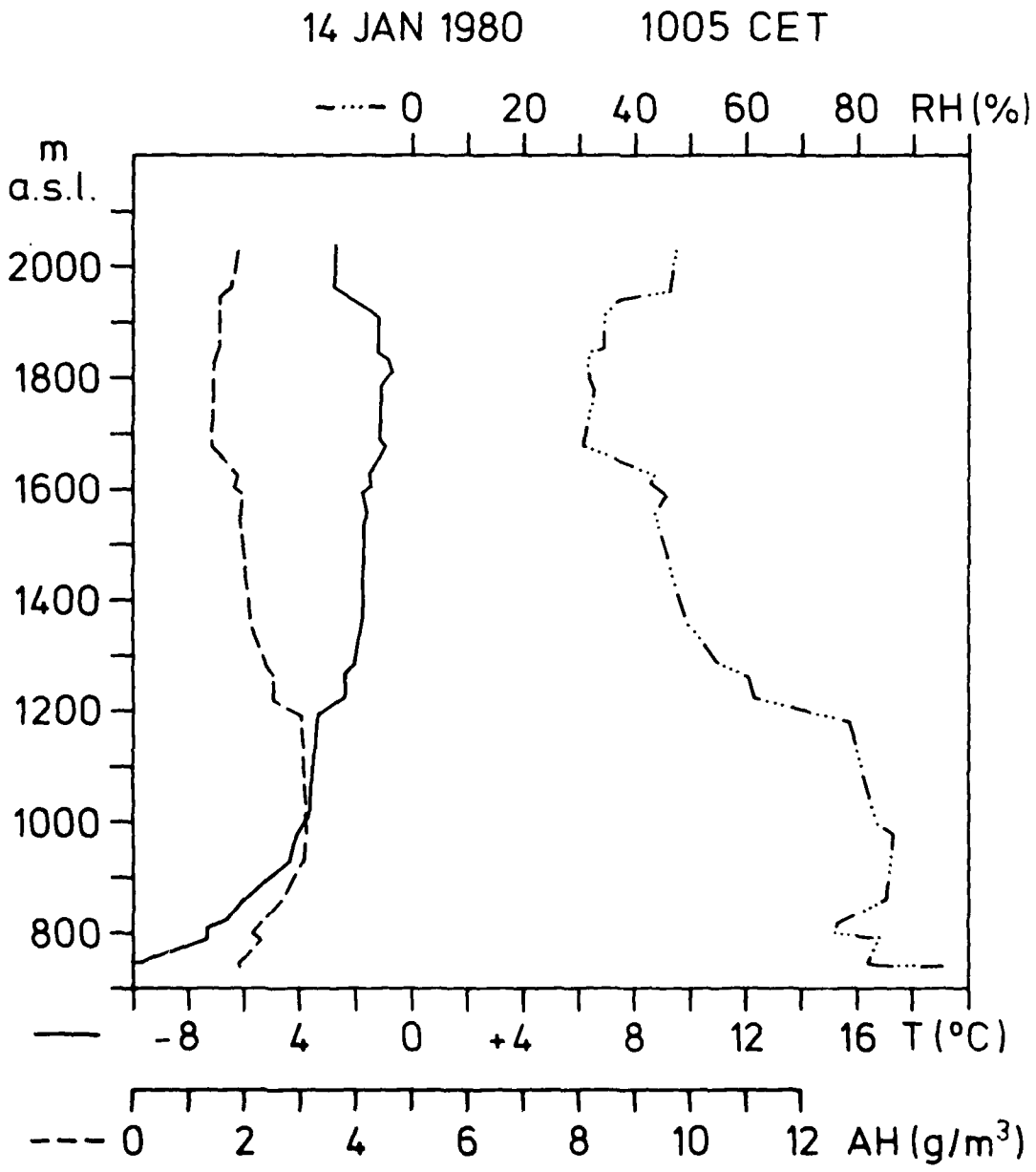
14 JAN 1980 1005 CET
0 20 40 60 80 RH (%)
m a.s.l.
2000
1800
1600
1400
1200
1000
800
-8 4 0 +4 8 12 16 T (°C)
0 2 4 6 8 10 12 AH (g/m³)

Fig. 4

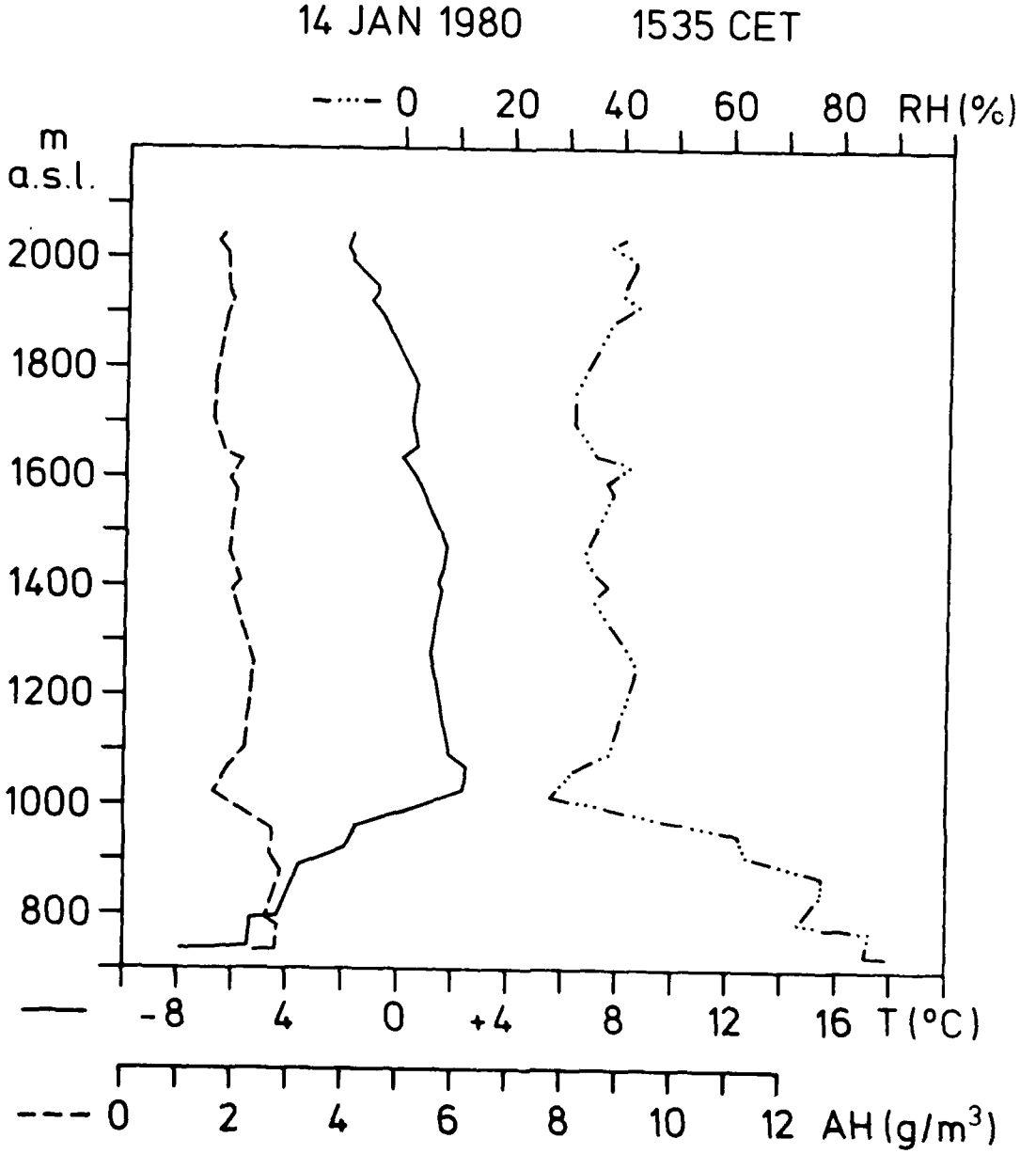
14 JAN 1980 1535 CET
0 20 40 60 80 RH(%)
m a.s.l.
2000
1800
1600
1400
1200
1000
800
-8 4 0 +4 8 12 16 T(°C)
0 2 4 6 8 10 12 AH(g/m³)

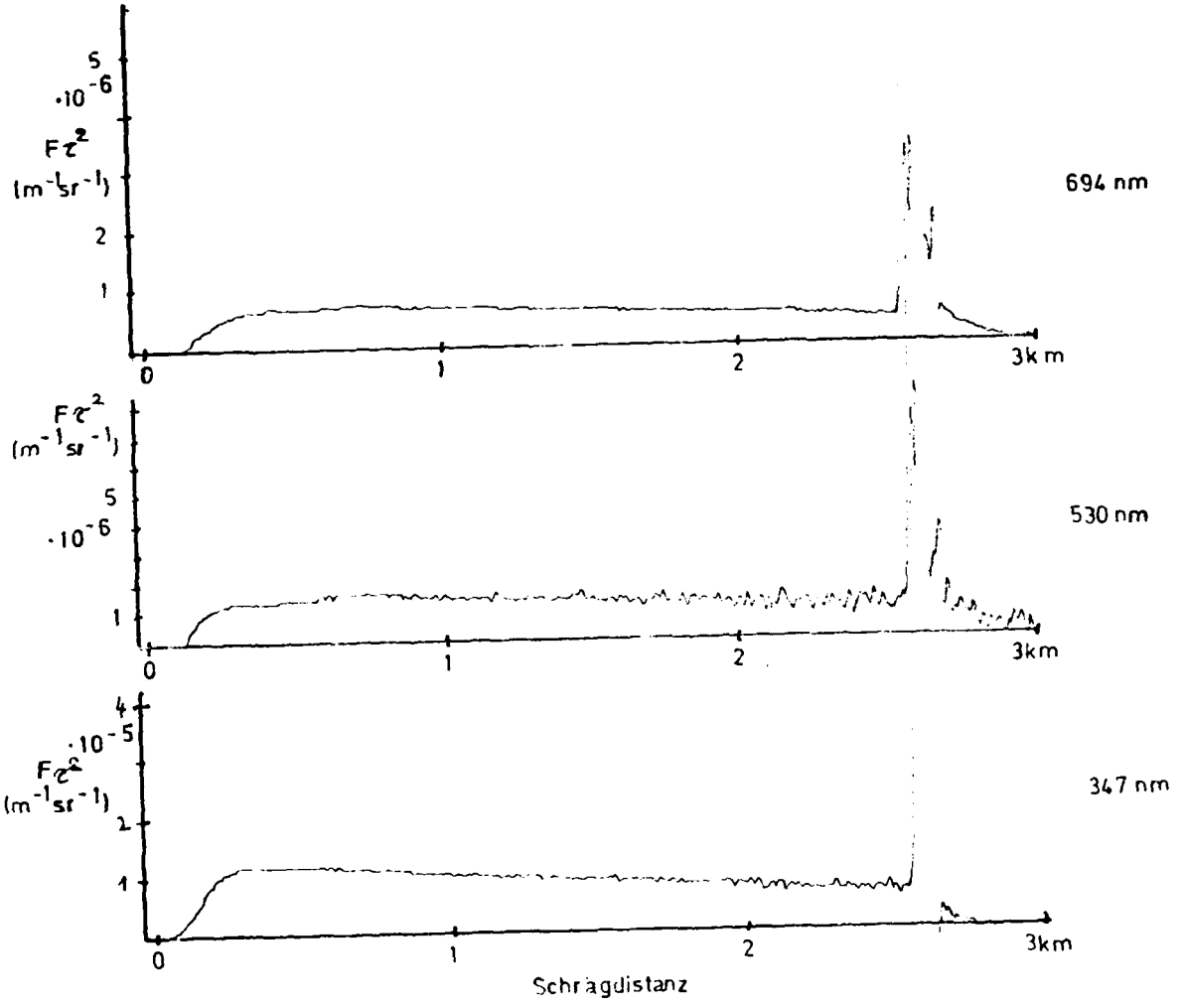

Datum:

14. Jan. 1980

Uhrzeit:

11.00 MEZ

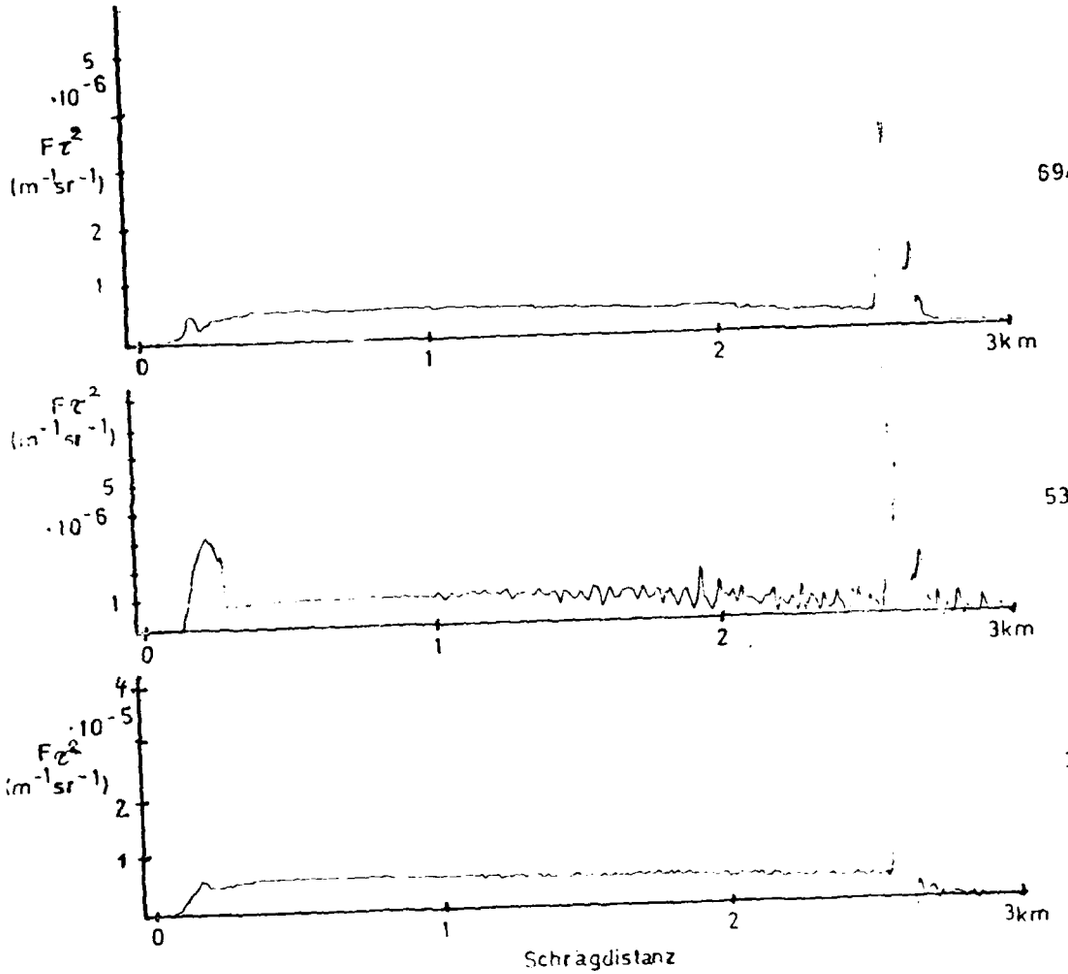

Datum:

14. Jan. 1980

Uhrzeit:

14.00 MEZ

Fig. 9

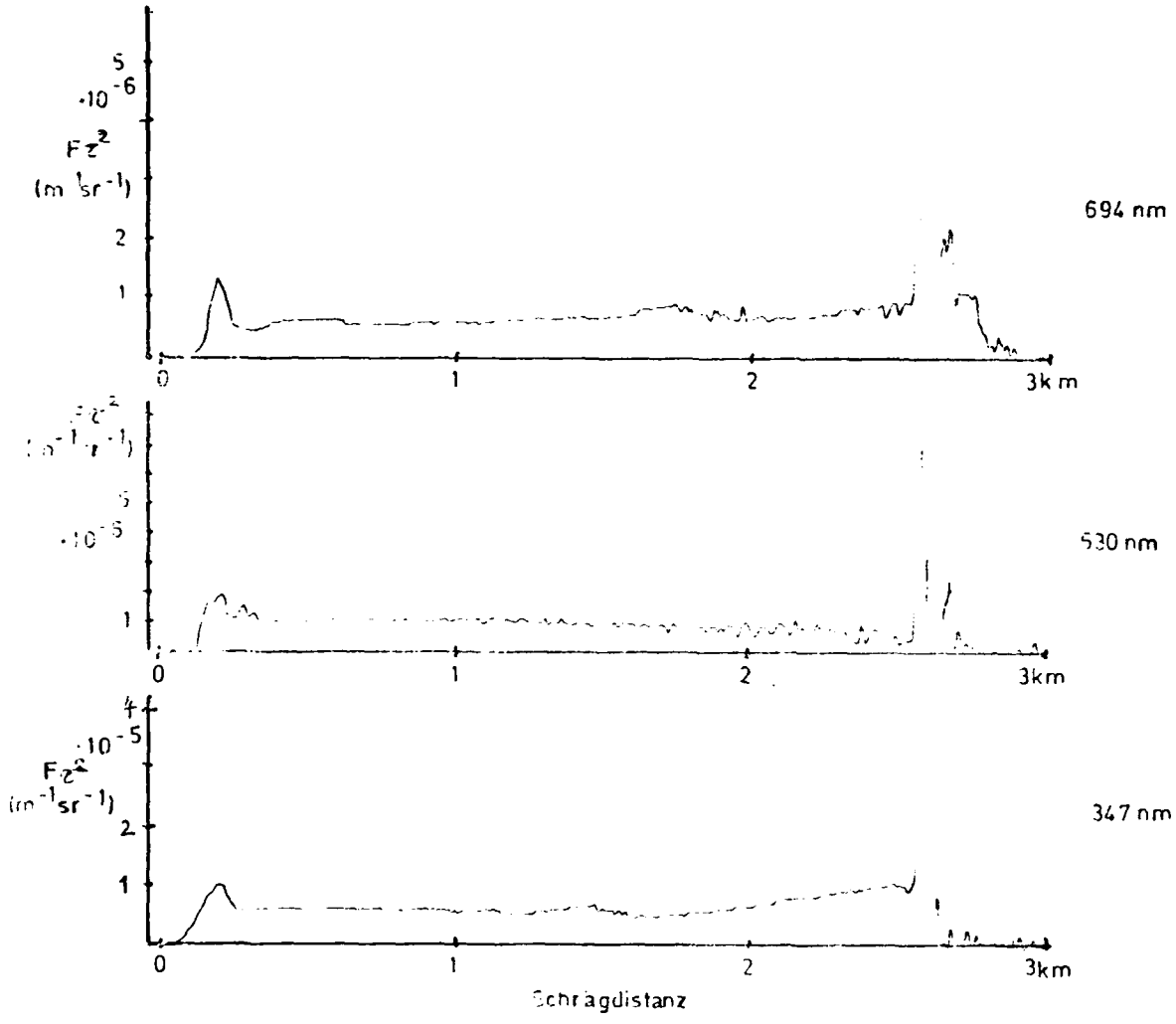

Datum:

14. Jan. 1980

Uhrzeit:

1440 MEZ

Fig. 7

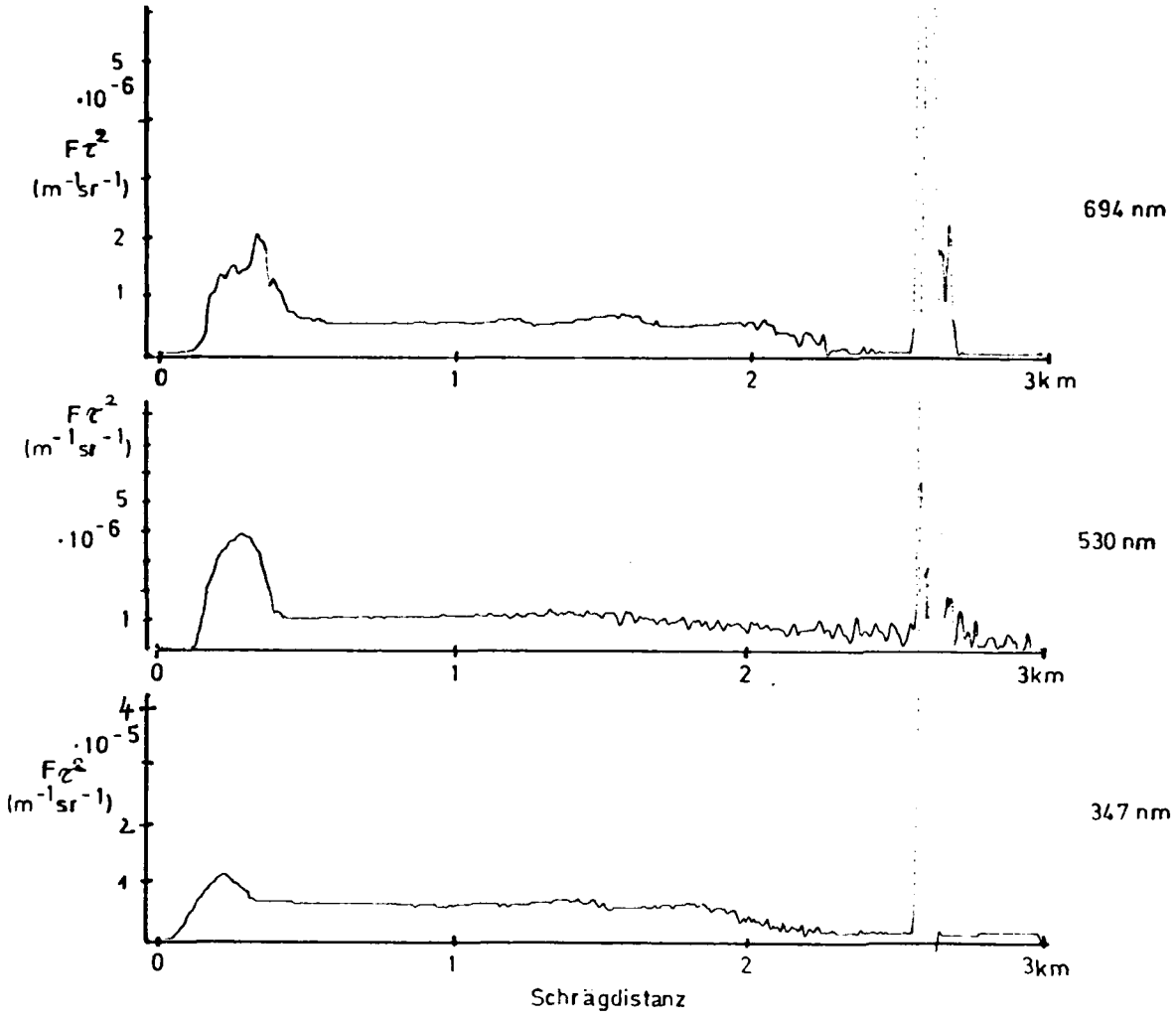

Datum:

14. Jan. 1980

Uhrzeit:

15.30 MEZ

Fig. 8

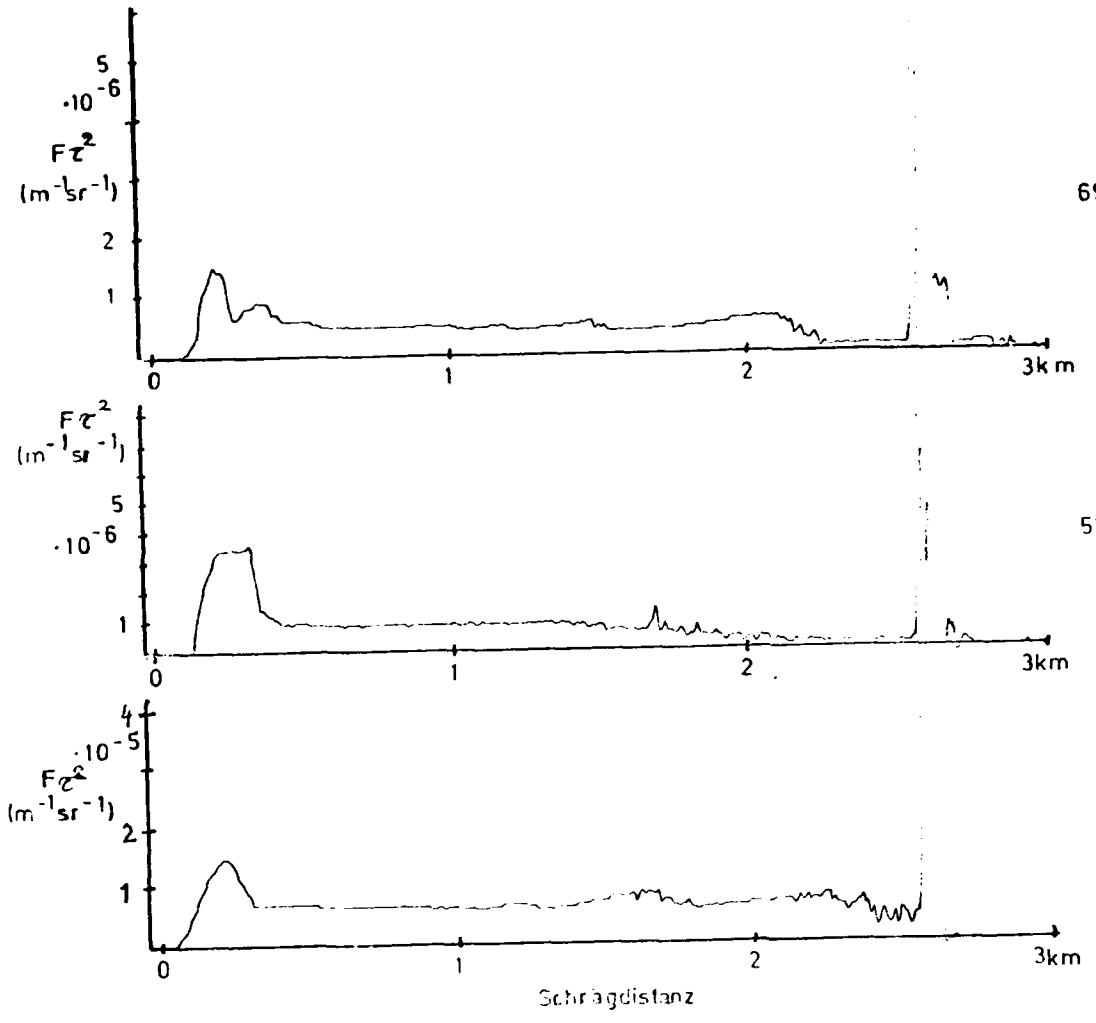

Datum:

14. Jan. 1980

Uhrzeit:

16.00 MEZ

Fig. 9

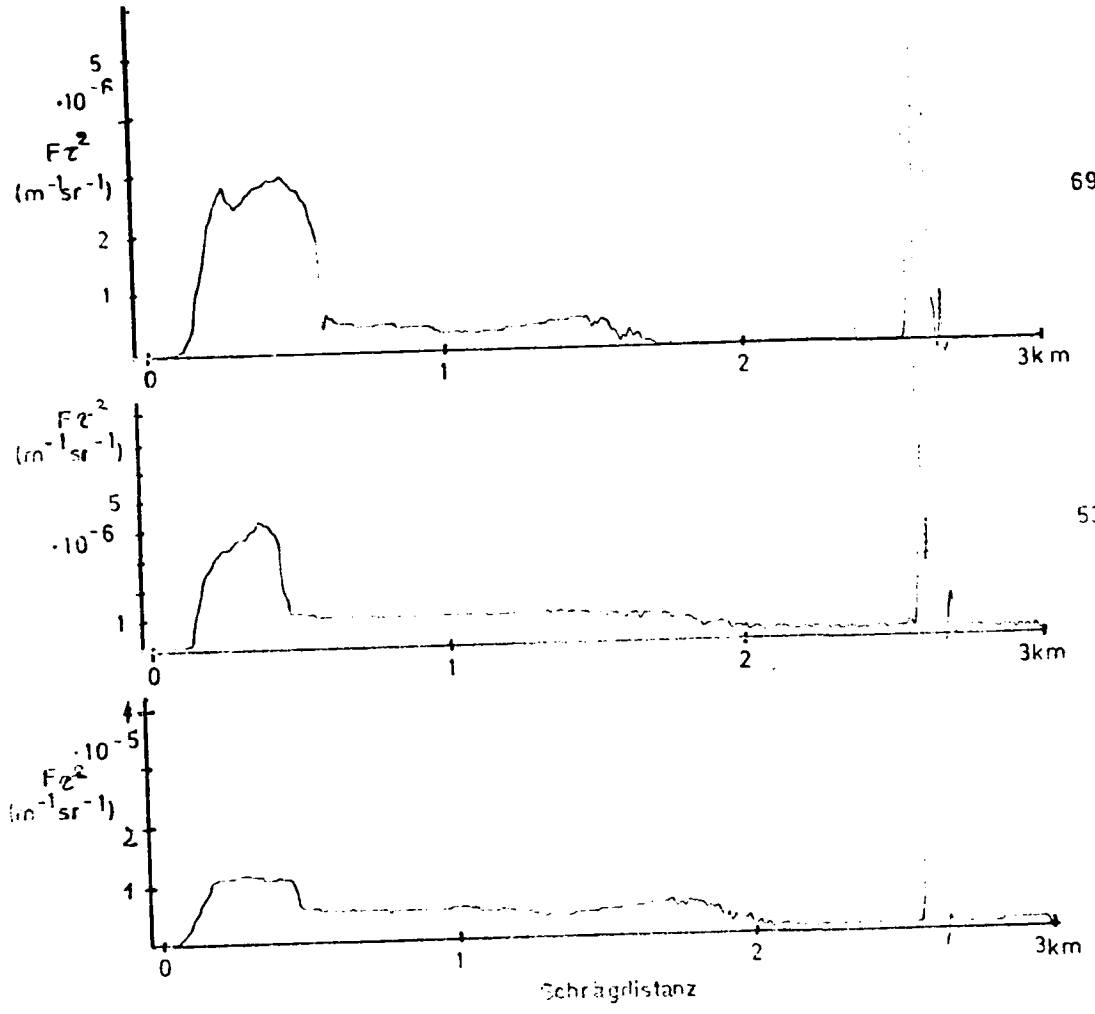

Datum:

14. Jan. 1980

Uhrzeit:

16.30 MEZ

Fig. 10

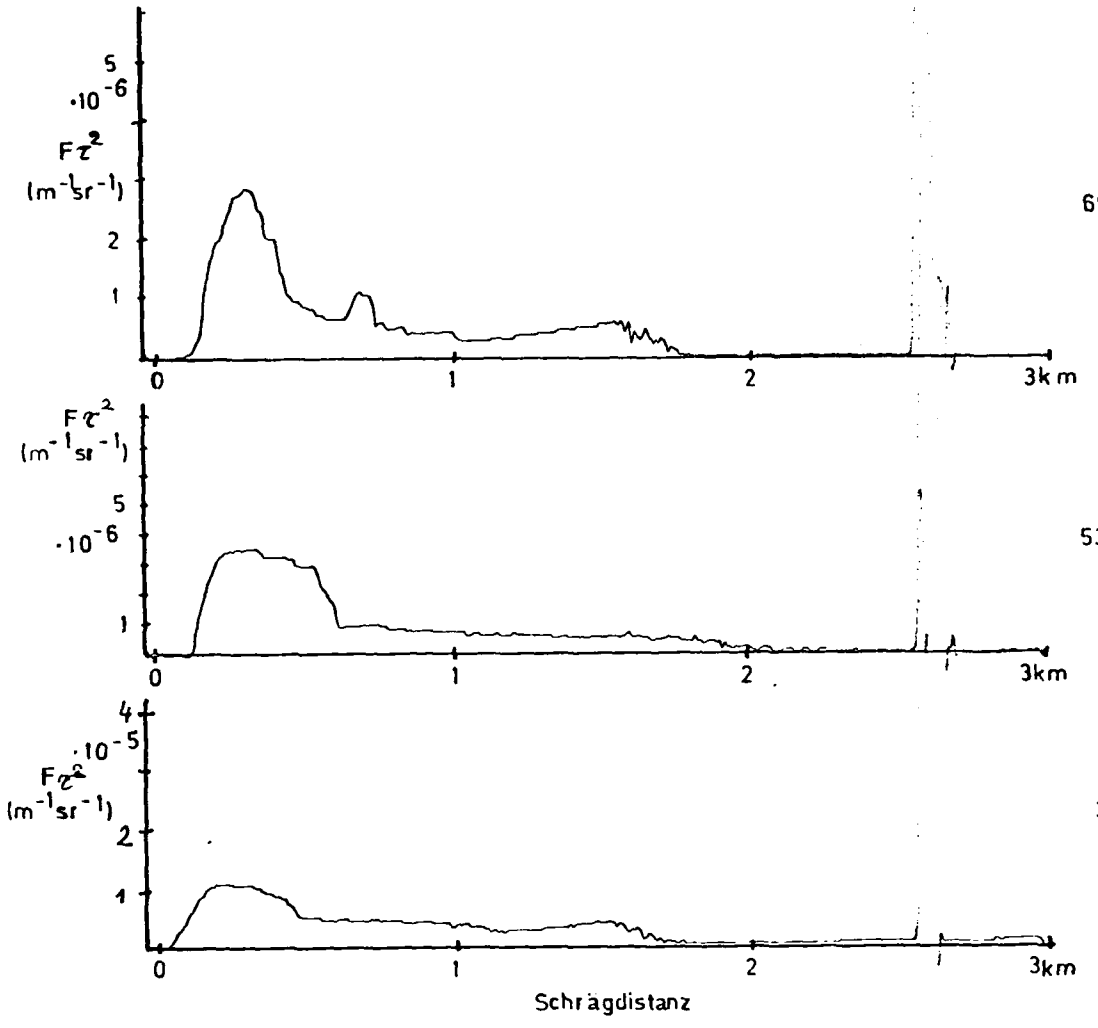

Datum:

14. Jan. 1980

Uhrzeit:

17.00 MEZ

Fig. 11

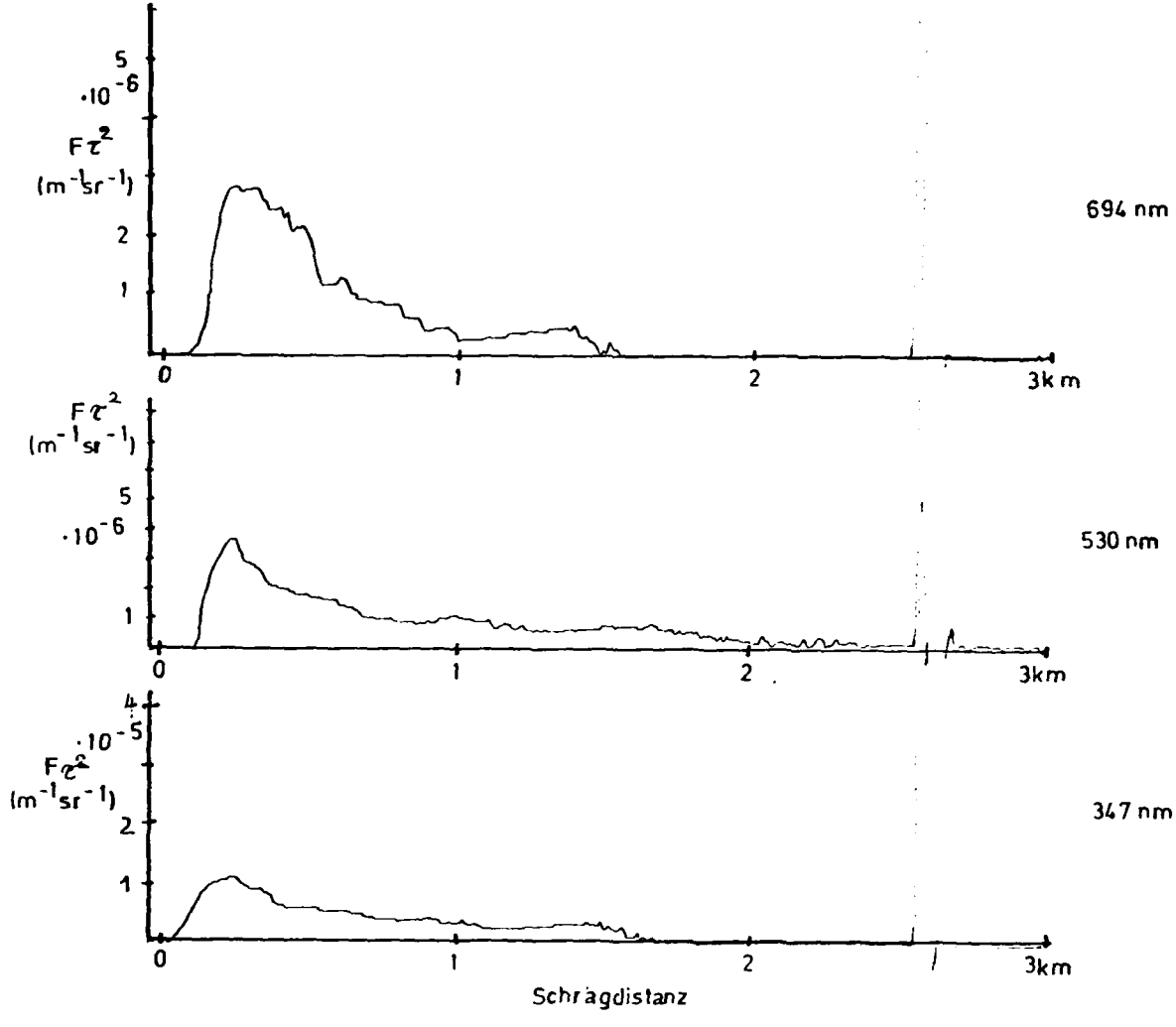

Datum:

14. Jan. 1980

Uhrzeit:

17.30 MEZ

Fig. 12

Fig. 13

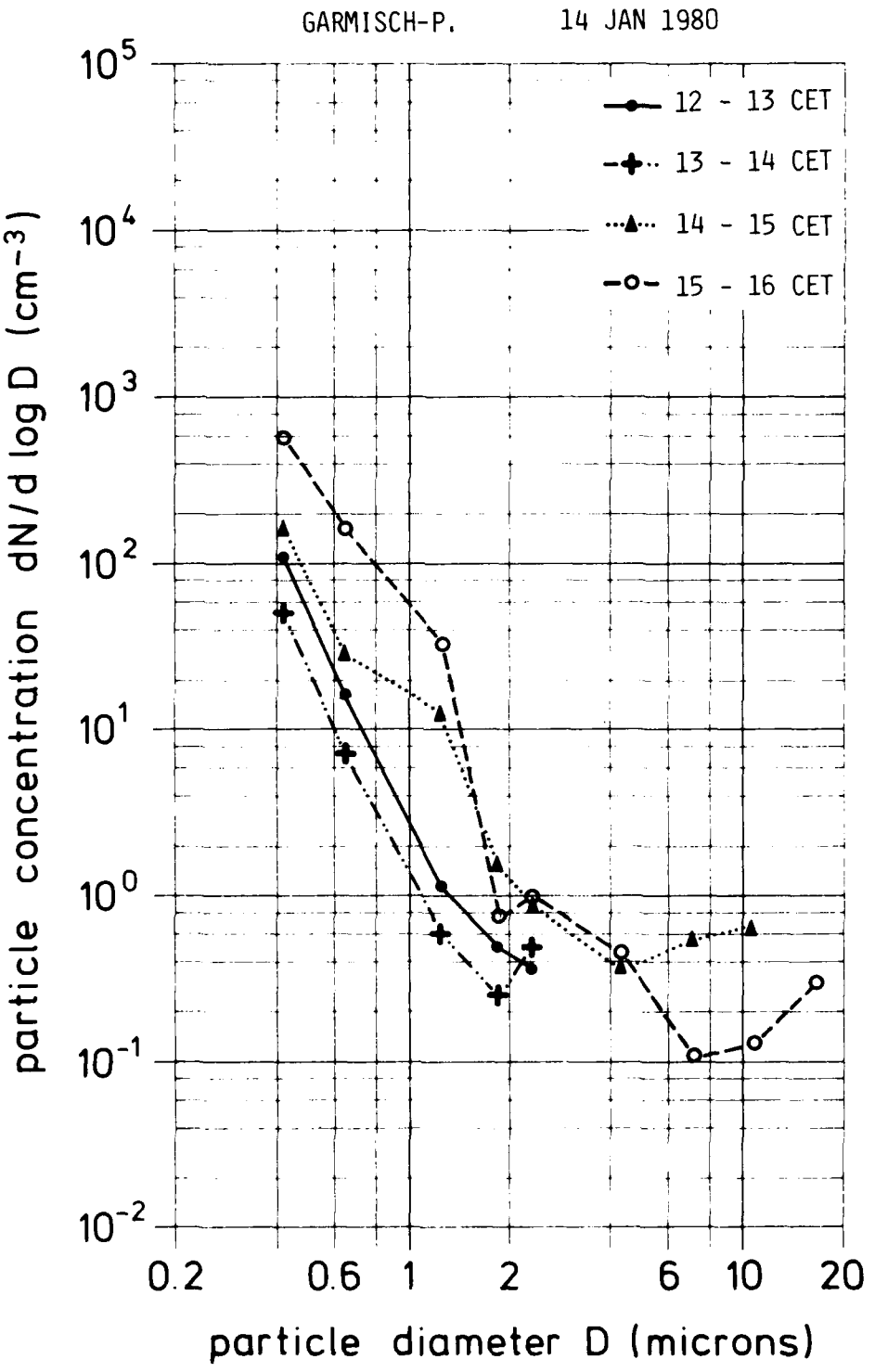
GARMISCH-P. 14 JAN 1980
12 - 13 CET
13 - 14 CET
14 - 15 CET
15 - 16 CET
particle concentration dN/d log D (cm⁻³)
10⁵
10⁴
10³
10²
10¹
10⁰
10⁻¹
10⁻²
0.2
0.6
1
2
6
10
20
particle diameter D (microns)

Fig. 14

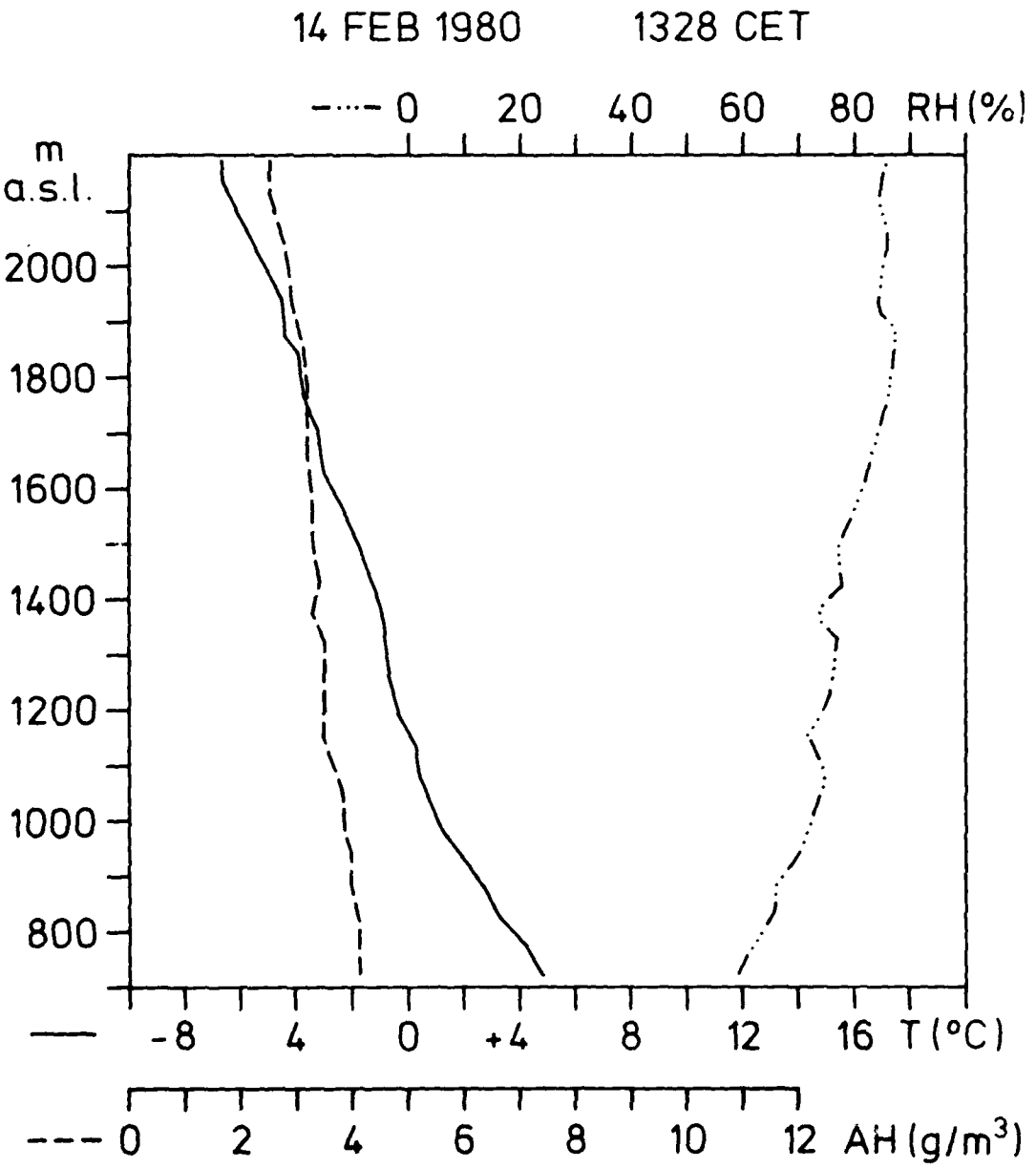
14 FEB 1980 1328 CET
0 20 40 60 80 RH (%)
m a.s.l.
2000
1800
1600
1400
1200
1000
800
-8 4 0 +4 8 12 16 T (°C)
0 2 4 6 8 10 12 AH (g/m³)

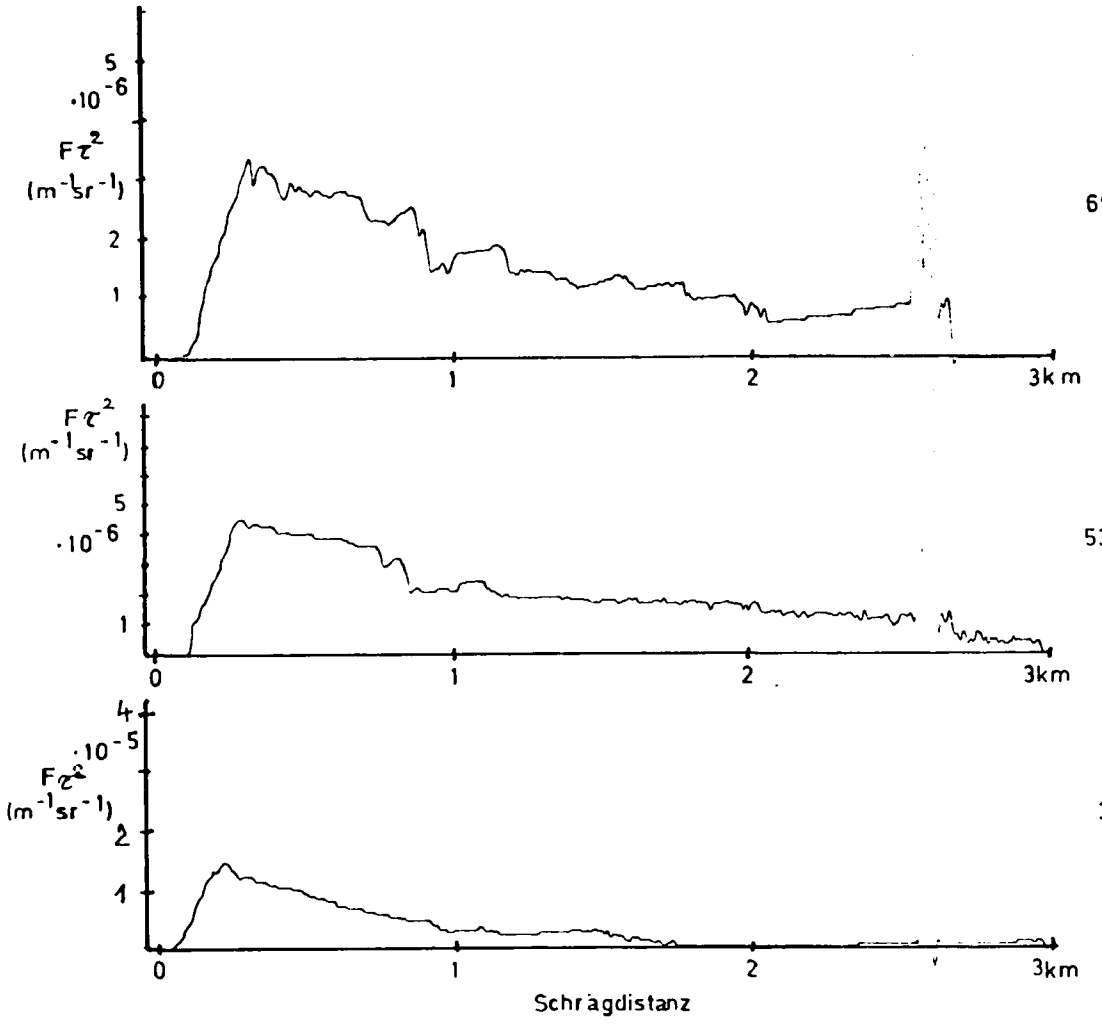

Datum:

14. Feb. 1980

Uhrzeit:

08.30 MEZ

Fig. 15

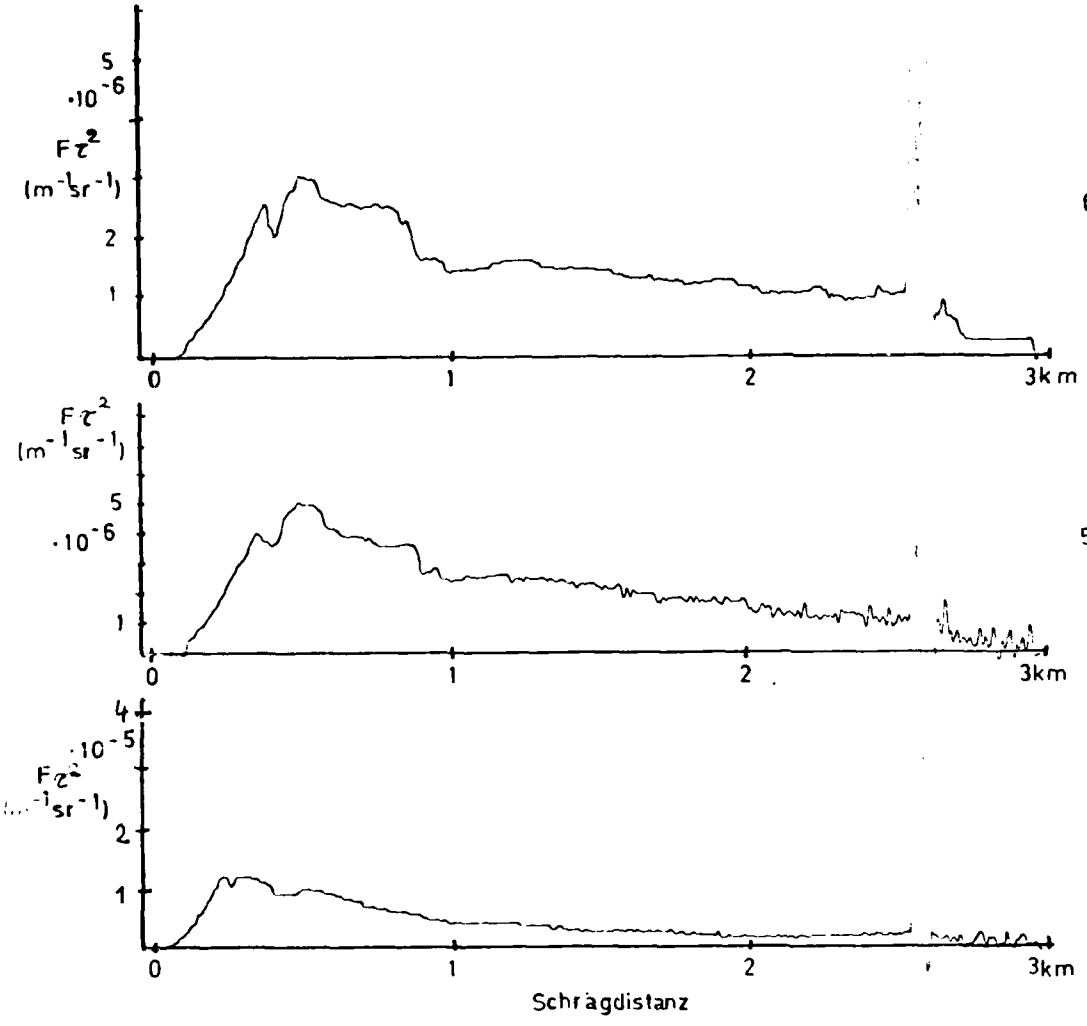

Datum:

14. Feb. 1980

Uhrzeit:

0900 MEZ

Fig. 16

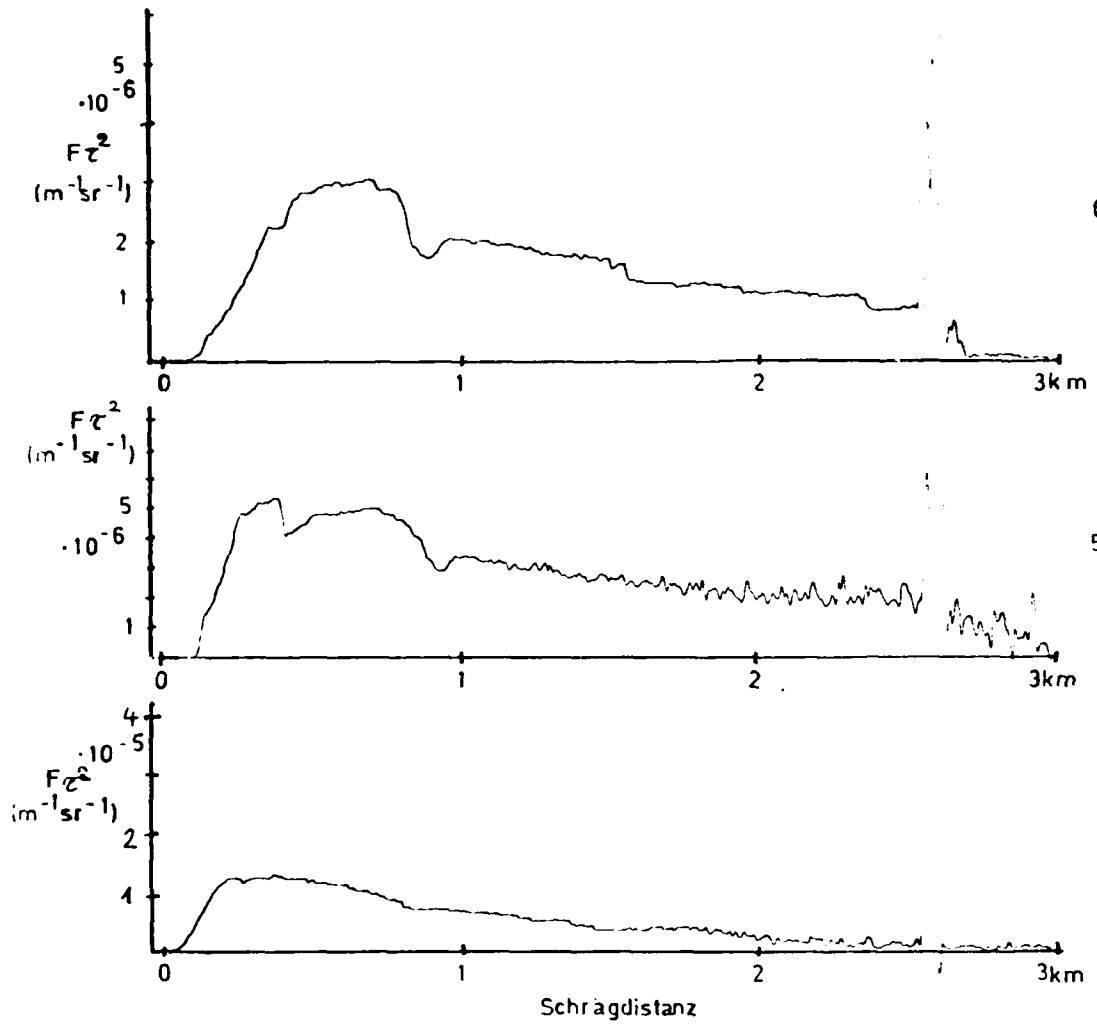

Datum:

14. Feb. 1980

Uhrzeit:

0925 MEZ

Fig. 17

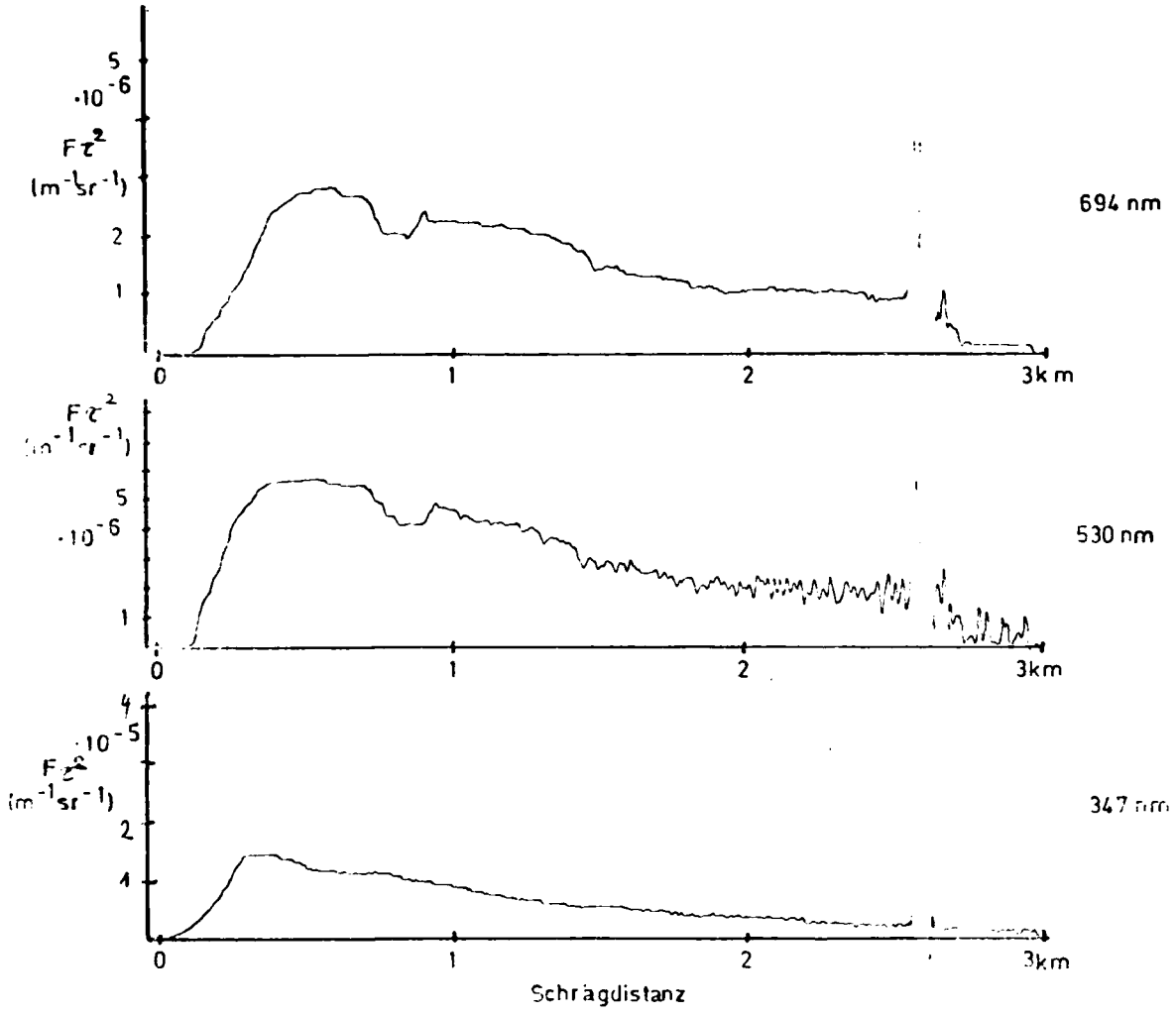

Datum:

14. Feb. 1980

Uhrzeit:

1000 MEZ

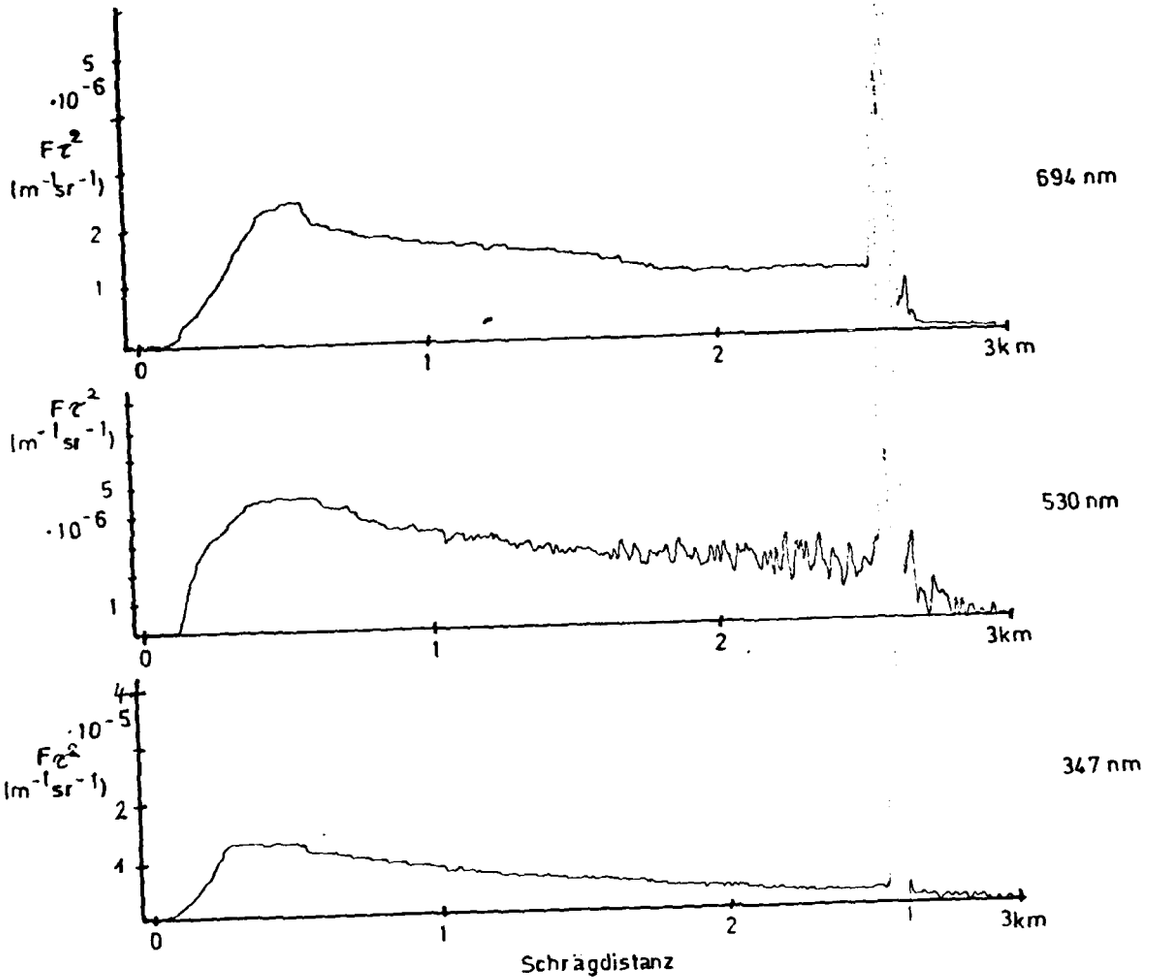

Datum:

14. Feb. 1980

Uhrzeit:

10.40 MEZ

Fig. 19

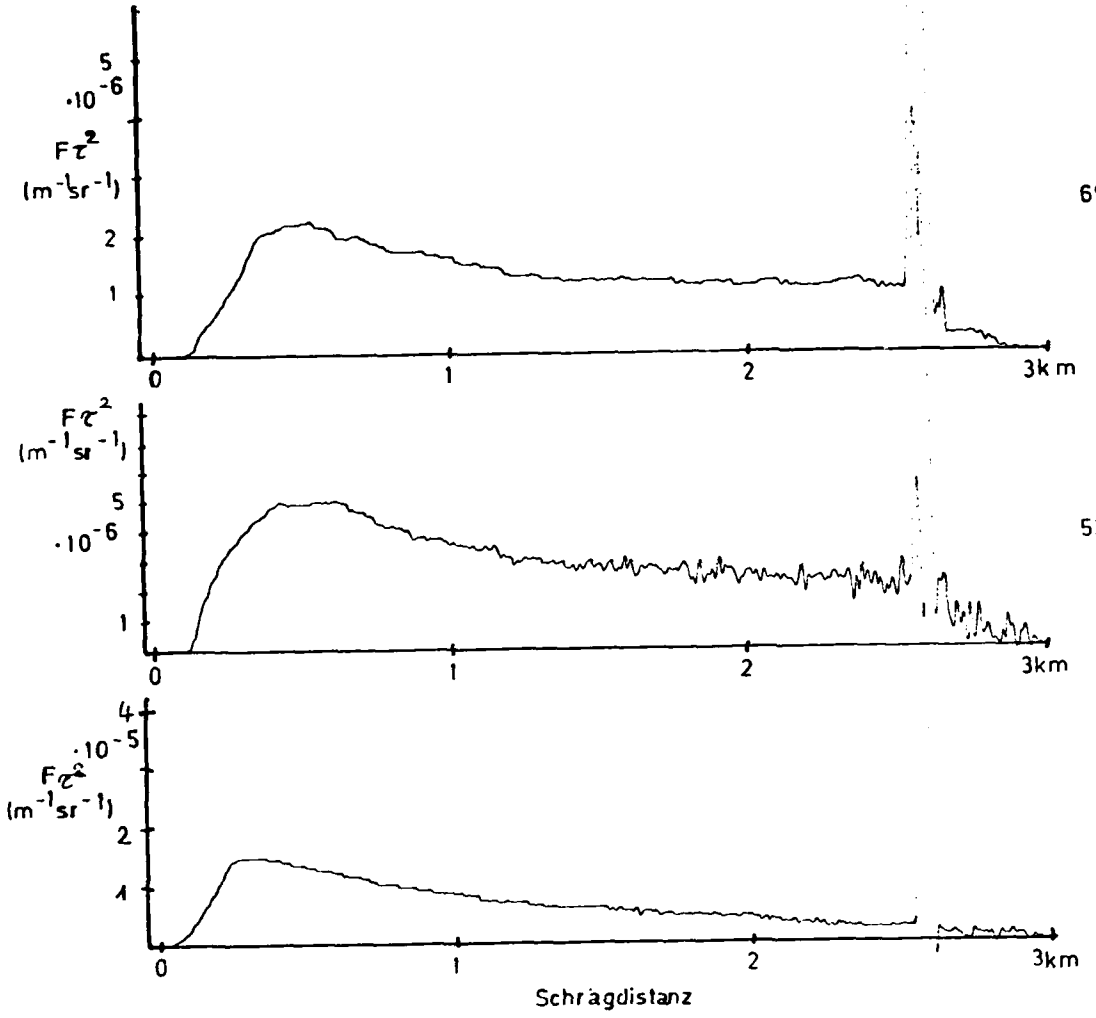

Datum:

14. Feb. 1980

Uhrzeit:

11.00 MEZ

Fig. 20

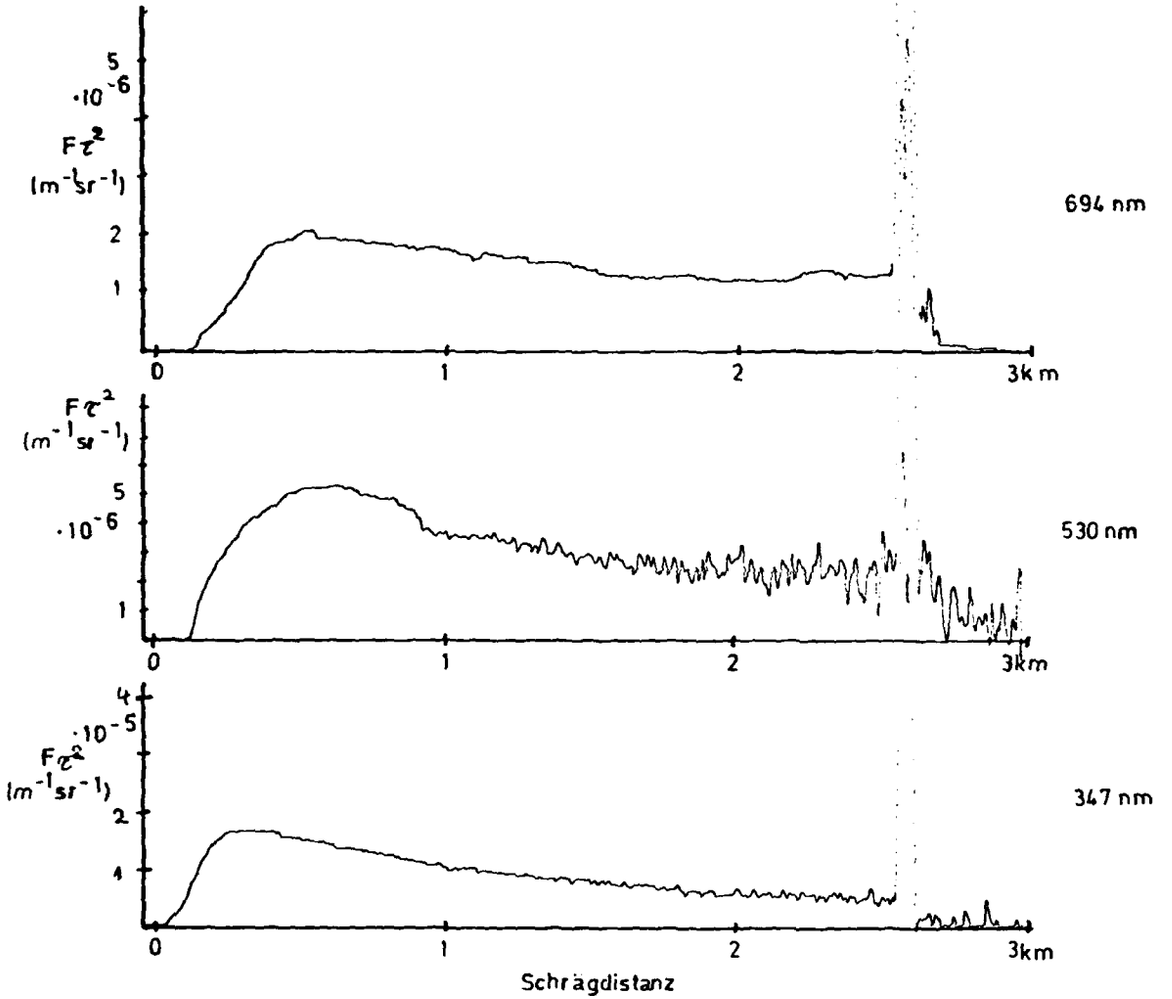

Datum:

14. Feb. 1980

Uhrzeit:

1130 MEZ

Fig. 21

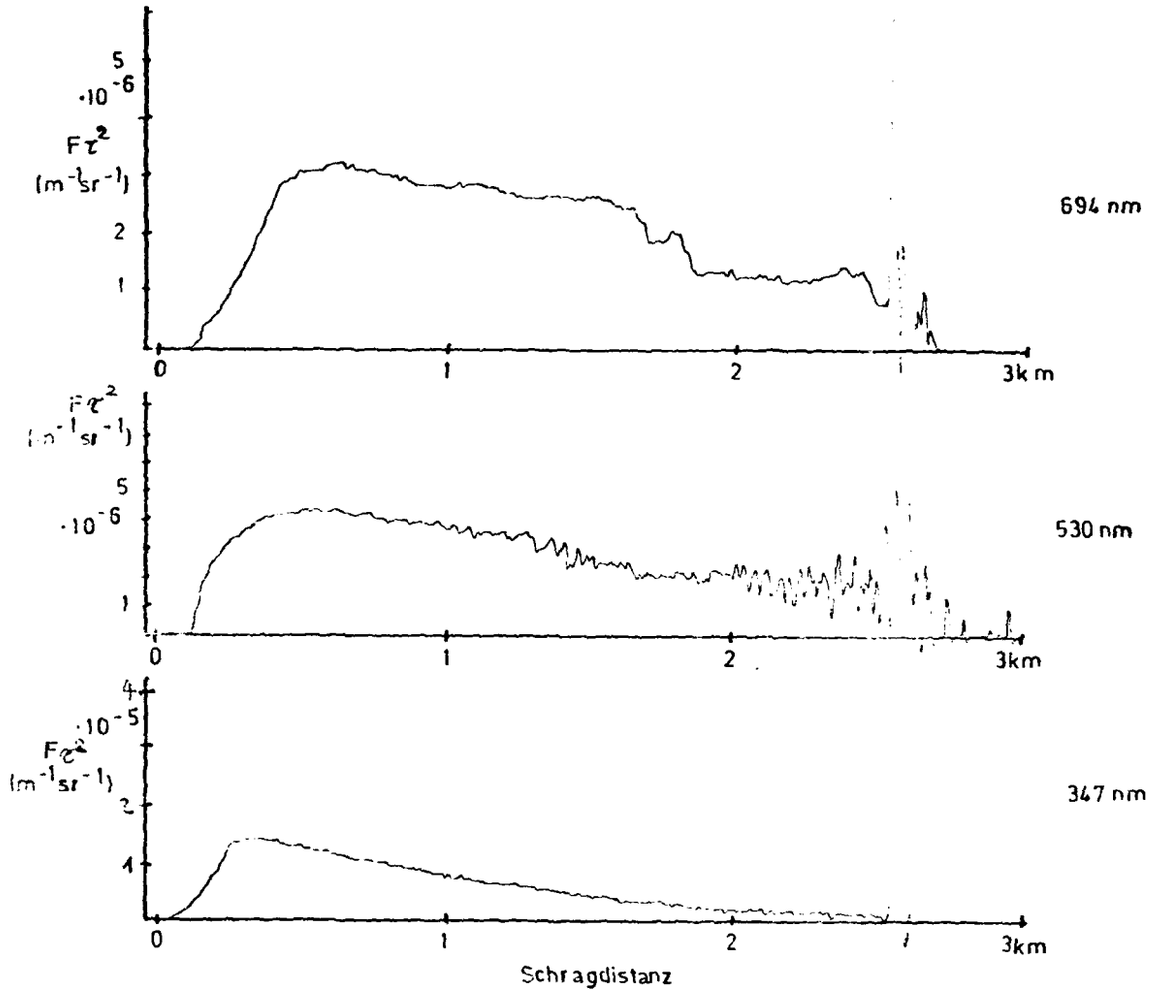

Datum:

14. Feb. 1980

Uhrzeit:

1400 MEZ

Fig. 22

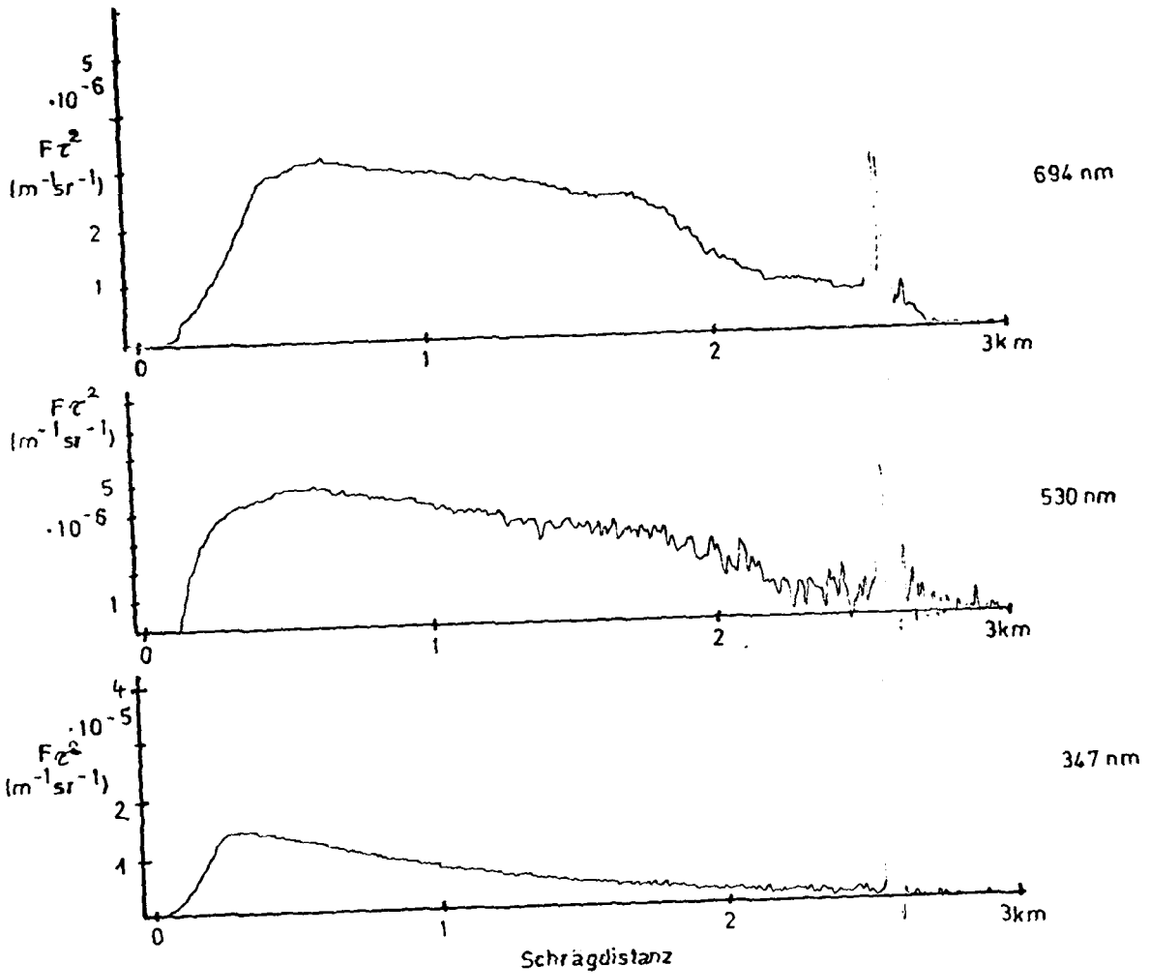

Datum:

14. Feb. 1980

Uhrzeit:

14,30 MEZ

Fig. 23

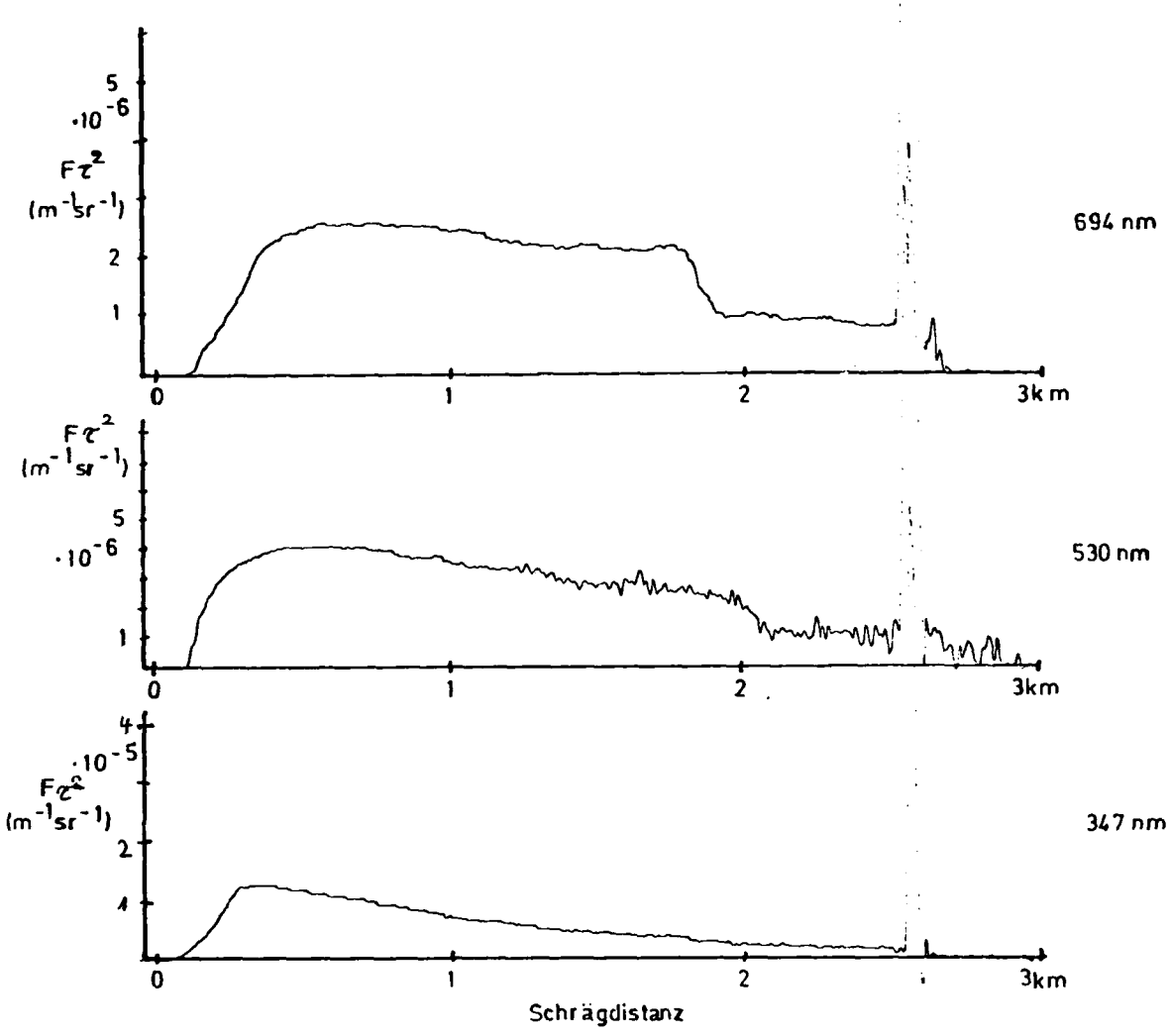

Datum:

14. Feb. 1980

Uhrzeit:

14.55 MEZ

Fig. 24

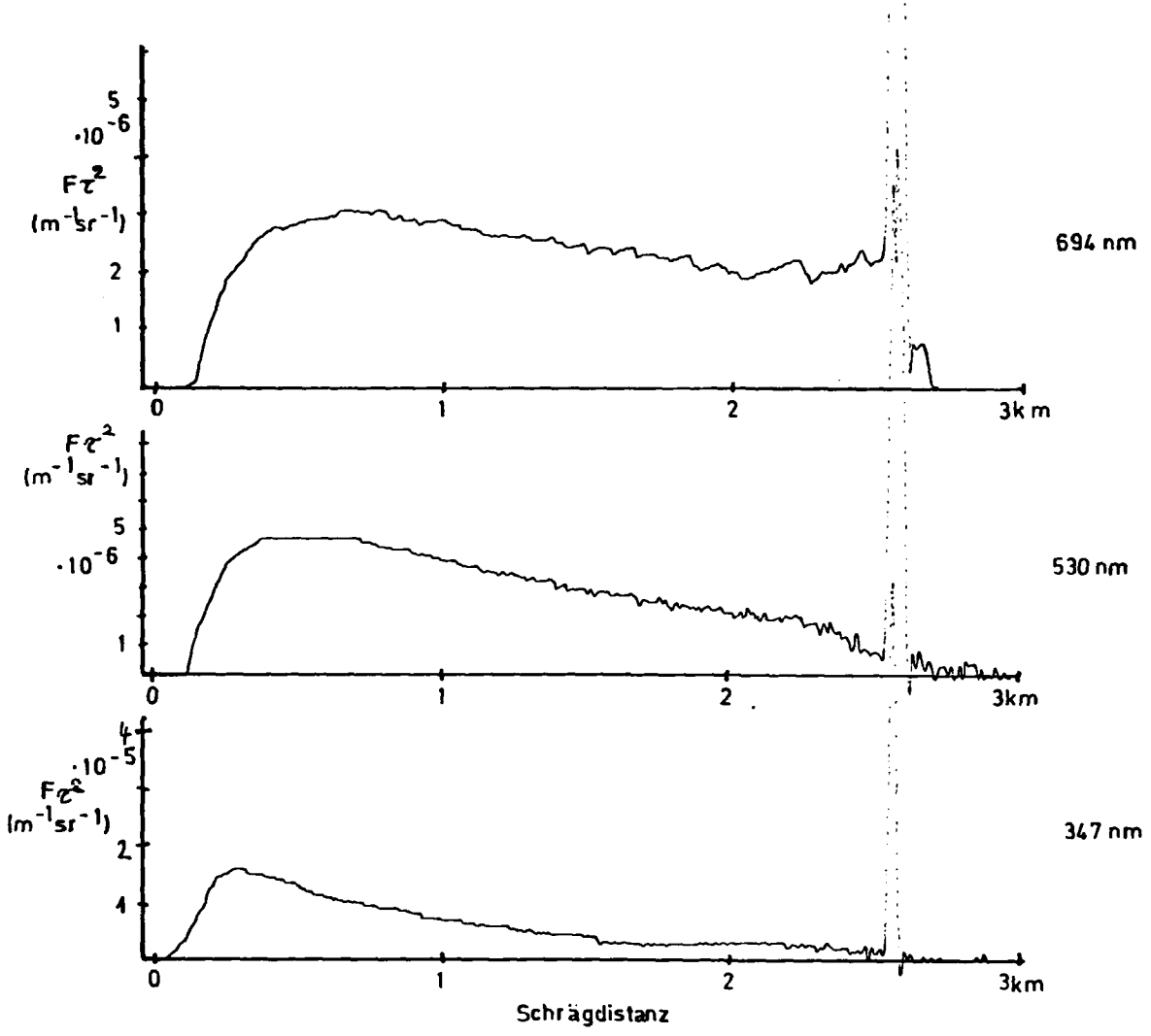

Datum:

14. Feb. 1980

Uhrzeit:

16.00 MEZ

Fig. 25

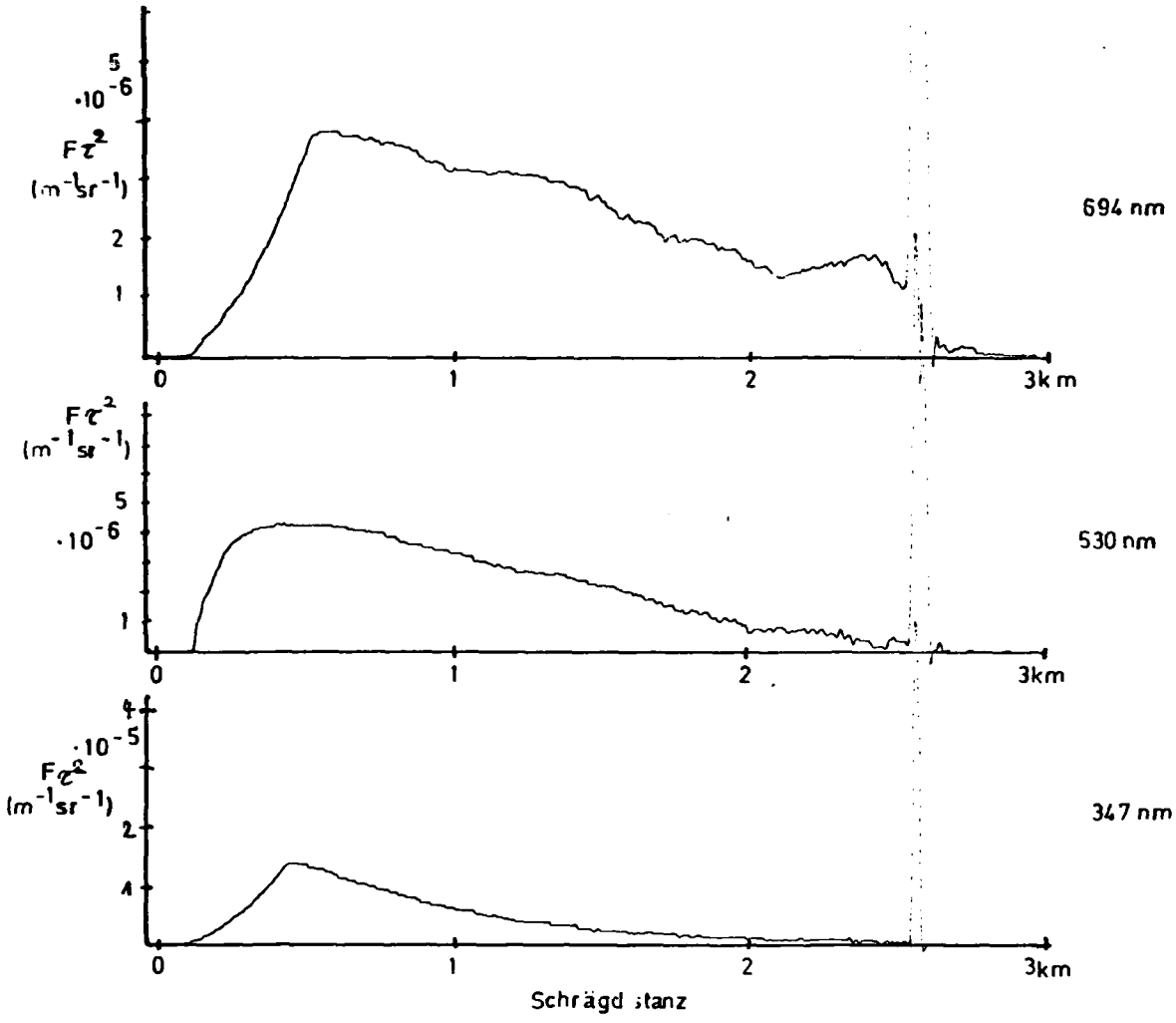

Datum:

14. Feb. 1980

Uhrzeit:

16.30 MEZ

Fig. 26

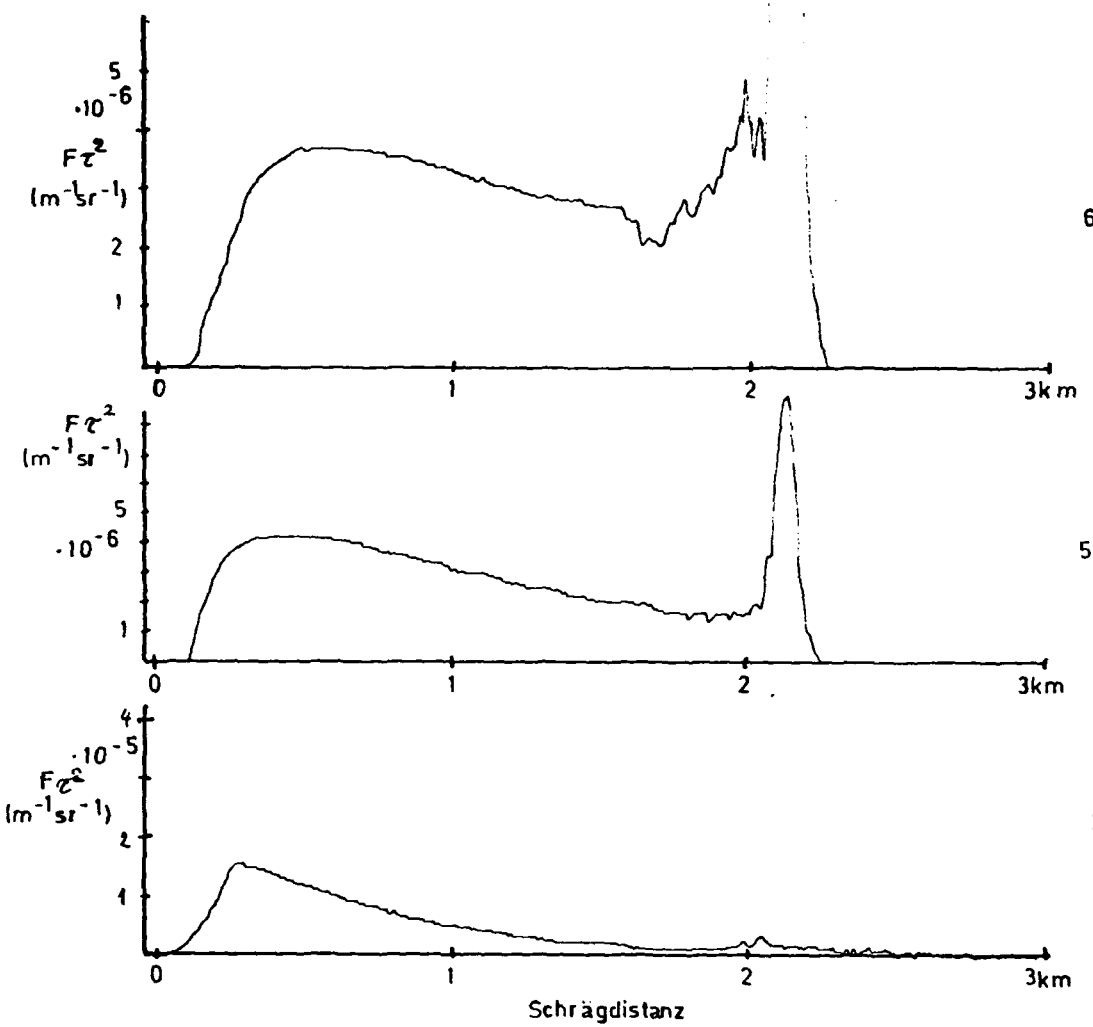

Datum:

14. Feb. 1980

Uhrzeit:

17.00 MEZ

Fig. 27

Fig. 28

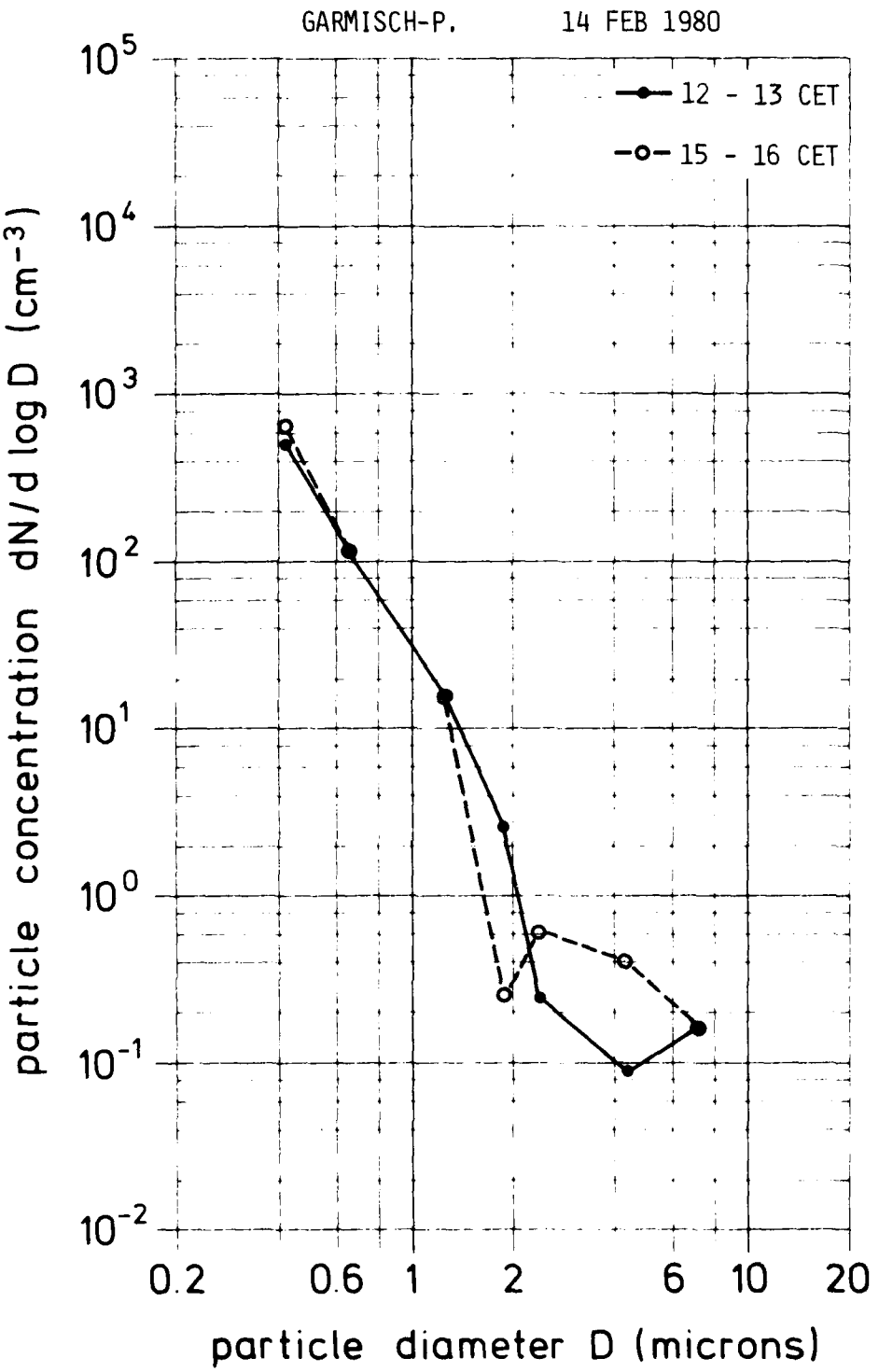
GARMISCH-P. 14 FEB 1980
12 - 13 CET
15 - 16 CET
particle concentration dN/d log D (cm⁻³)
10⁵
10⁴
10³
10²
10¹
10⁰
10⁻¹
10⁻²
0.2
0.6
1
2
6
10
20
particle diameter D (microns)

Fig. 29

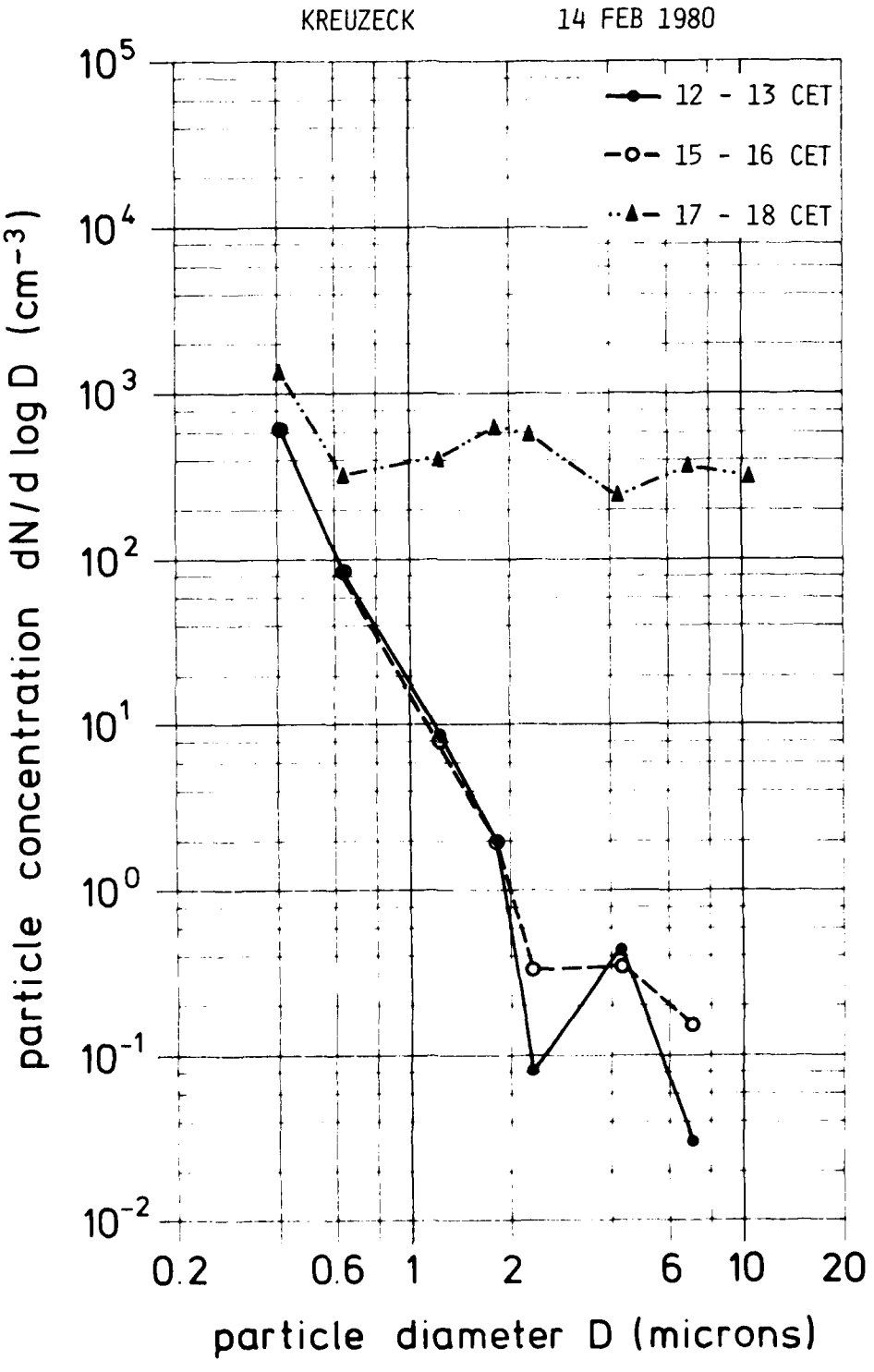
KREUZECK
14 FEB 1980
12 - 13 CET
15 - 16 CET
17 - 18 CET
particle concentration dN/d log D (cm⁻³)
10⁵
10⁴
10³
10²
10¹
10⁰
10⁻¹
10⁻²
0.2
0.6
1
2
6
10
20
particle diameter D (microns)

Fig. 30

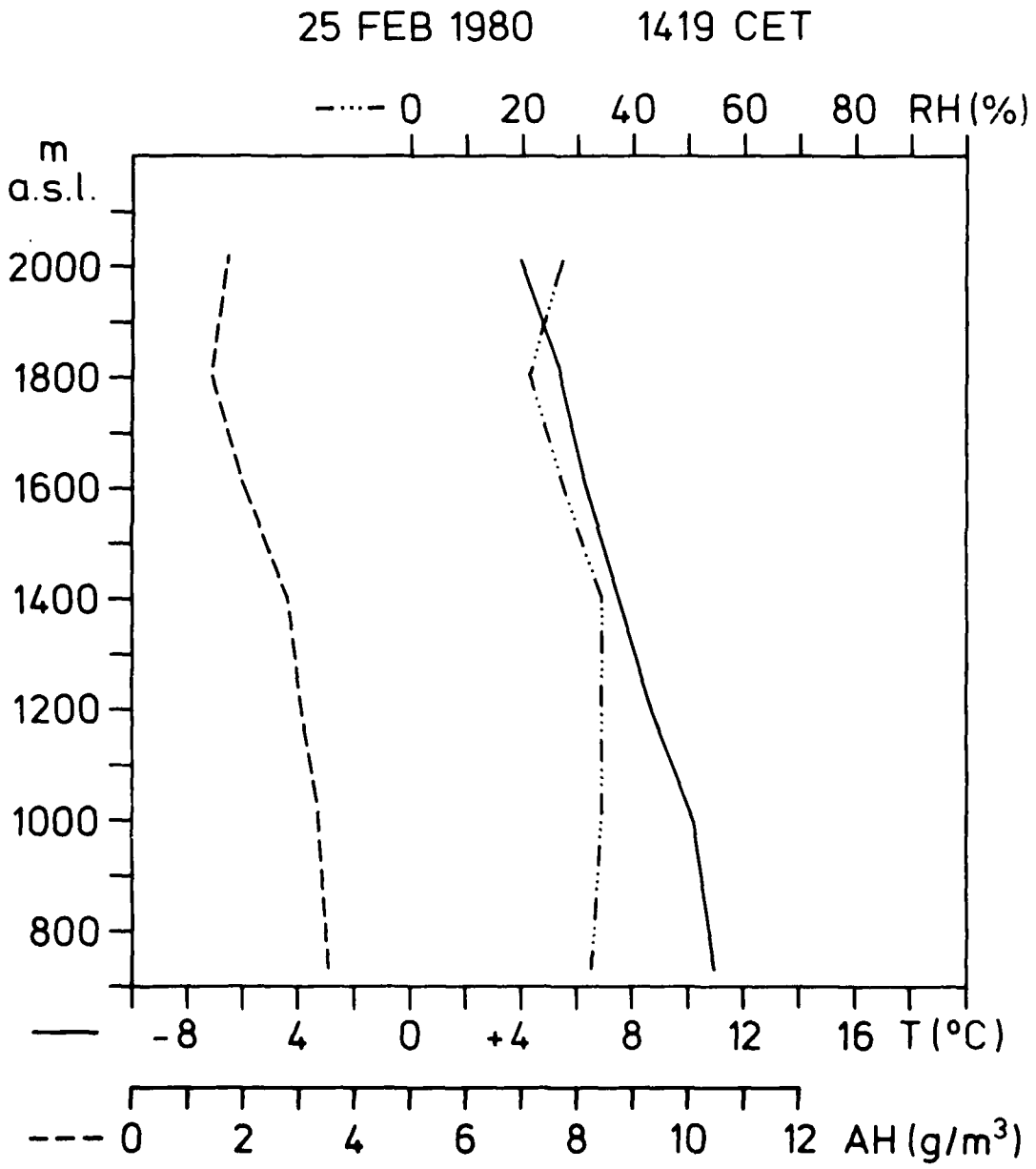
25 FEB 1980 1419 CET
0 20 40 60 80 RH(%)
m
a.s.l.
2000
1800
1600
1400
1200
1000
800
-8 4 0 +4 8 12 16 T(°C)
0 2 4 6 8 10 12 AH(g/m³)

Fig. 31

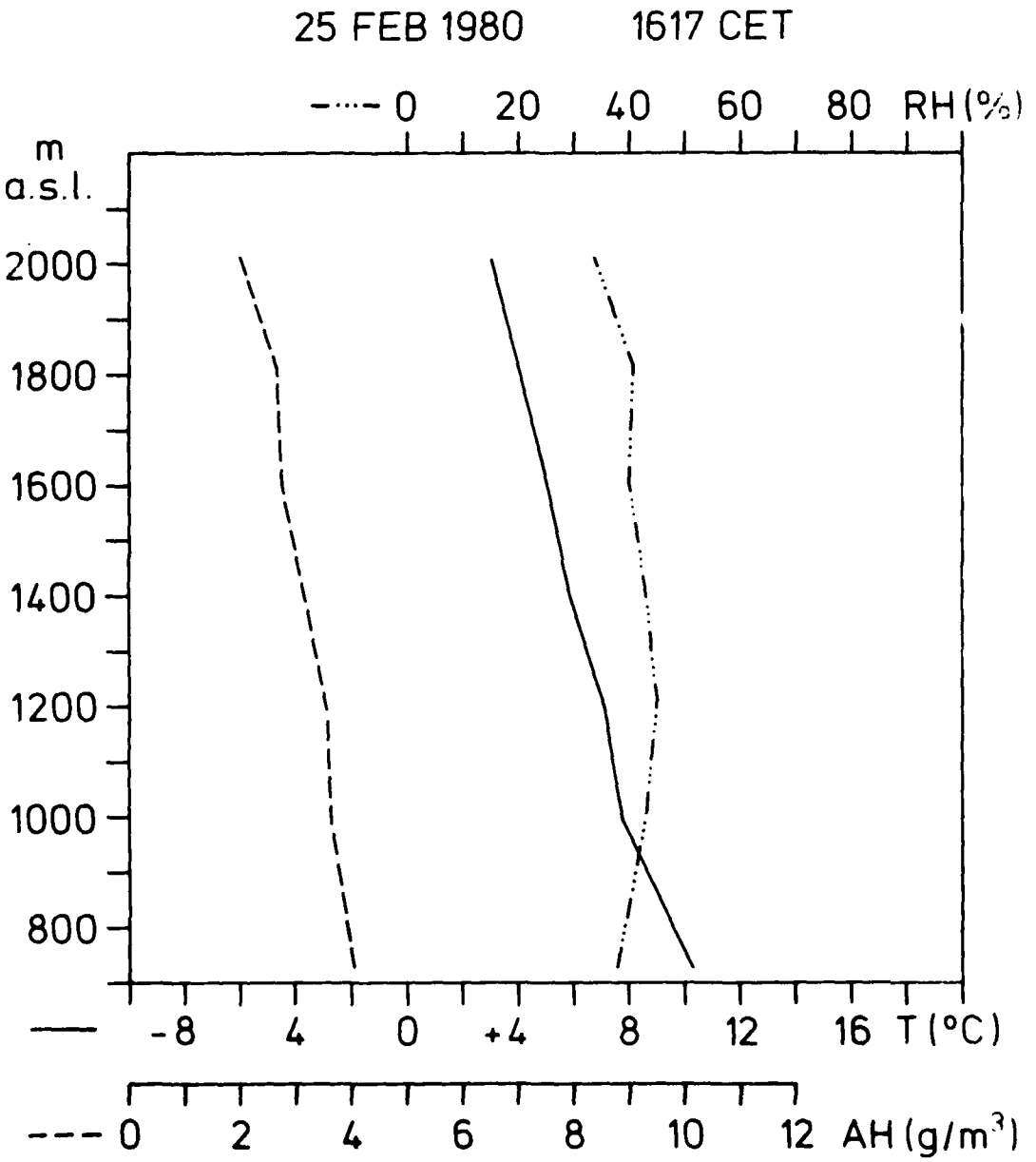
25 FEB 1980 1617 CET
0 20 40 60 80 RH (%)
m a.s.l.
2000
1800
1600
1400
1200
1000
800
-8 4 0 +4 8 12 16 T (°C)
0 2 4 6 8 10 12 AH (g/m³)

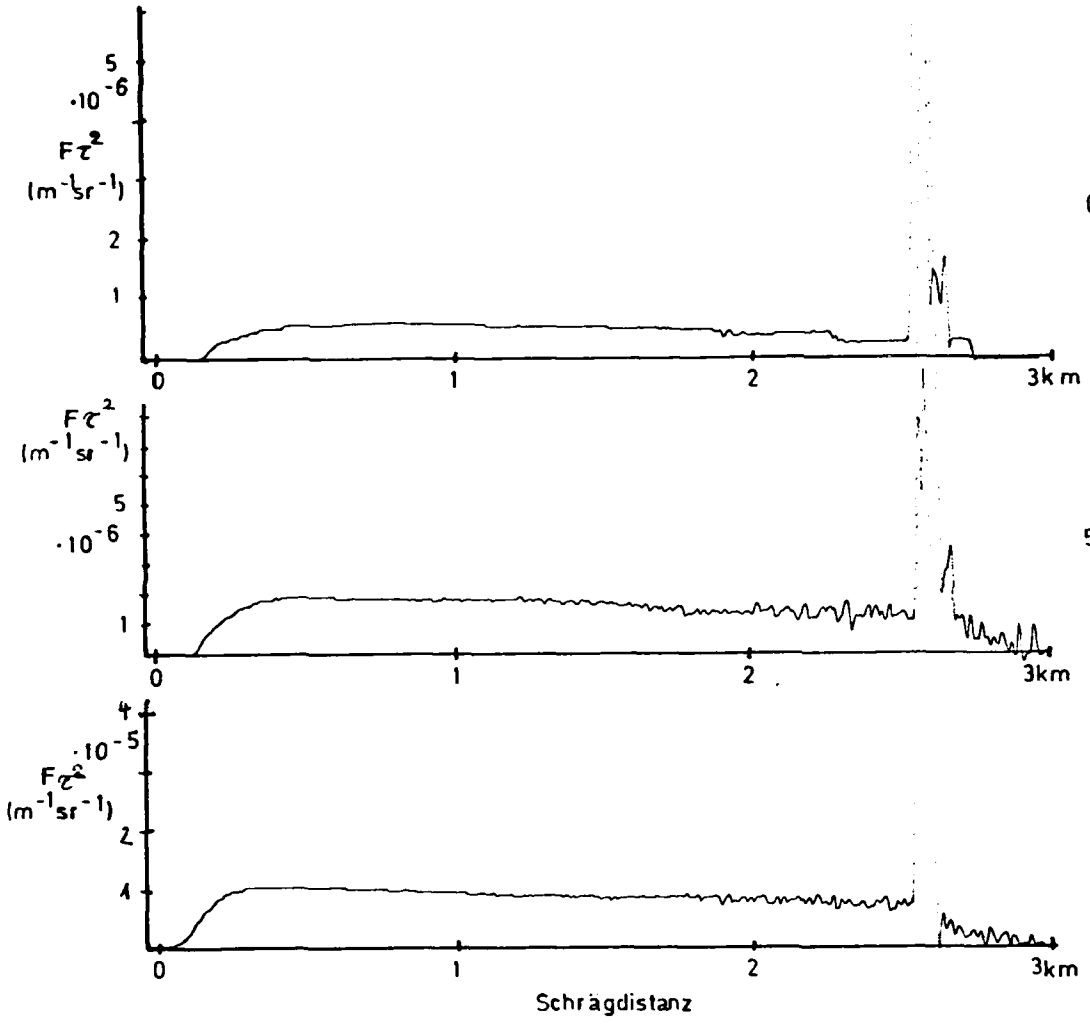

Datum:

25. Feb. 1980

Uhrzeit:

10.00

~~0900~~ MEZ

Fig. 32

Fig. 33

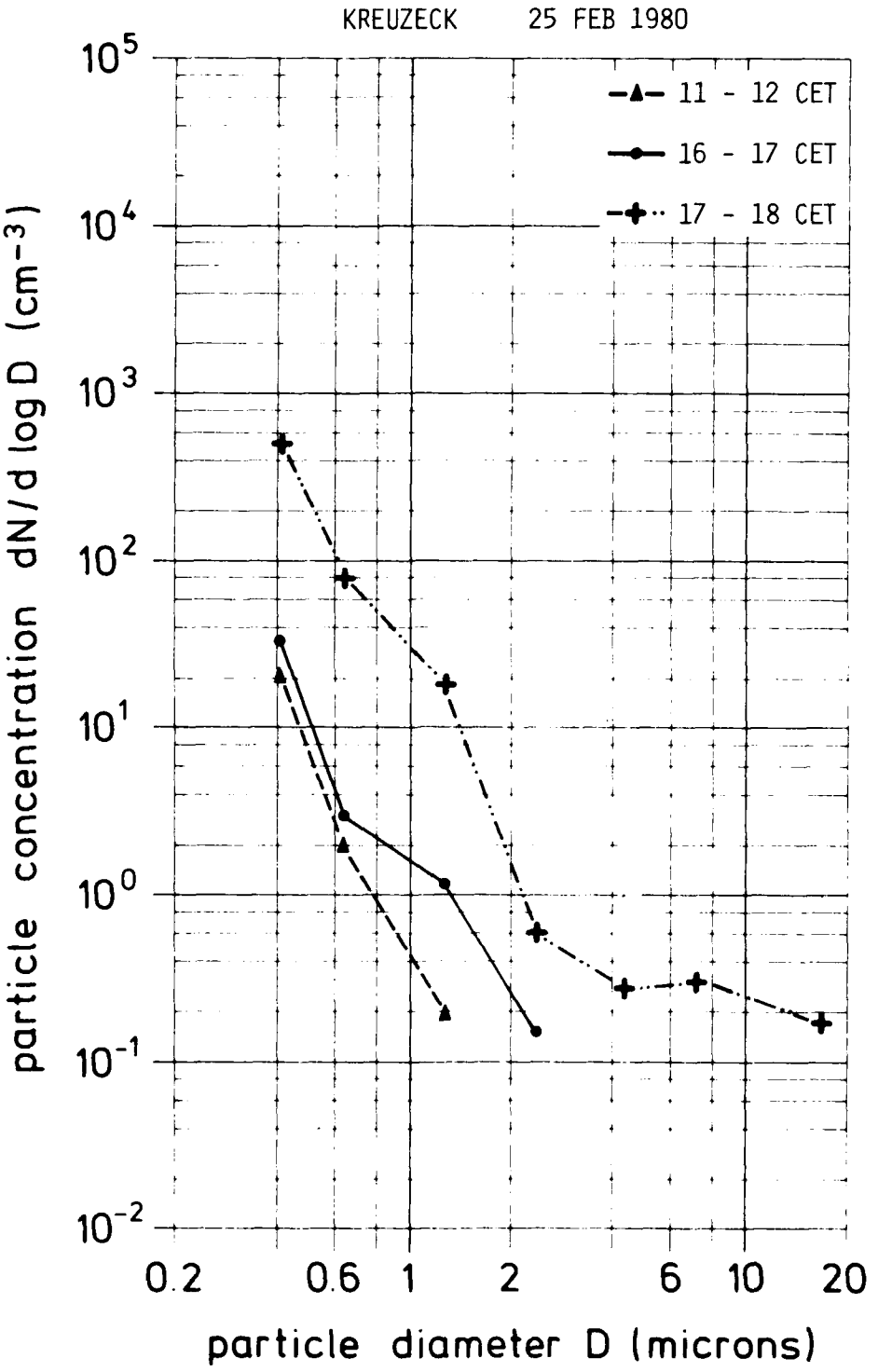
KREUZECK 25 FEB 1980
11 - 12 CET
16 - 17 CET
17 - 18 CET
particle concentration dN/d log D (cm⁻³)
10⁵
10⁴
10³
10²
10¹
10⁰
10⁻¹
10⁻²
0.2
0.6
1
2
6
10
20
particle diameter D (microns)

Fig. 34

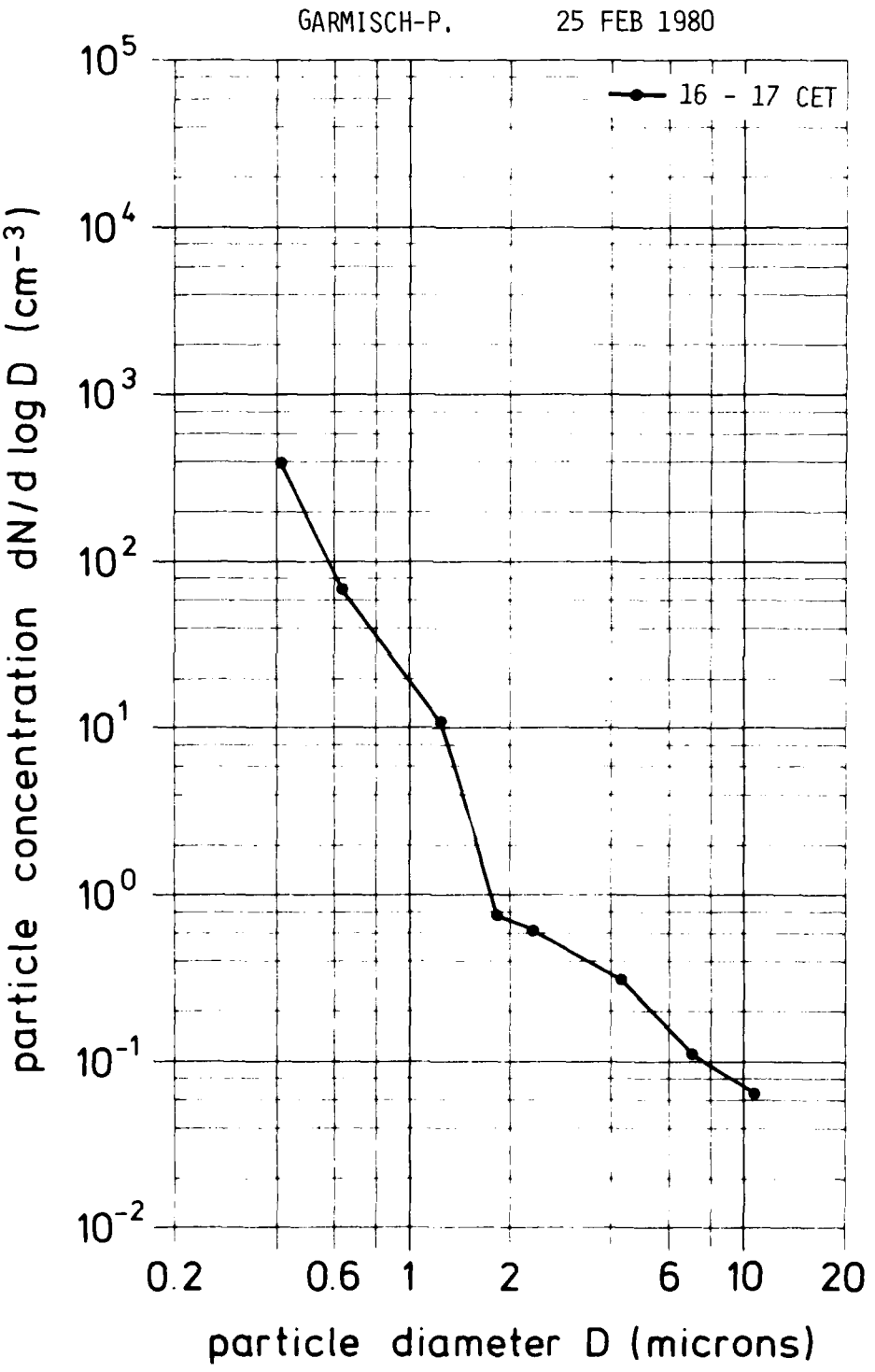
GARMISCH-P. 25 FEB 1980
16 - 17 CET
particle concentration dN/d log D (cm⁻³)
10⁵
10⁴
10³
10²
10¹
10⁰
10⁻¹
10⁻²
0.2
0.6
1
2
6
10
20
particle diameter D (microns)

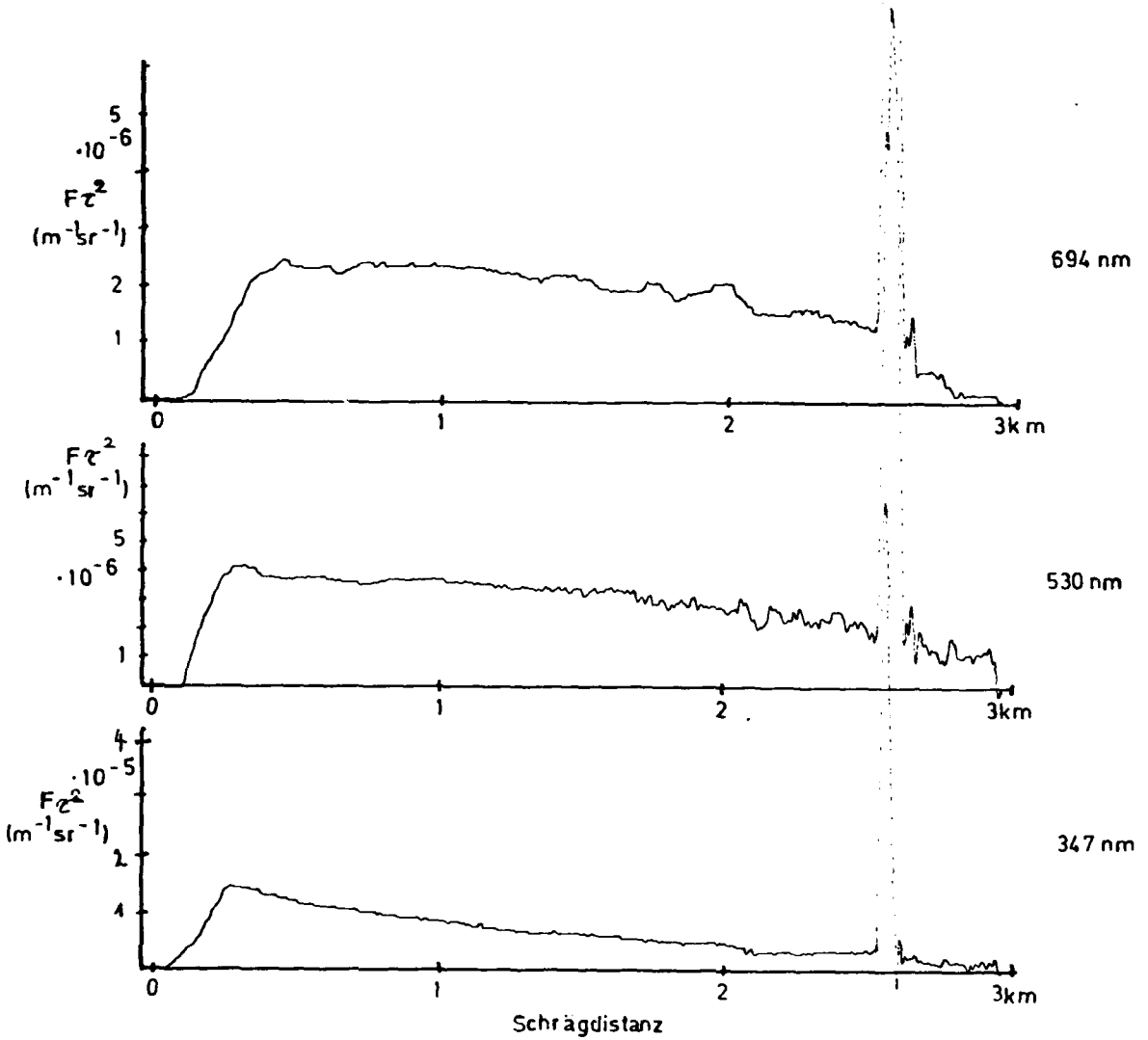

Datum:
28. Feb. 1980

Uhrzeit:

08.55 MEZ

Fig. 35

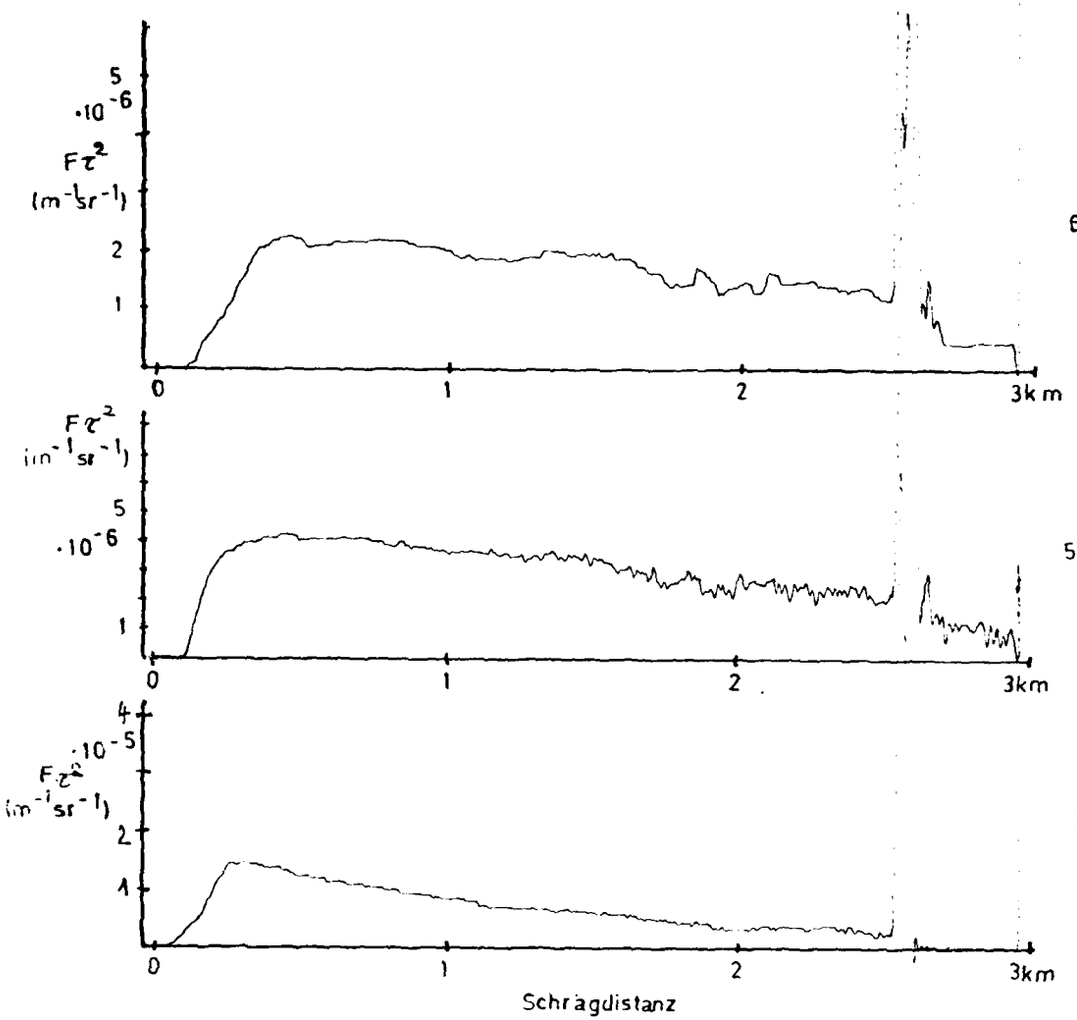

Datum:

28. Feb. 1980

Uhrzeit:

09.25 MEZ

Fig. 36

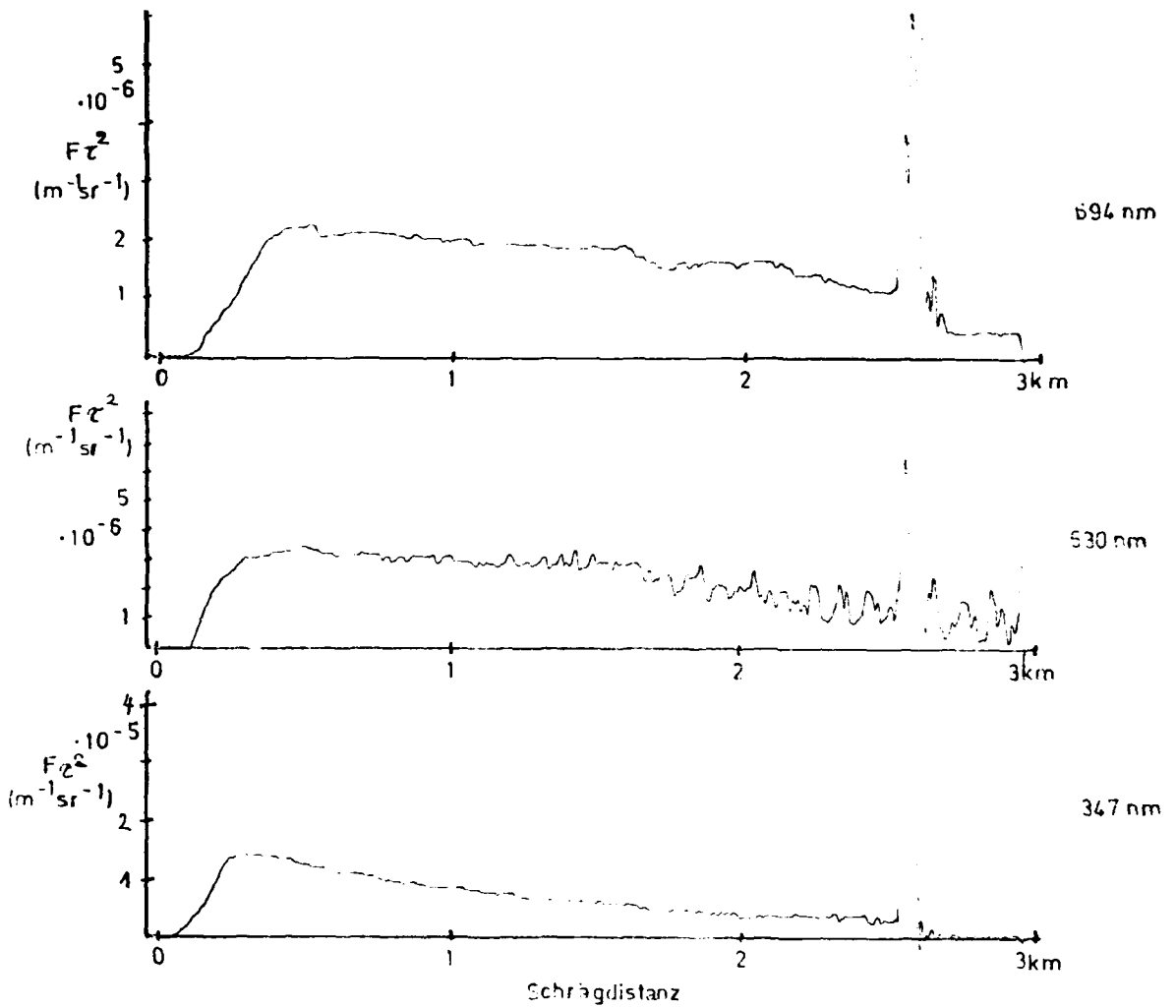

Datum:

28. Feb. 1980

Uhrzeit:

1000 MEZ

Fig. 37

AD-A096 723 FRAUNHOFER-GESELLSCHAFT GARMISCH-PARTENKIRCHEN (GERMA--ETC F/G 4/1
SLANT PATH LOW VISIBILITY ATMOSPHERIC CONDITIONS.(U)
SEP 80 R REITER, W CARNUTH, R SLADKOVIC DA-ERO-77-G-064

UNCLASSIFIED NL

2 OF 2
AD A096 723

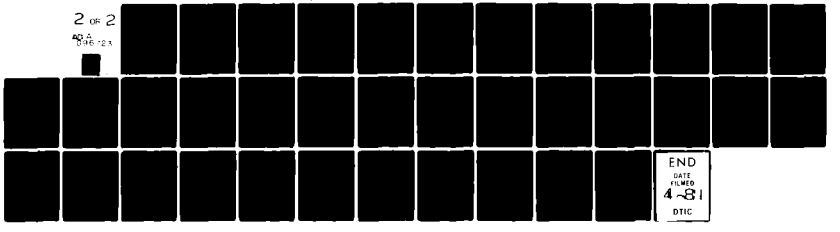

END
DATE FILMED
4-81
DTIC

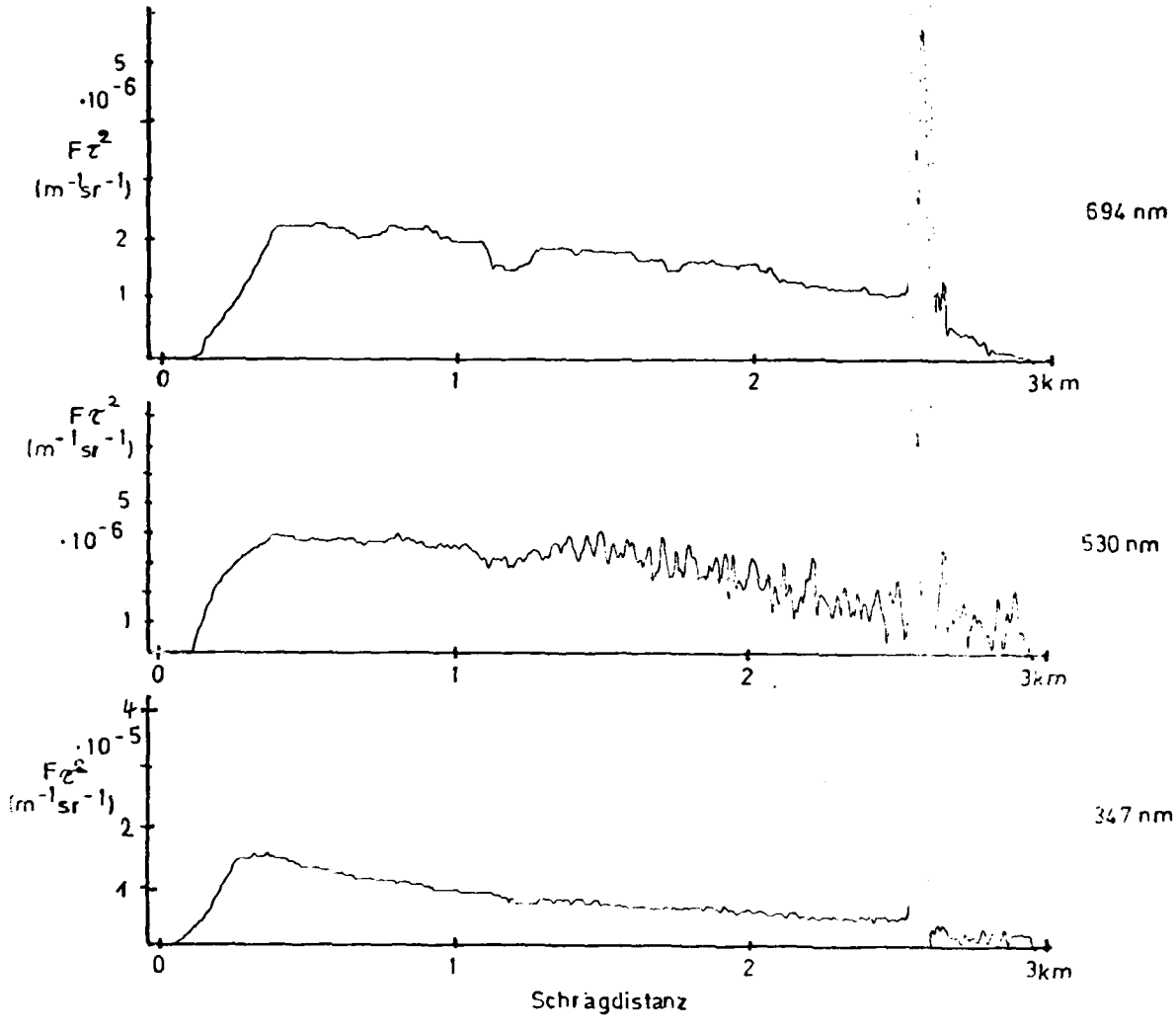

Datum:

28. Feb. 1980

Uhrzeit:

1030 MEZ

fig. 38

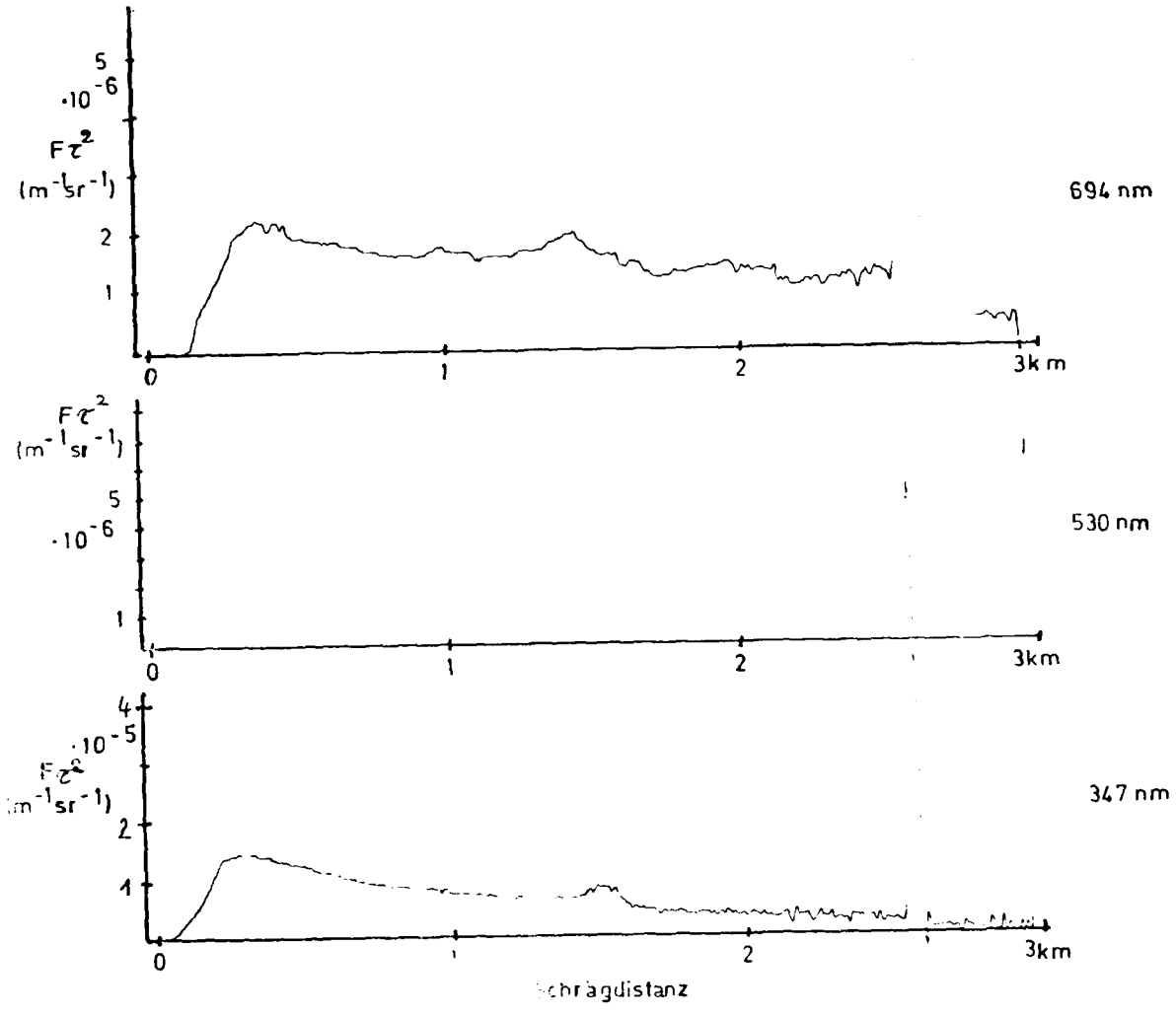

Datum:

28. Feb. 1980

Uhrzeit:

11.05 MEZ

Fig. 29

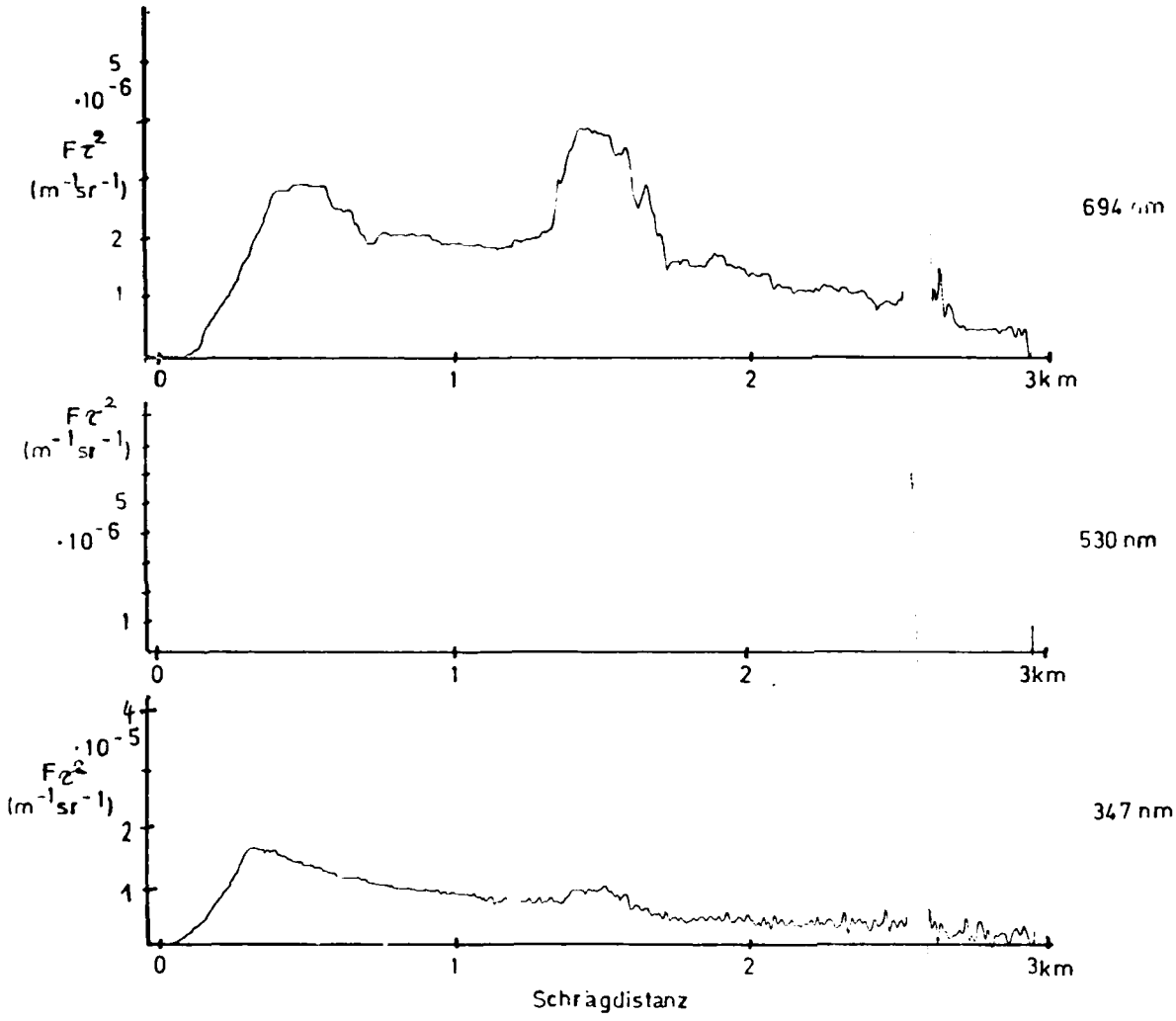

Datum:

28. Feb. 1980

Uhrzeit:

11.15 MEZ

Fig. 40

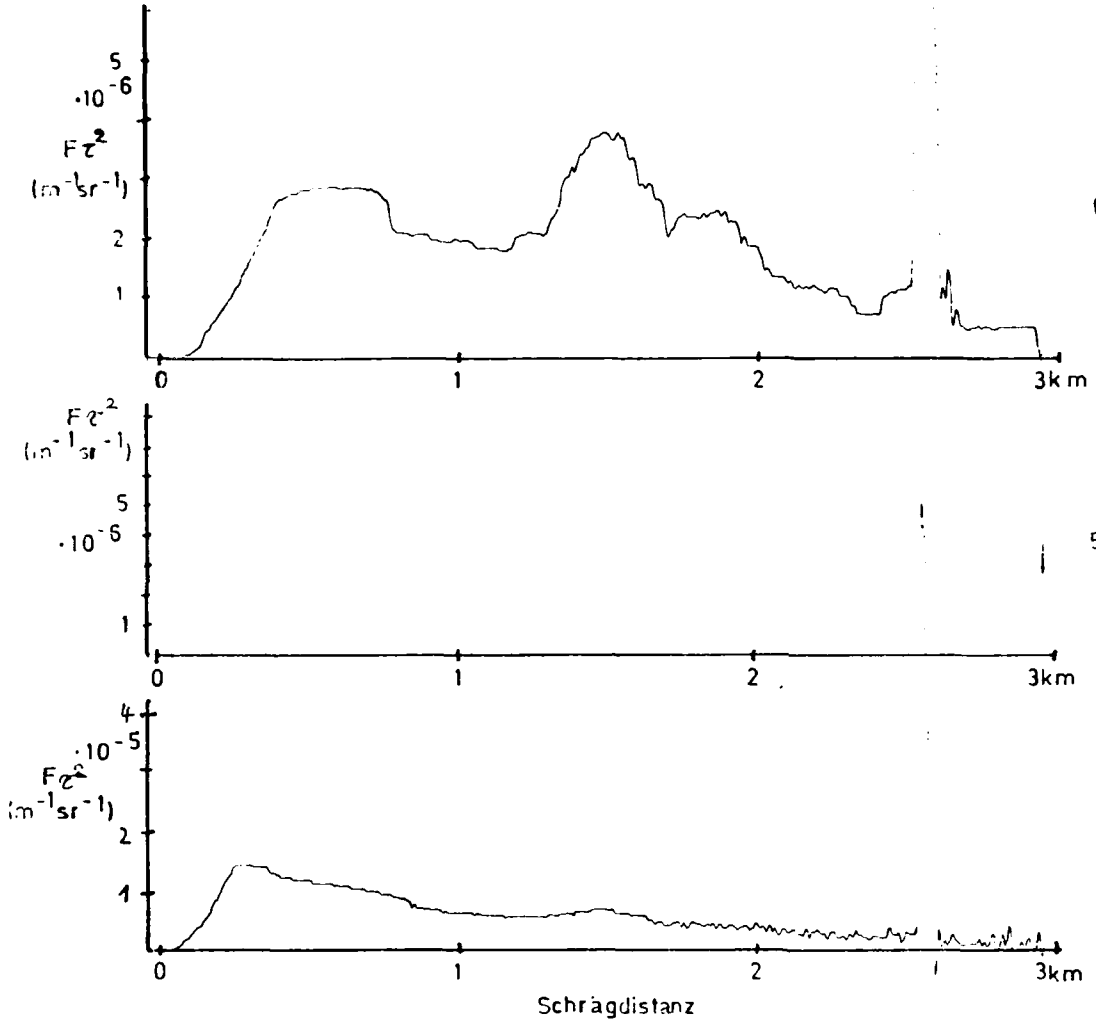

Datum:

28. Feb. 1980

Uhrzeit:

11.40 MEZ

Fig. 4

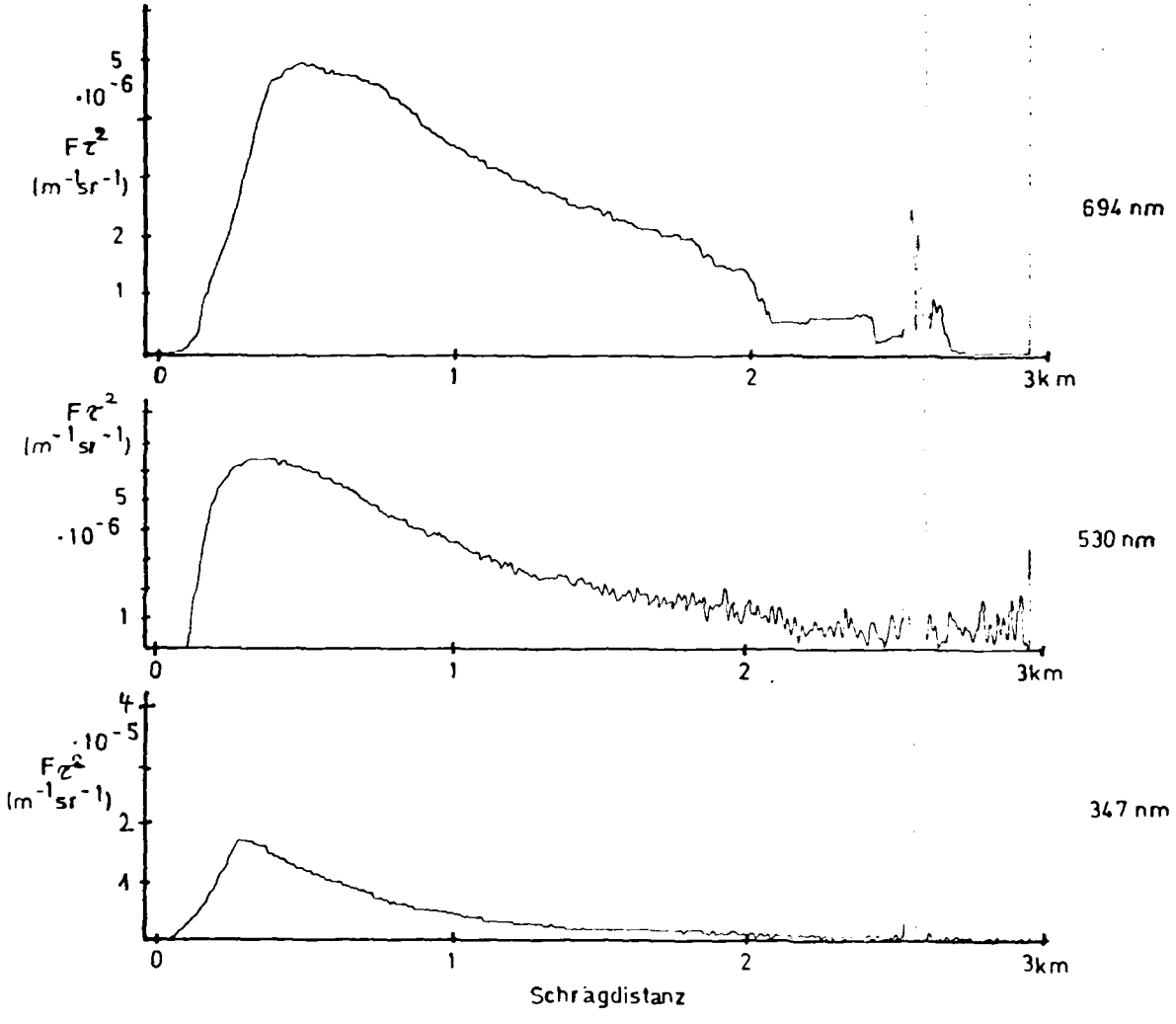

Datum:

28. Feb. 1980

Uhrzeit:

13.46 MEZ

Fig. 42

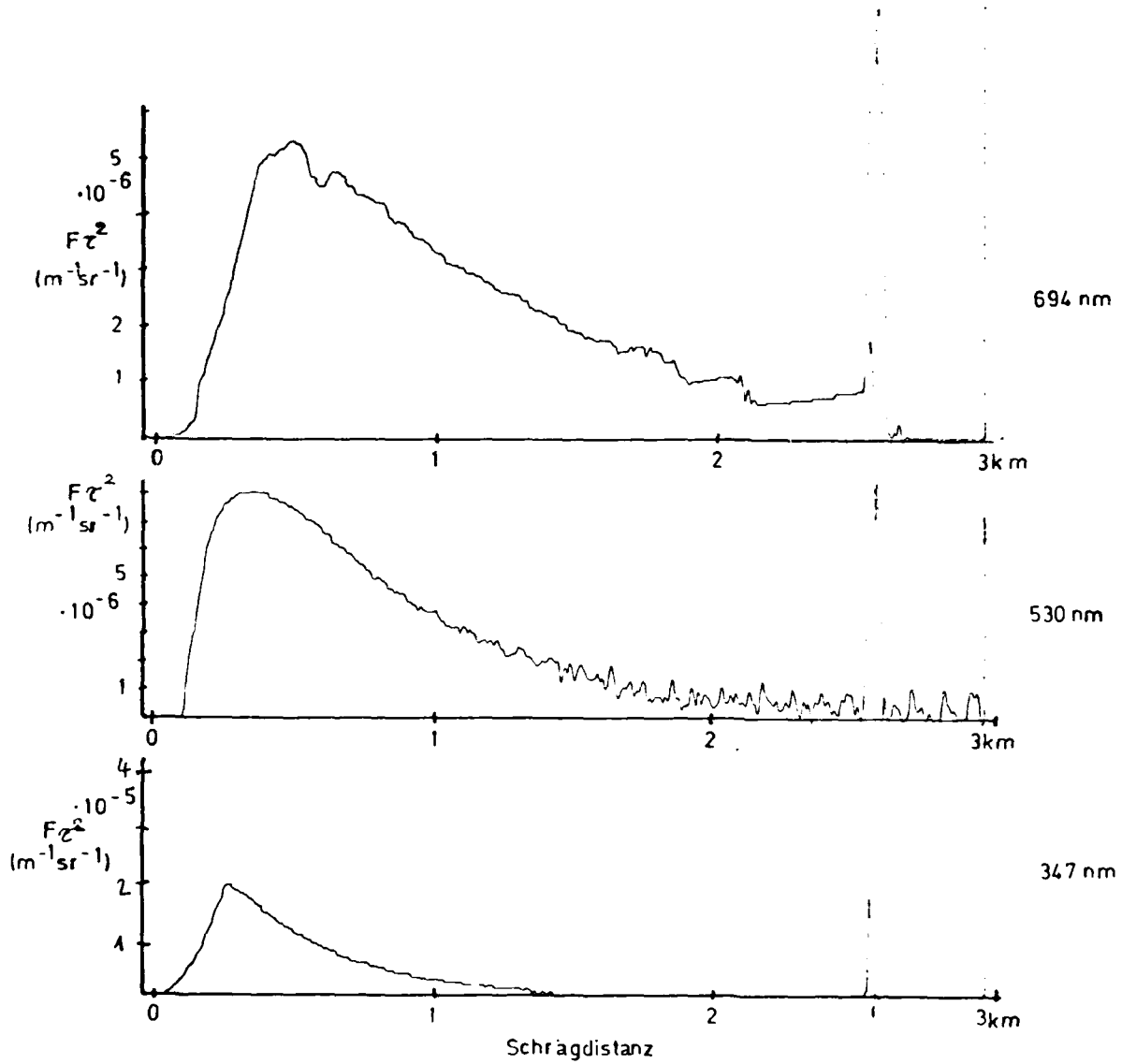

Datum:

28. Feb. 1980

Uhrzeit:

14.30 MEZ

Fig. 43

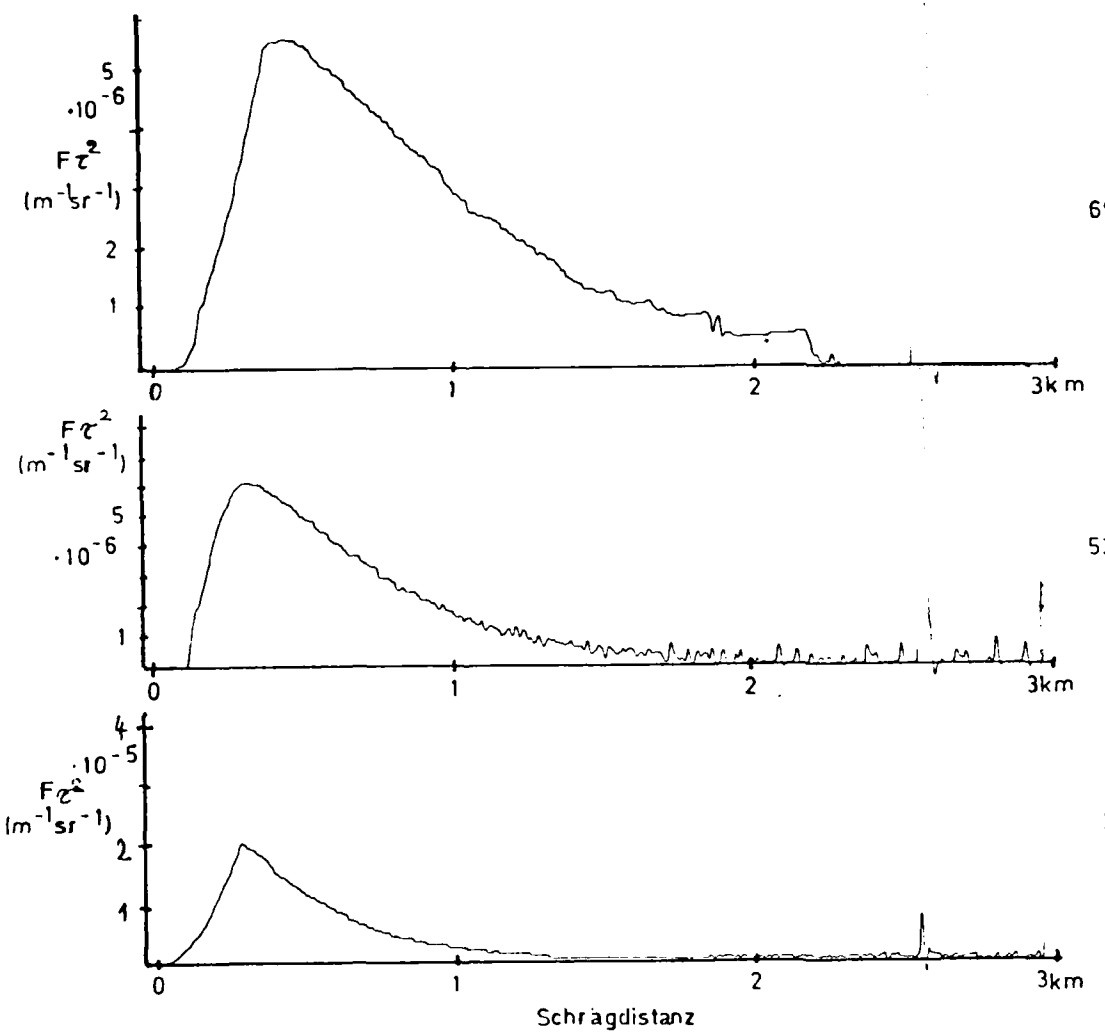

Datum:

28. Feb. 1980

Uhrzeit:

15.08 MEZ

Fig. 44

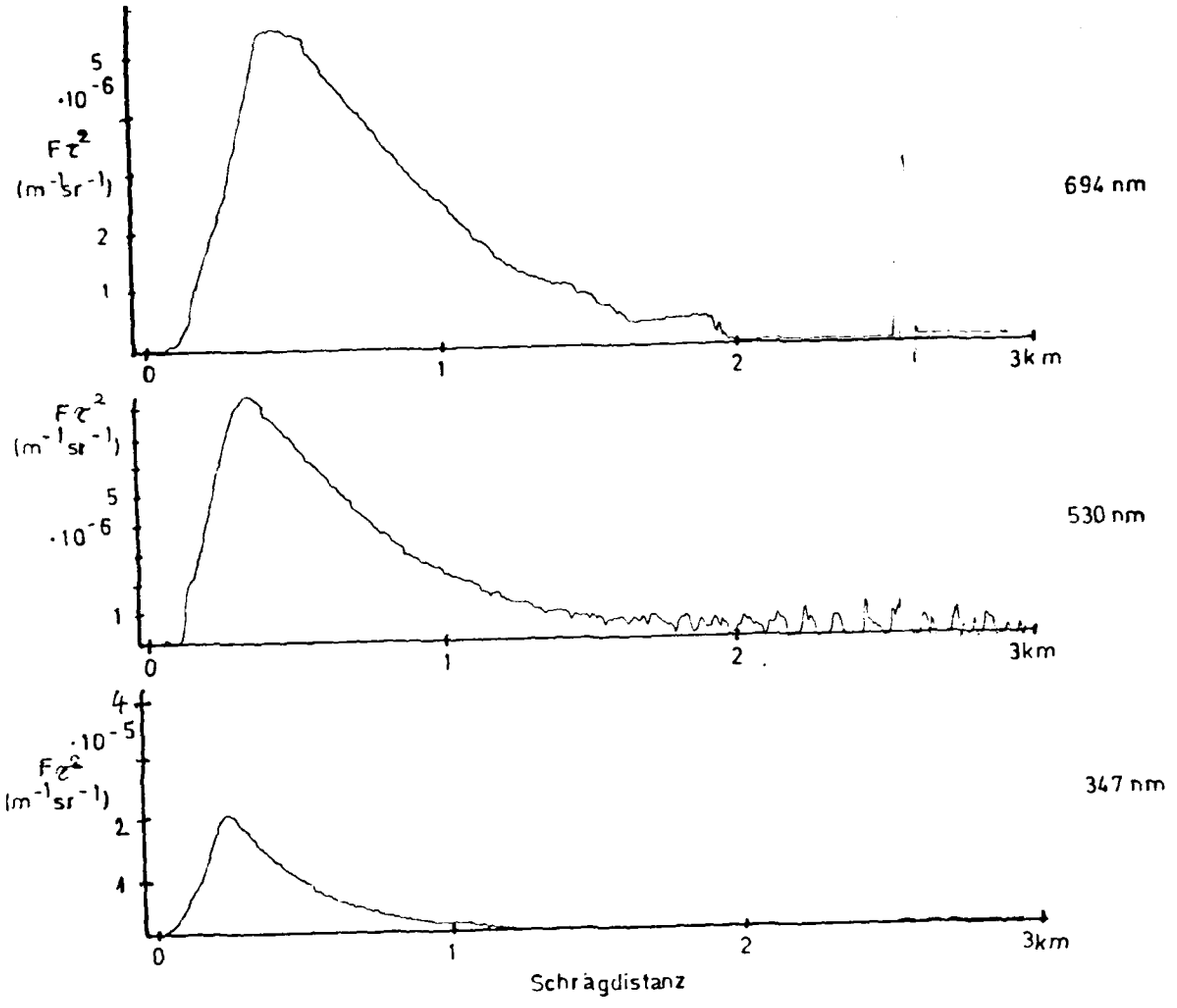

Datum:

28. Feb. 1980

Uhrzeit:

15.40 MEZ

Fig. 45

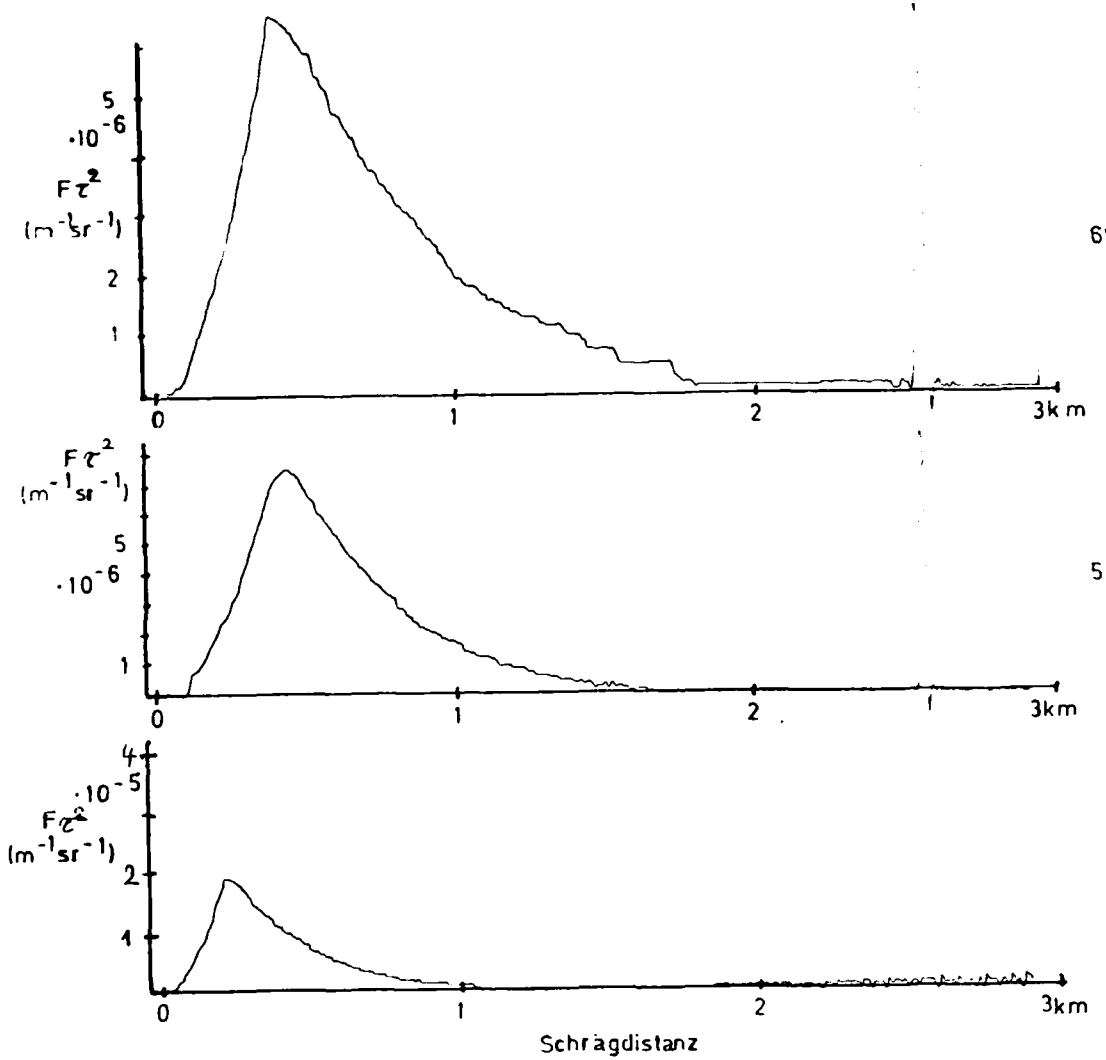

Datum:

28. Feb. 1980

Uhrzeit:

16.20 MEZ

Fig. 46

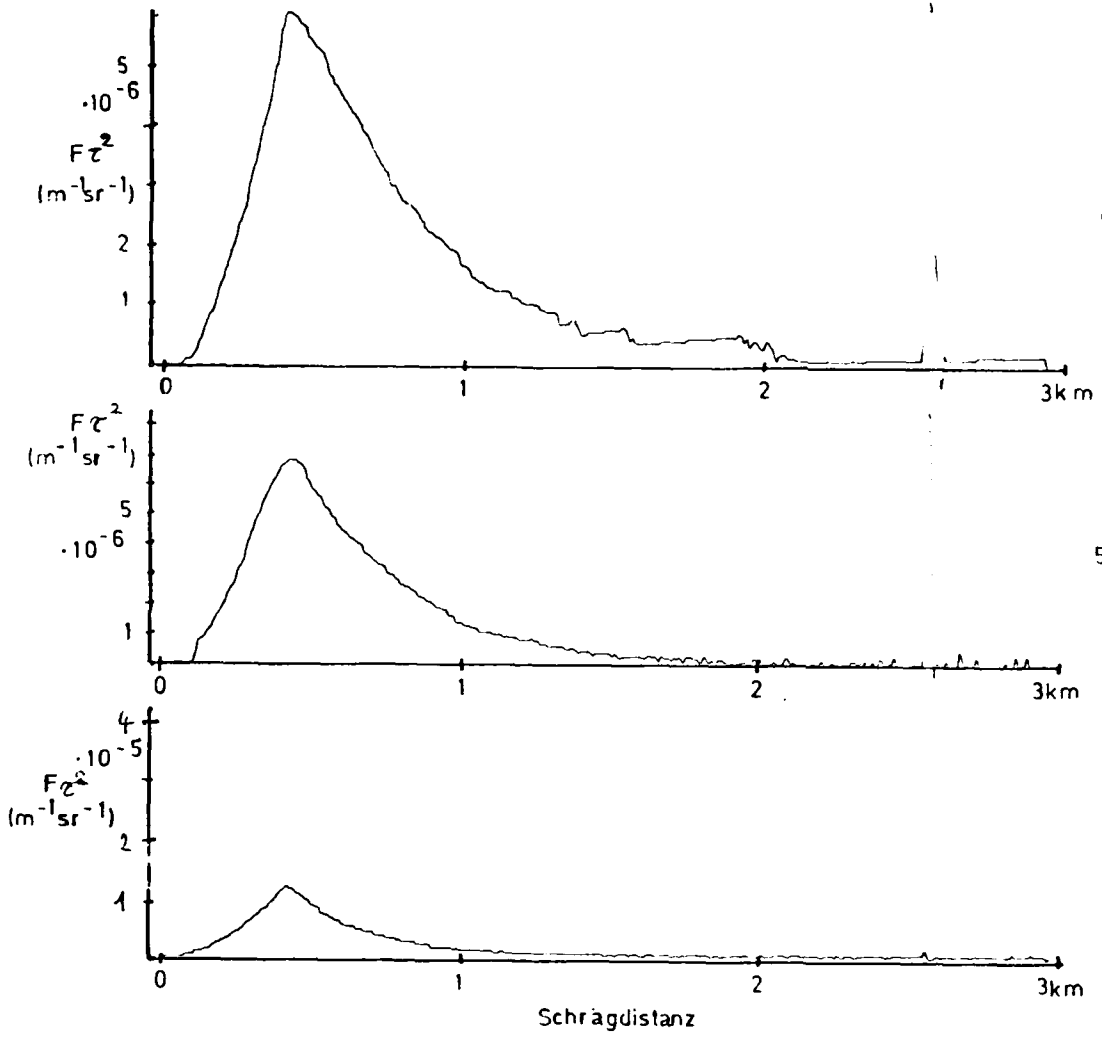

Datum:

28. Feb. 1980

Uhrzeit:

17.0[illegible] MEZ

Fig. 47

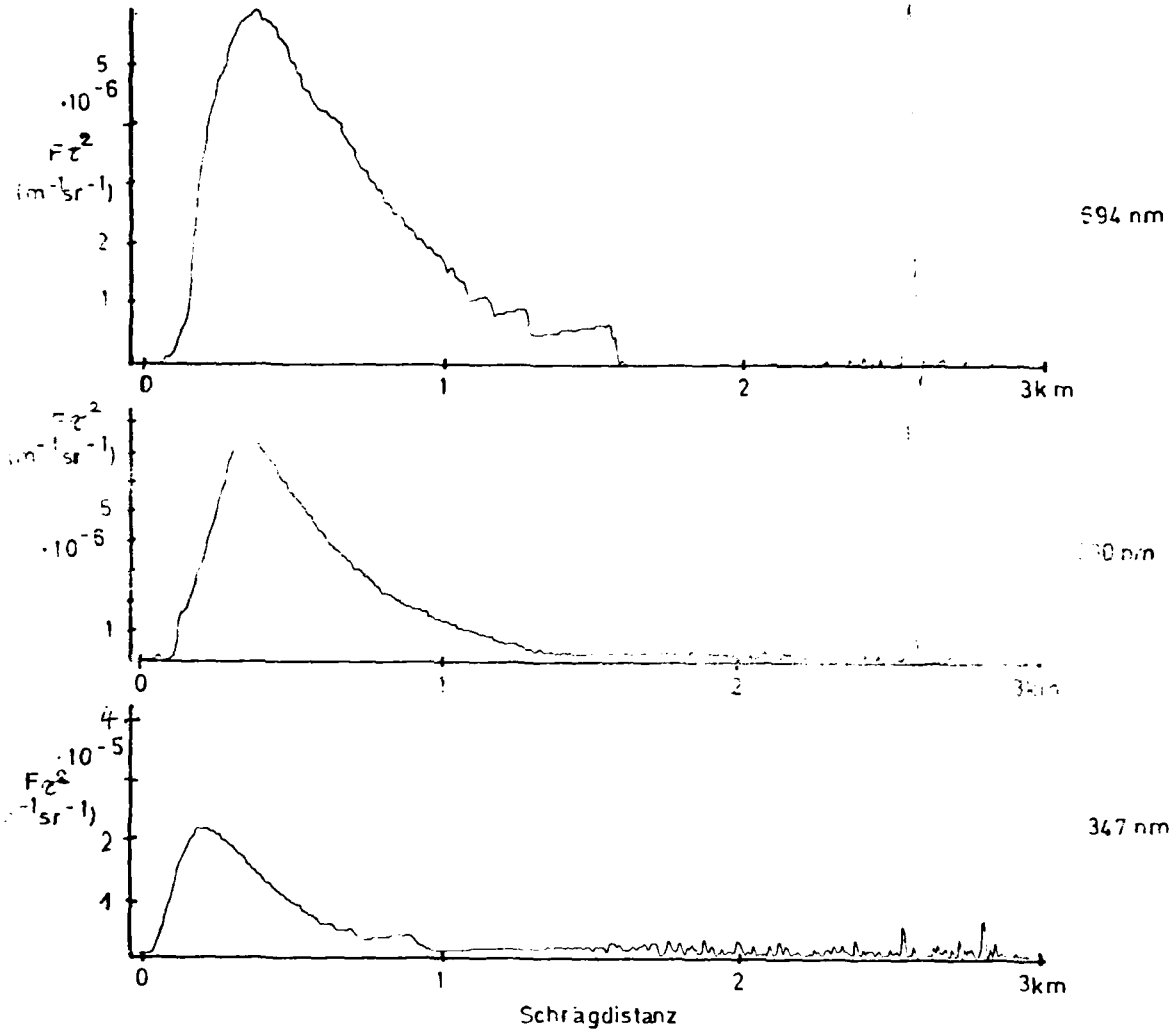

Datum:

28. Feb. 1980

Uhrzeit:

17.20 MEZ

Fig. 48

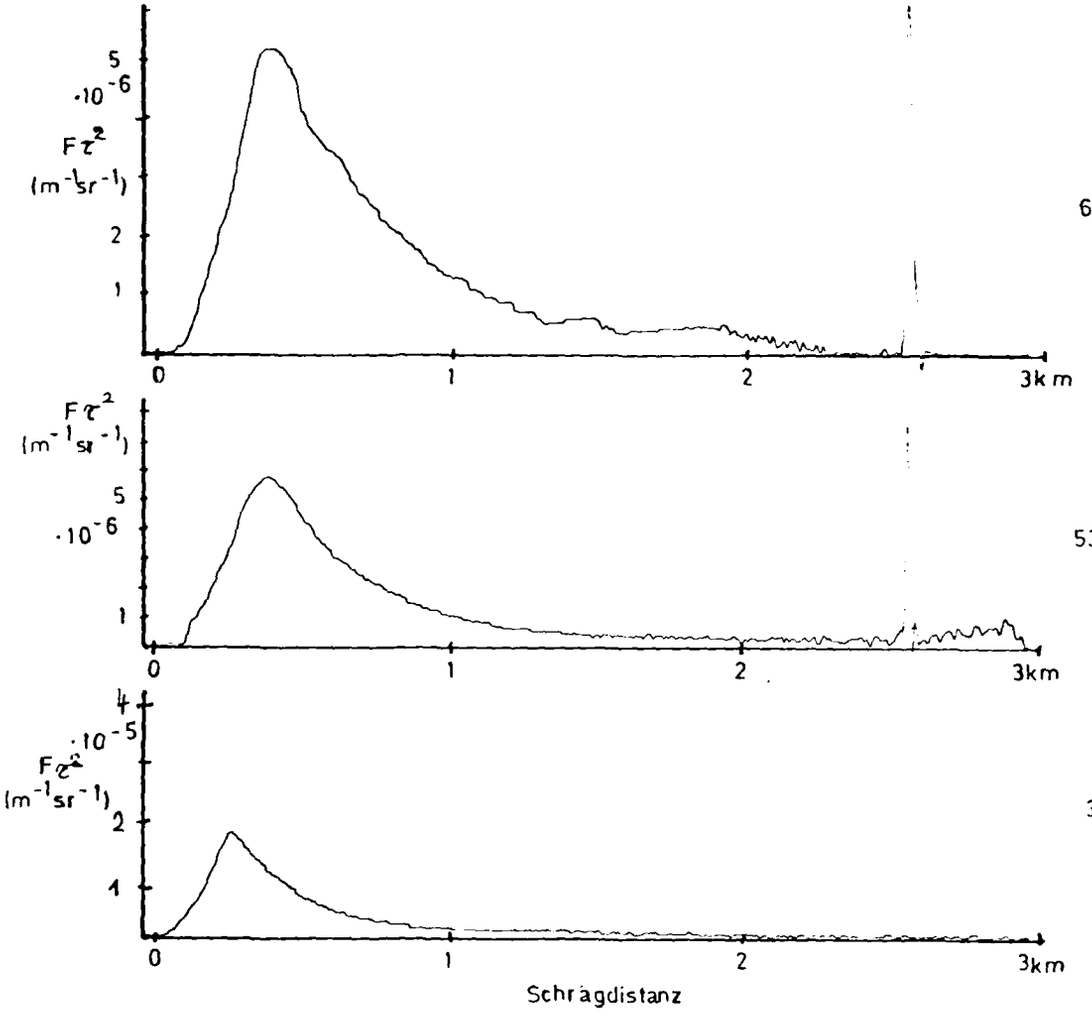

Datum:

28. Feb. 1980

Uhrzeit:

1800 MEZ

Fig. 49

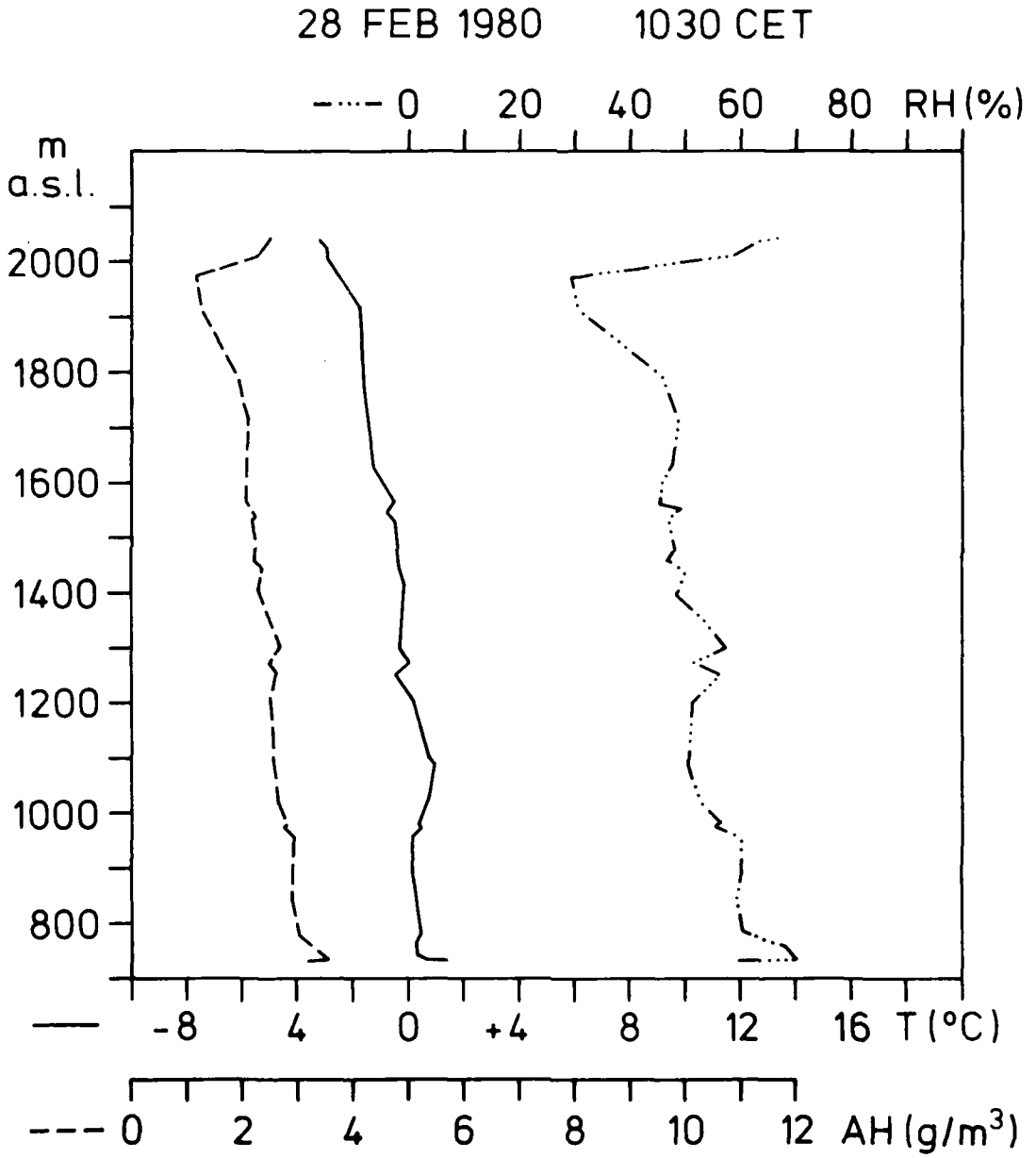
28 FEB 1980 1030 CET
0 20 40 60 80 RH(%)
m a.s.l.
2000
1800
1600
1400
1200
1000
800
-8 4 0 +4 8 12 16 T(°C)
0 2 4 6 8 10 12 AH(g/m³)

Fig. 51

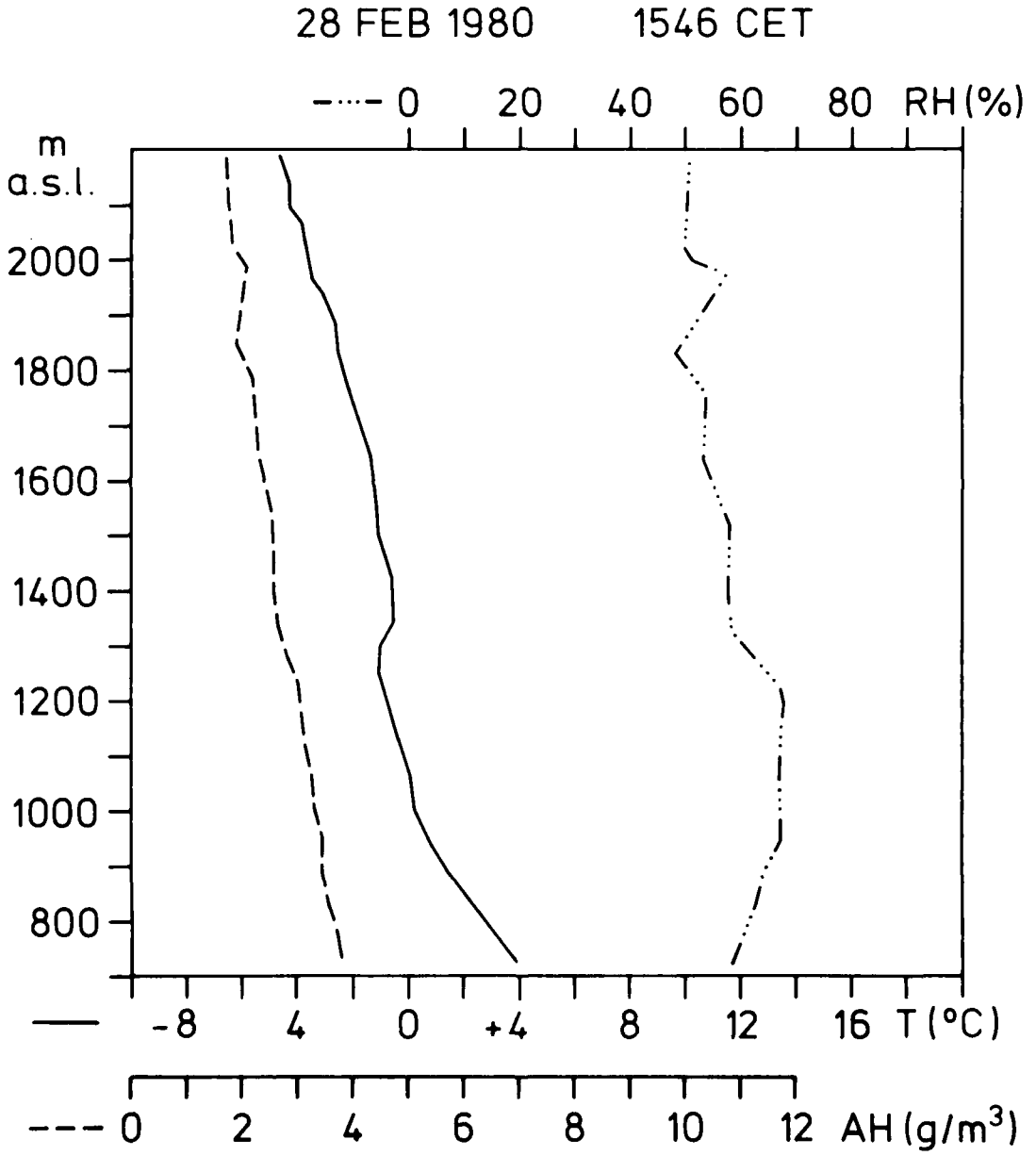
28 FEB 1980 1546 CET
0 20 40 60 80 RH(%)
m a.s.l.
2000
1800
1600
1400
1200
1000
800
-8 4 0 +4 8 12 16 T(°C)
0 2 4 6 8 10 12 AH(g/m³)

Fig. 52

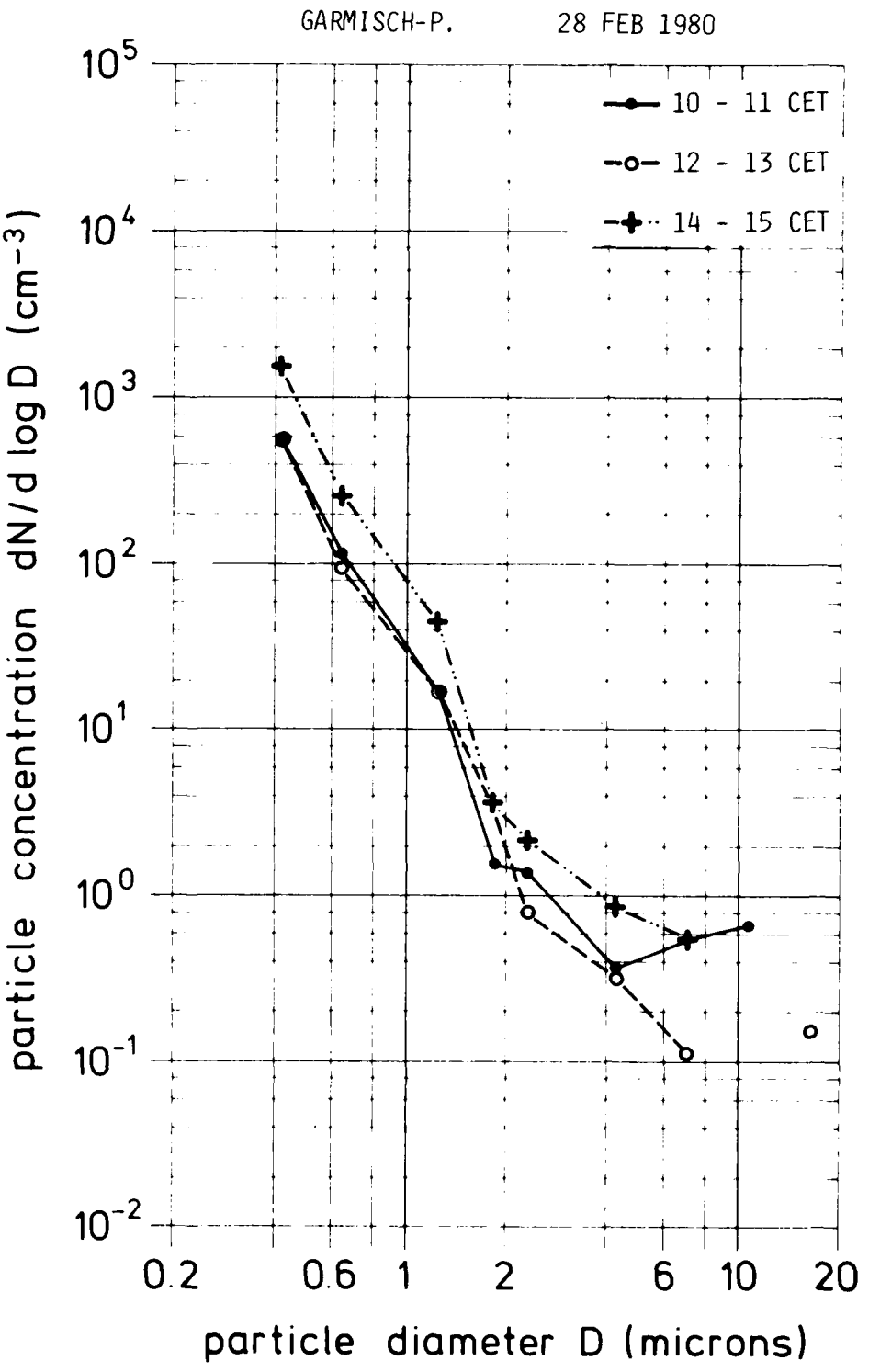
GARMISCH-P.
28 FEB 1980
10 - 11 CET
12 - 13 CET
14 - 15 CET
particle concentration dN/d log D (cm⁻³)
10⁵
10⁴
10³
10²
10¹
10⁰
10⁻¹
10⁻²
0.2
0.6
1
2
6
10
20
particle diameter D (microns)

Fig. 53

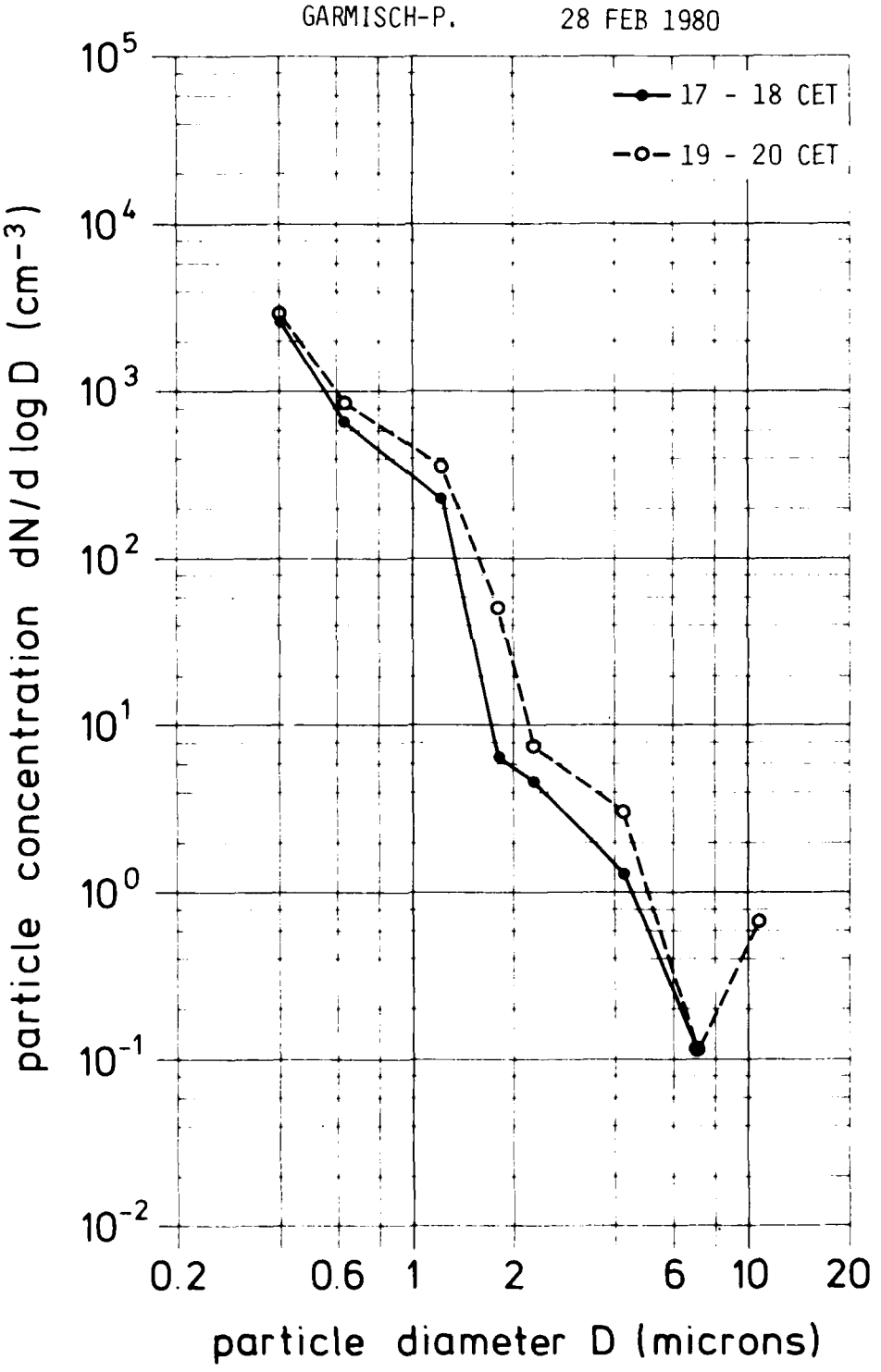
GARMISCH-P.
28 FEB 1980
17 - 18 CET
19 - 20 CET
particle concentration dN/d log D (cm⁻³)
10⁵
10⁴
10³
10²
10¹
10⁰
10⁻¹
10⁻²
0.2
0.6
1
2
6
10
20
particle diameter D (microns)

Fig. 54

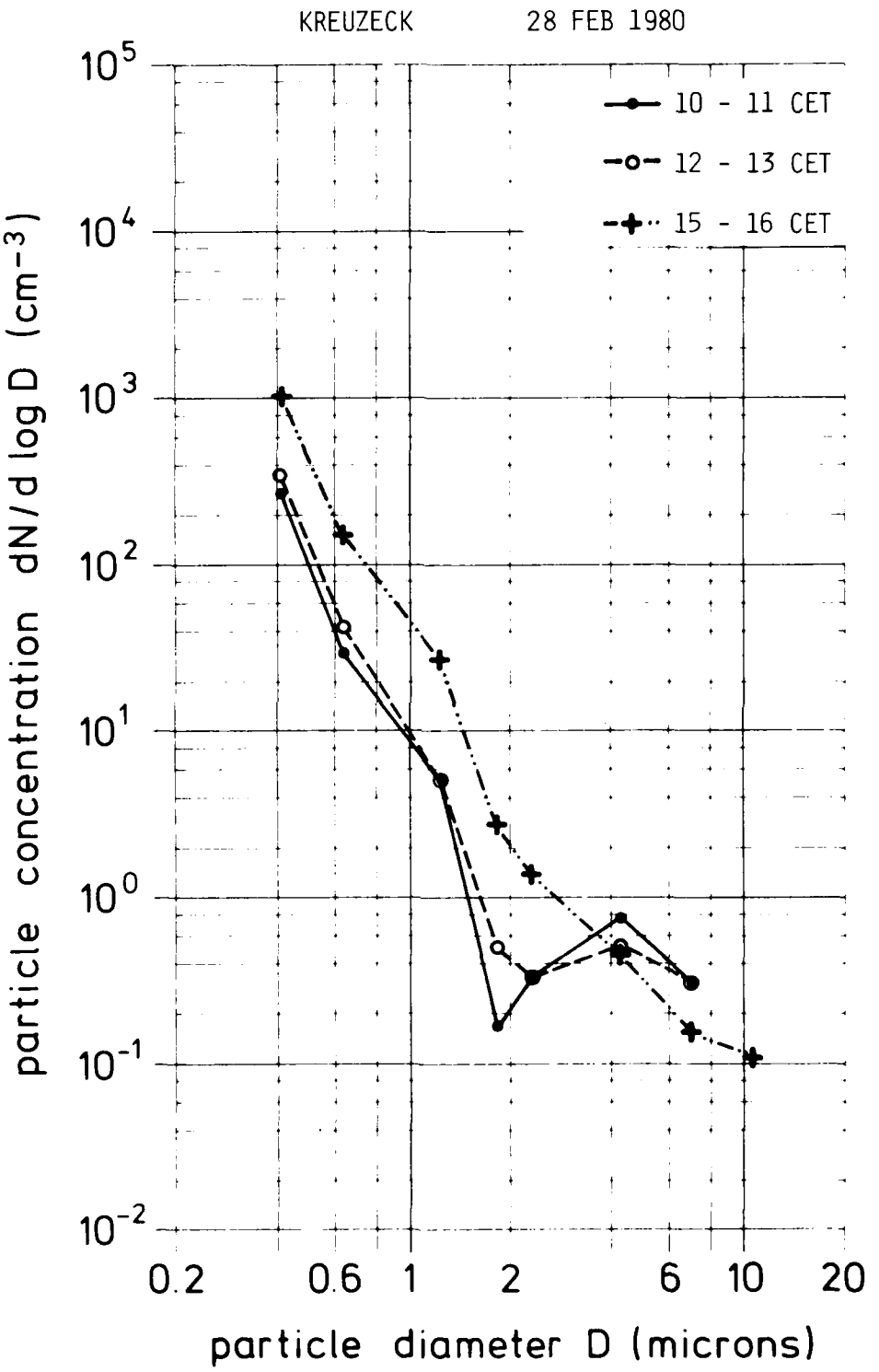
KREUZECK
28 FEB 1980
10 - 11 CET
12 - 13 CET
15 - 16 CET
particle concentration dN/d log D (cm⁻³)
10⁵
10⁴
10³
10²
10¹
10⁰
10⁻¹
10⁻²
0.2
0.6
1
2
6
10
20
particle diameter D (microns)

Fig. 55

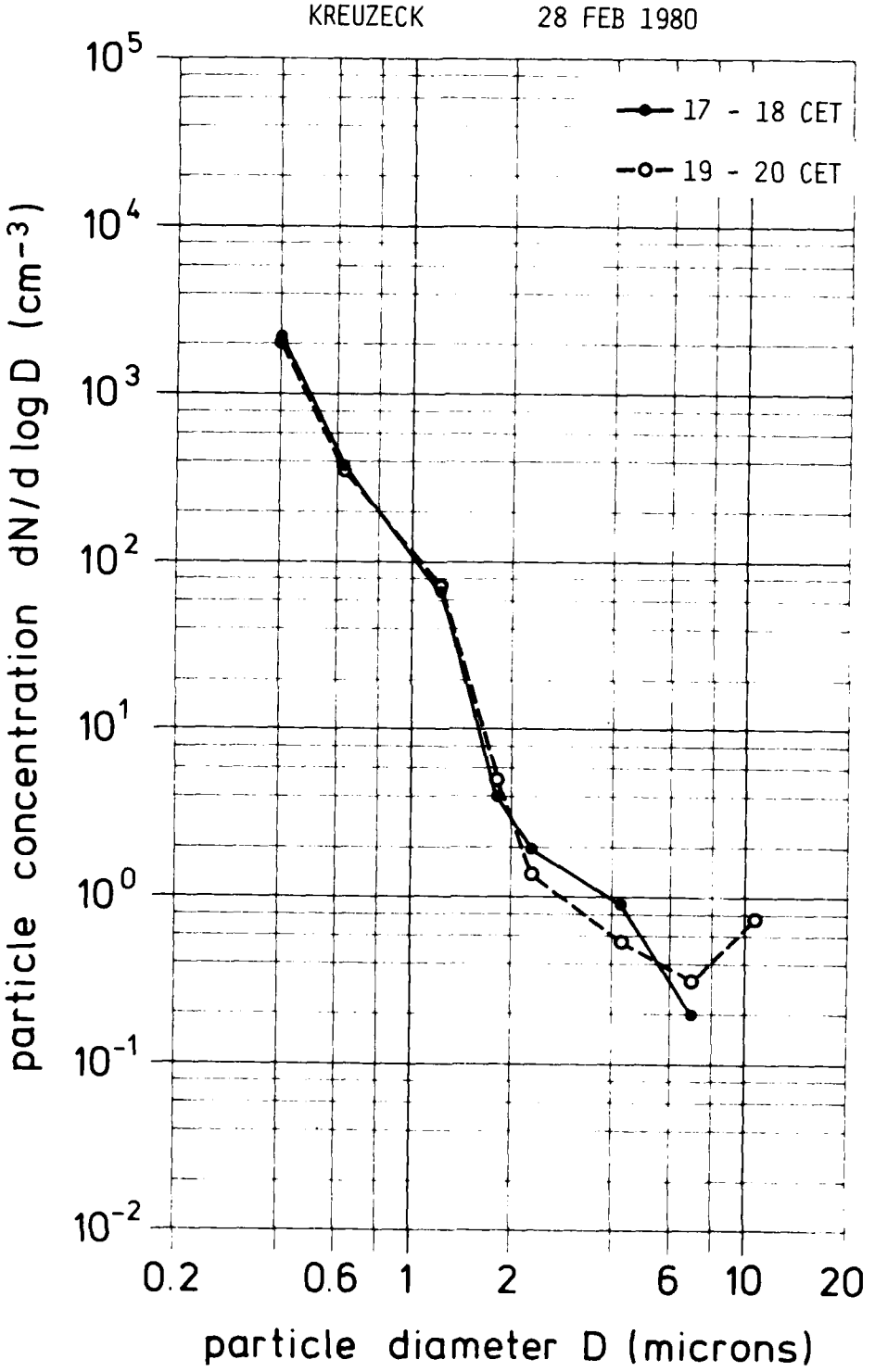
KREUZECK
28 FEB 1980
17 - 18 CET
19 - 20 CET
particle concentration dN/d log D (cm⁻³)
10⁵
10⁴
10³
10²
10¹
10⁰
10⁻¹
10⁻²
0.2
0.6
1
2
6
10
20
particle diameter D (microns)

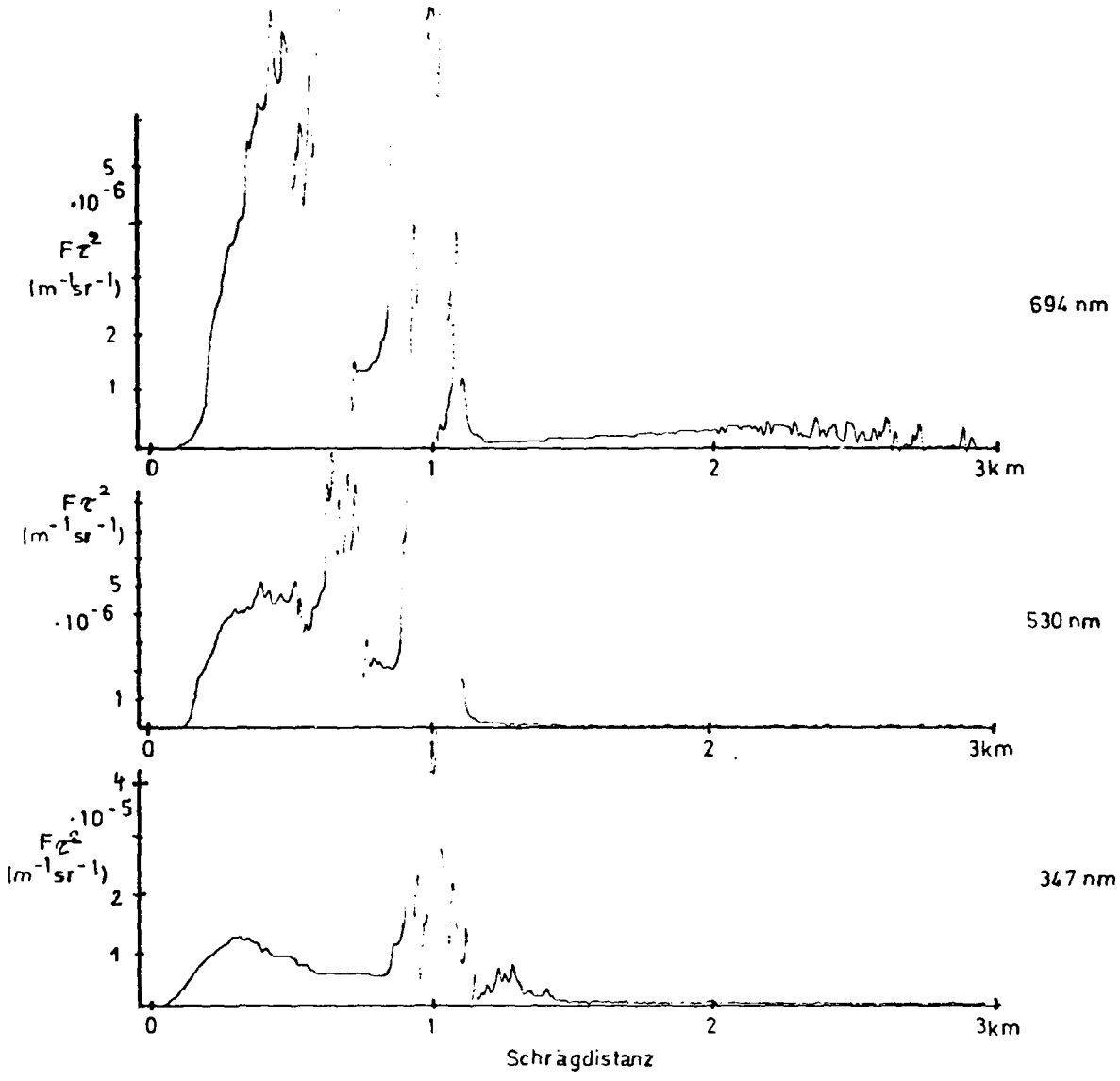

Datum:

19. Mai 1980

Uhrzeit:

08.15 MEZ

Fig. 56

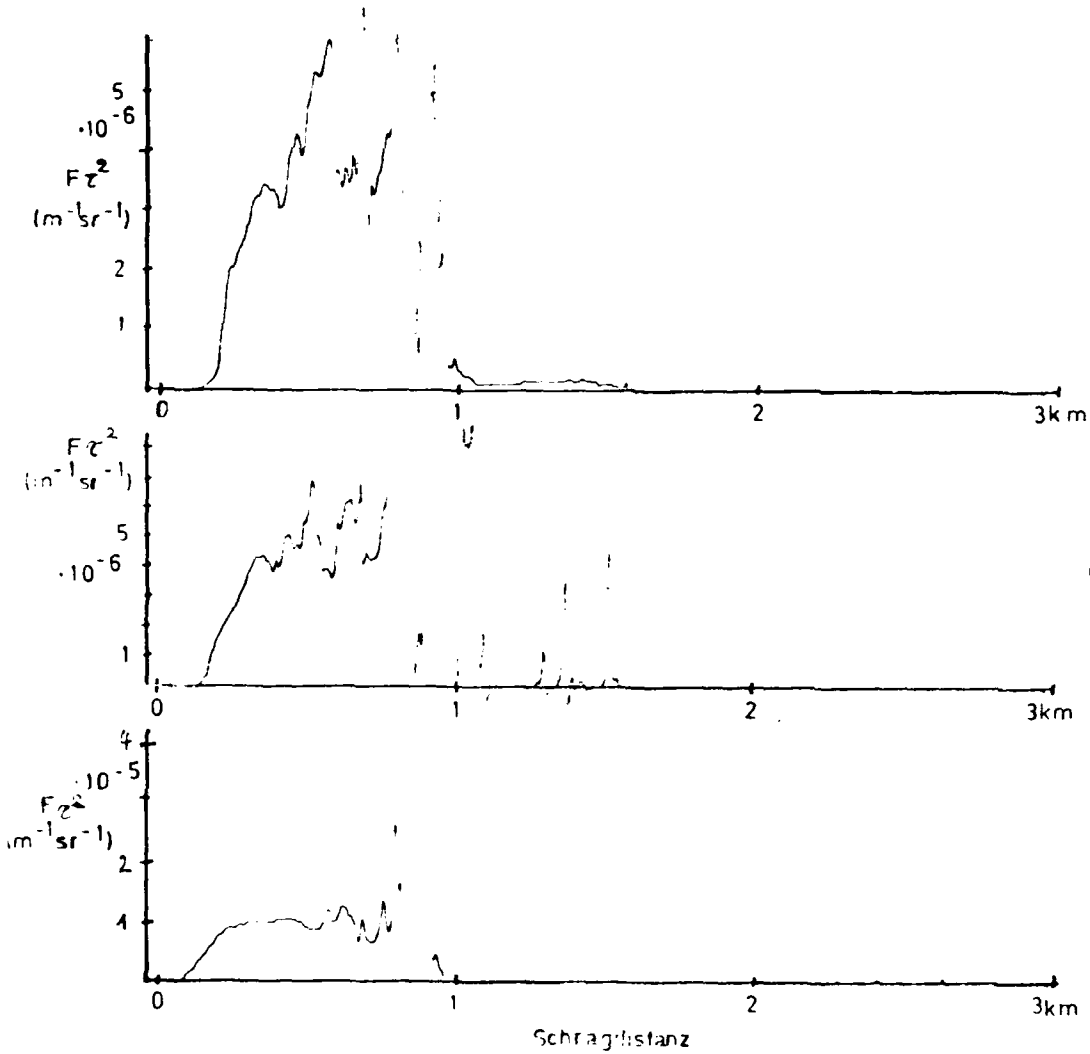

Datum:

19. Mai 1980

Uhrzeit:

0900 MEZ

Fig. 57

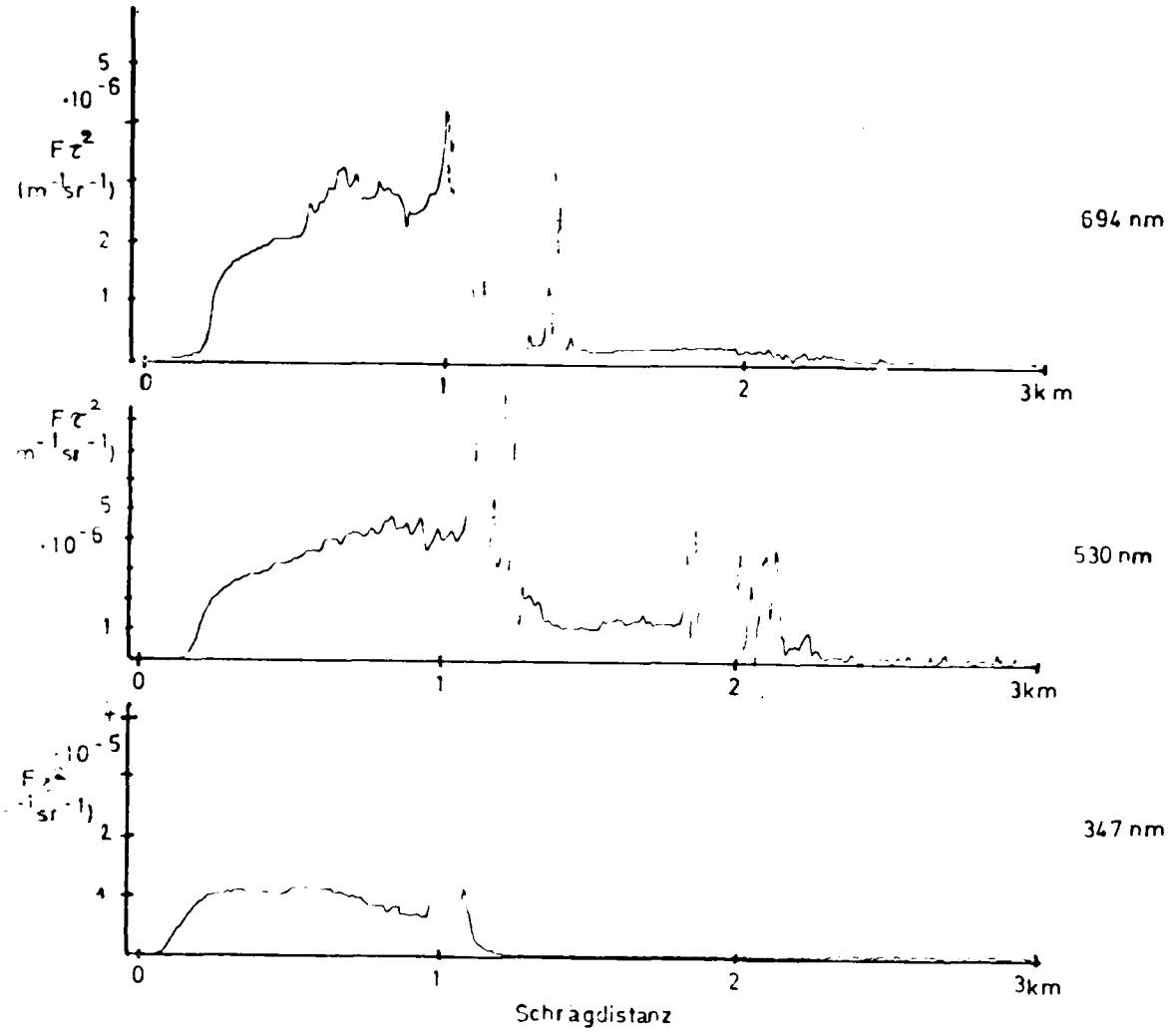

Datum:

19. Mai 1980

Uhrzeit:

0930 MEZ

Fig. 58

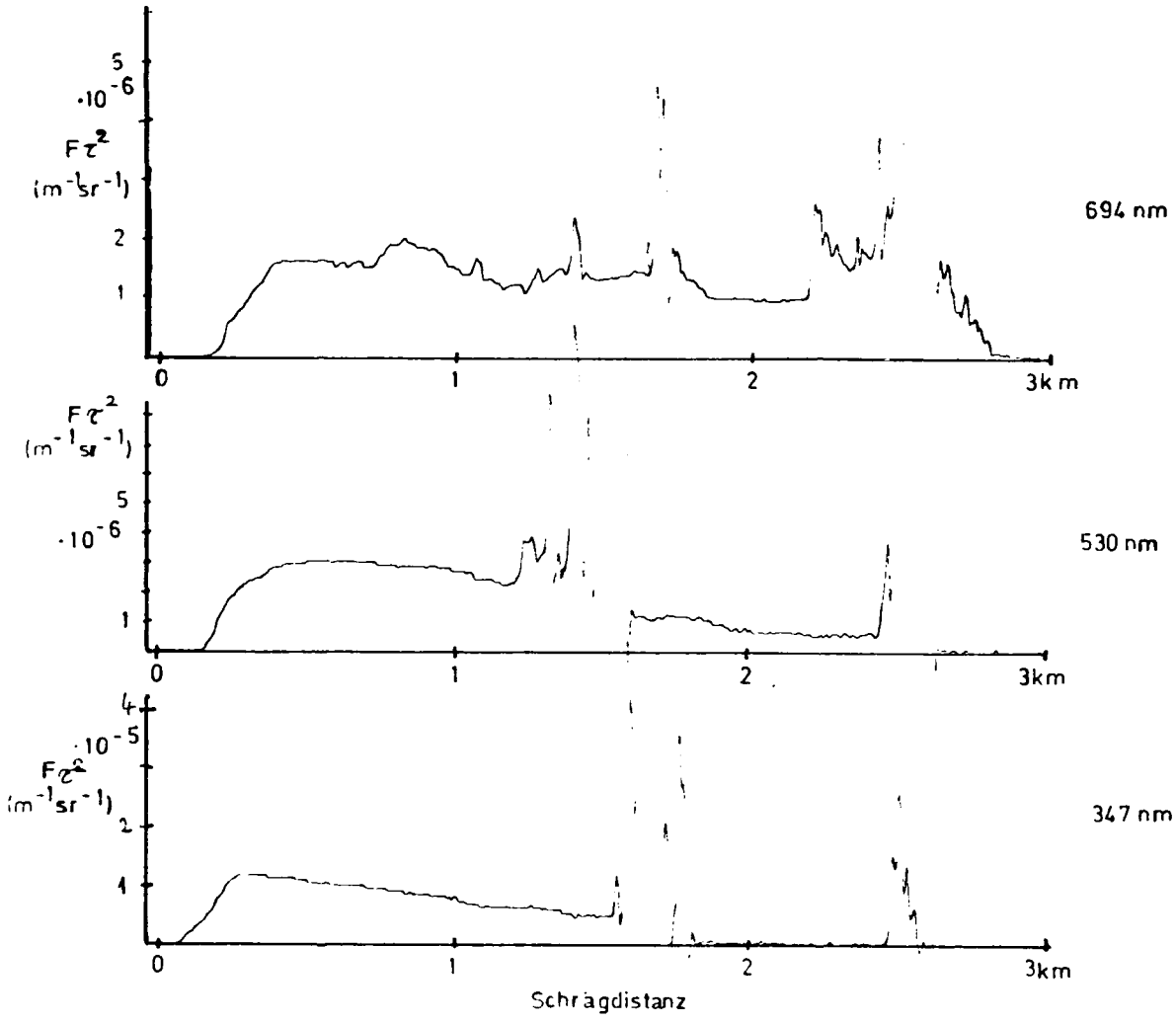

Datum:

19. Mai 1980

Uhrzeit:

10.00 MEZ

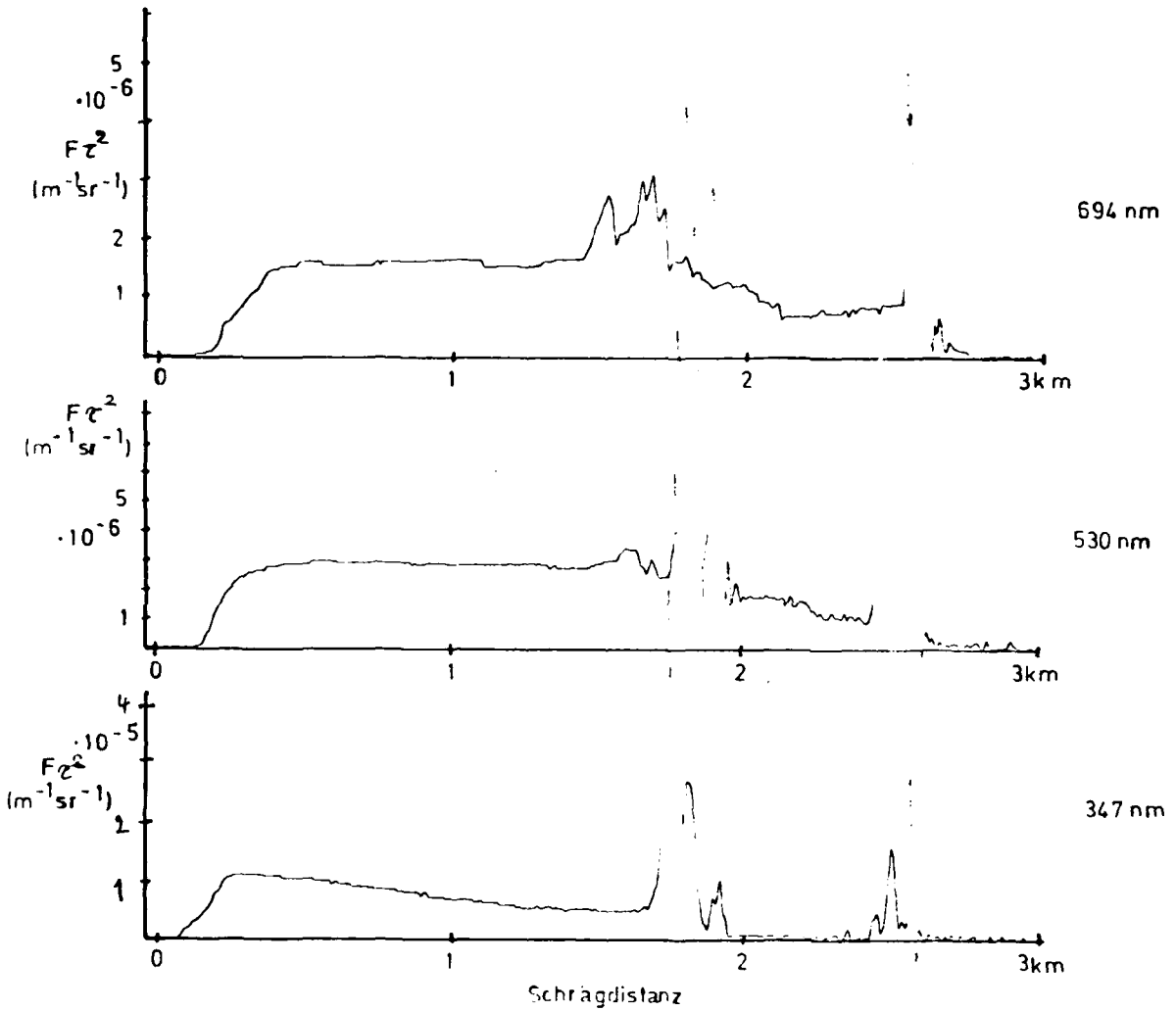

Datum:

19. Mai 1980

Uhrzeit:

1030 MEZ

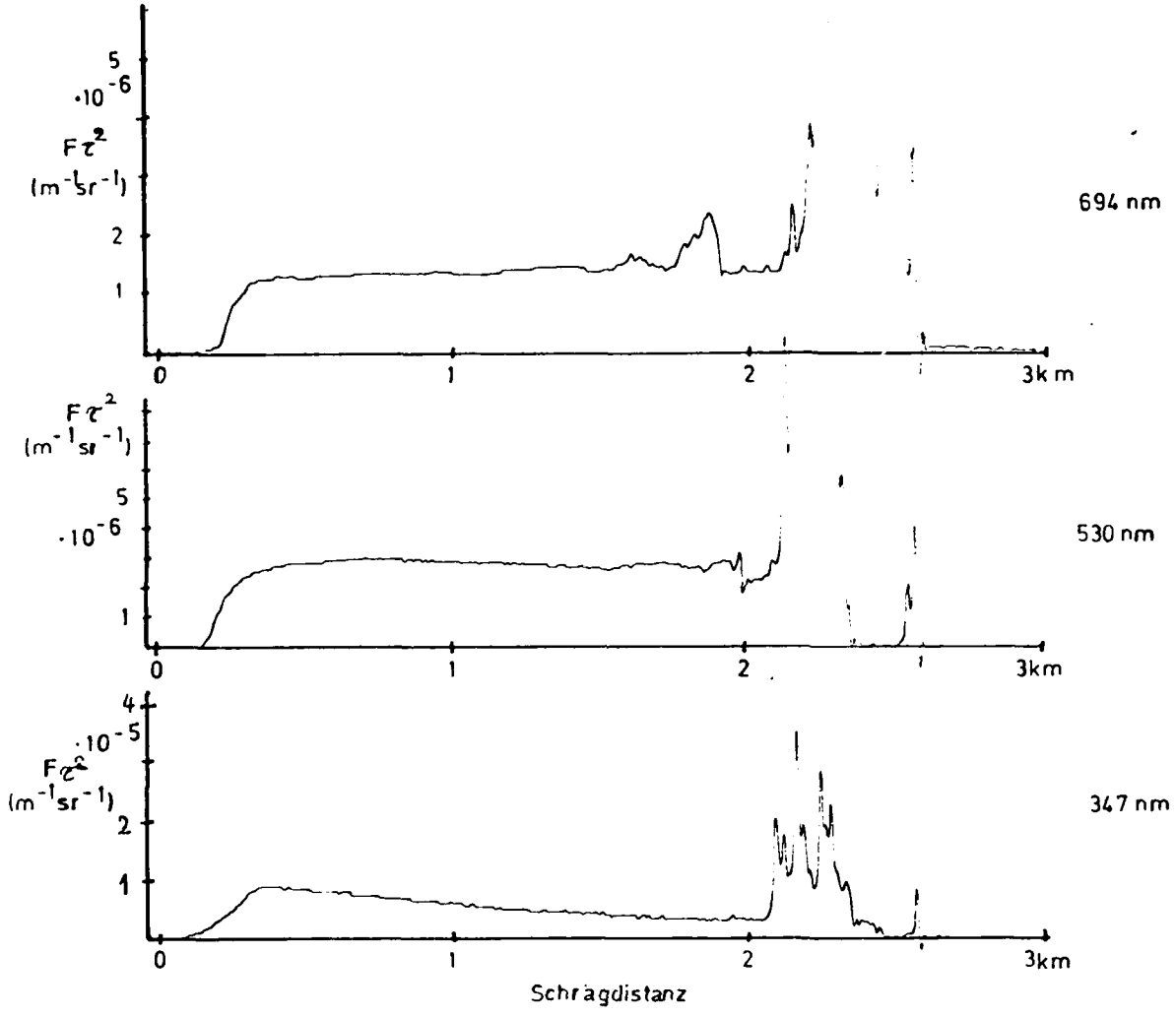

Datum:

19. Mai 1980

Uhrzeit:

11.05 MEZ

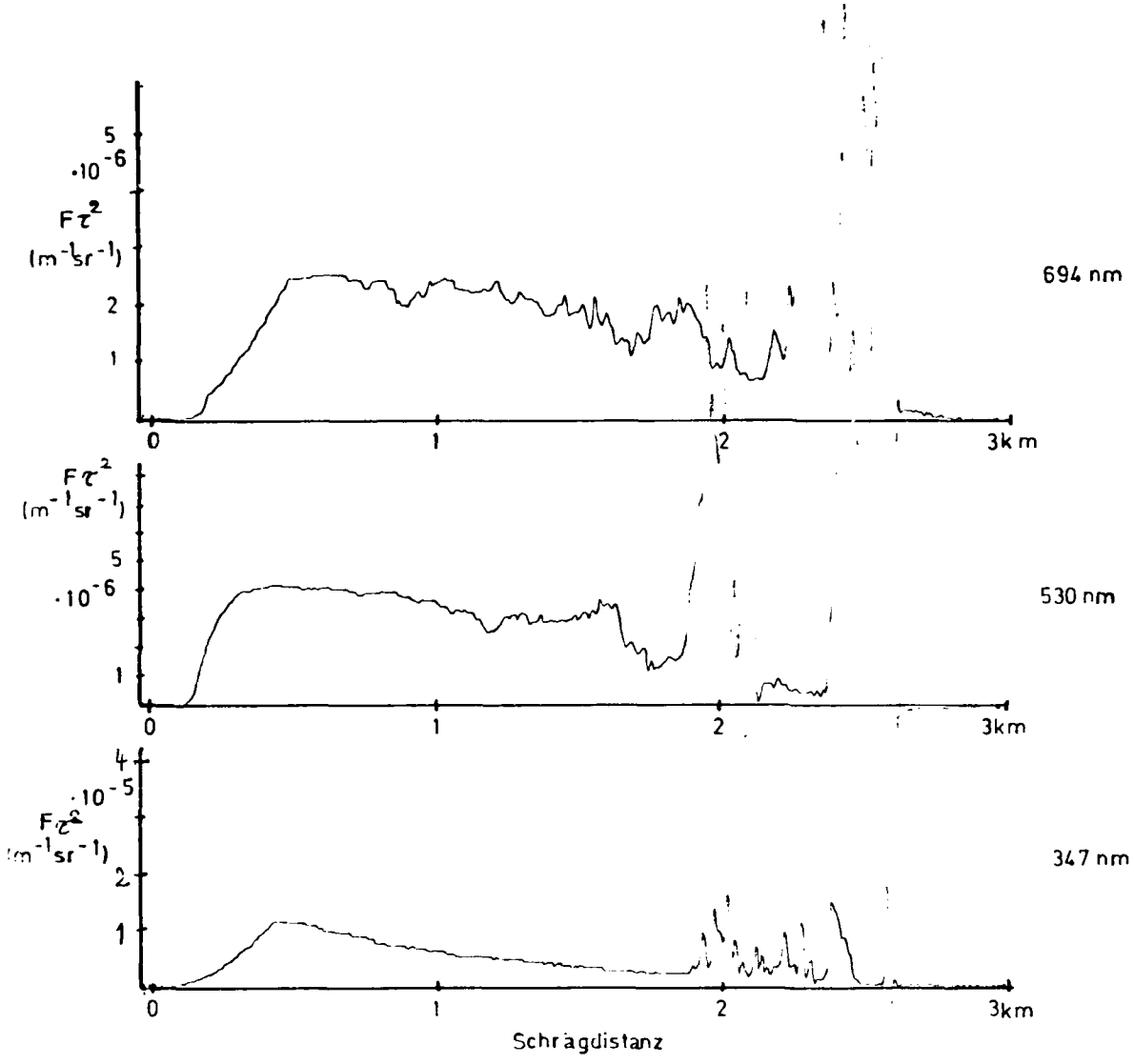

Datum:

19. Mai 1980

Uhrzeit:

13.05 MEZ

Fig. 62

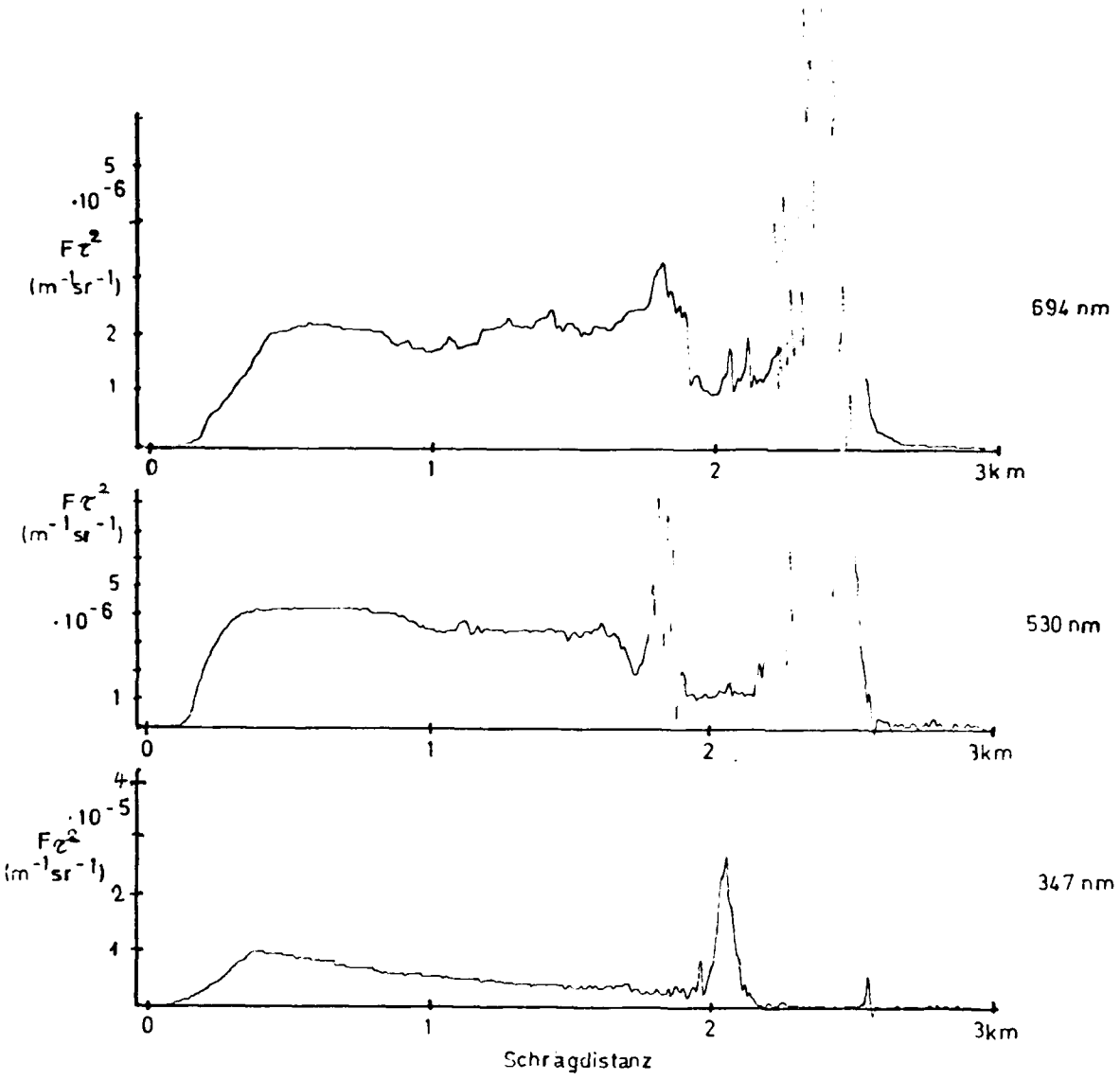

Datum:

19. Mai 1980

Uhrzeit:

13.38 MEZ

Fig. 63

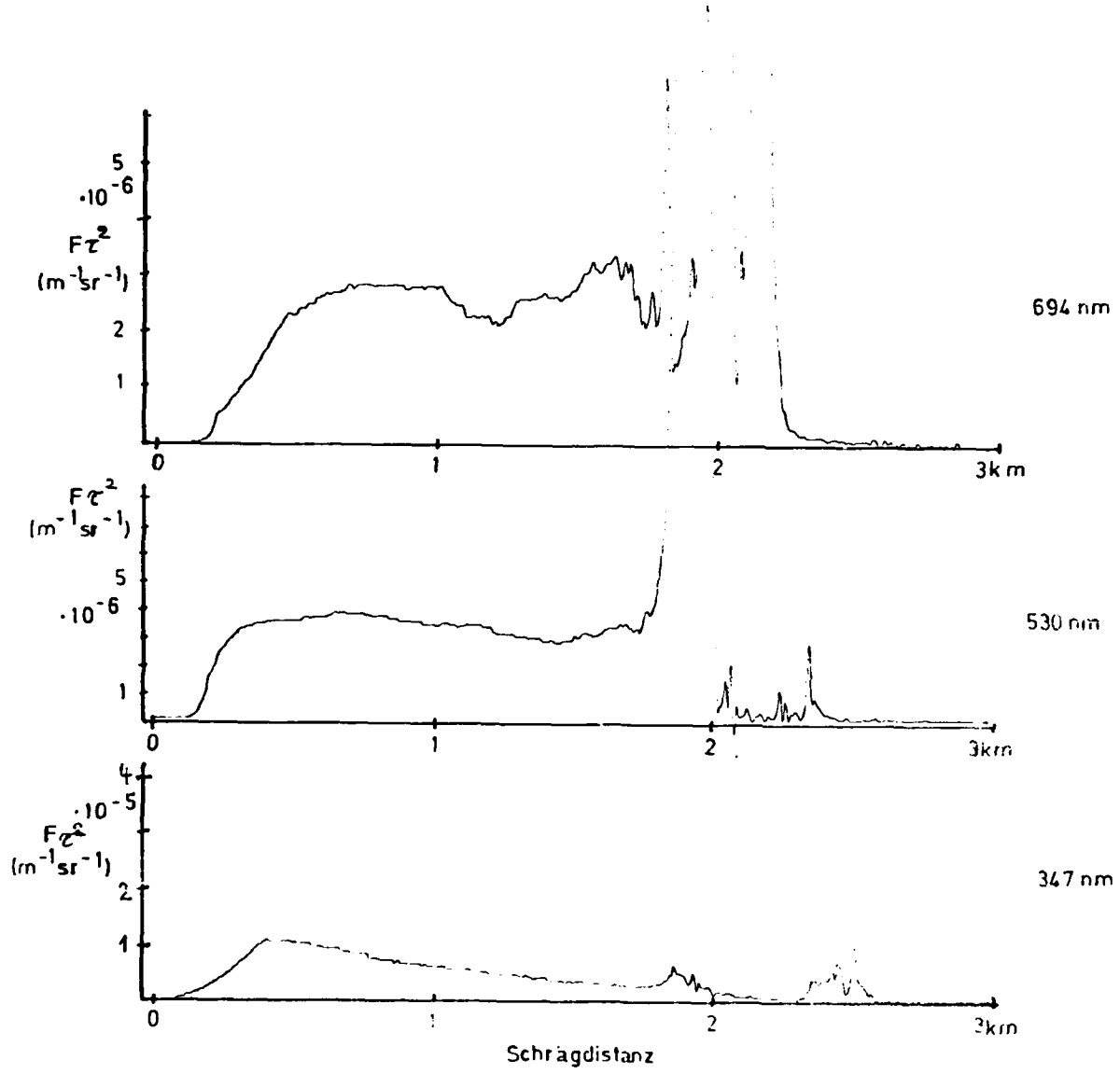

Datum:

19. Mai 1980

Uhrzeit:

14.00 MEZ

Fig. 44

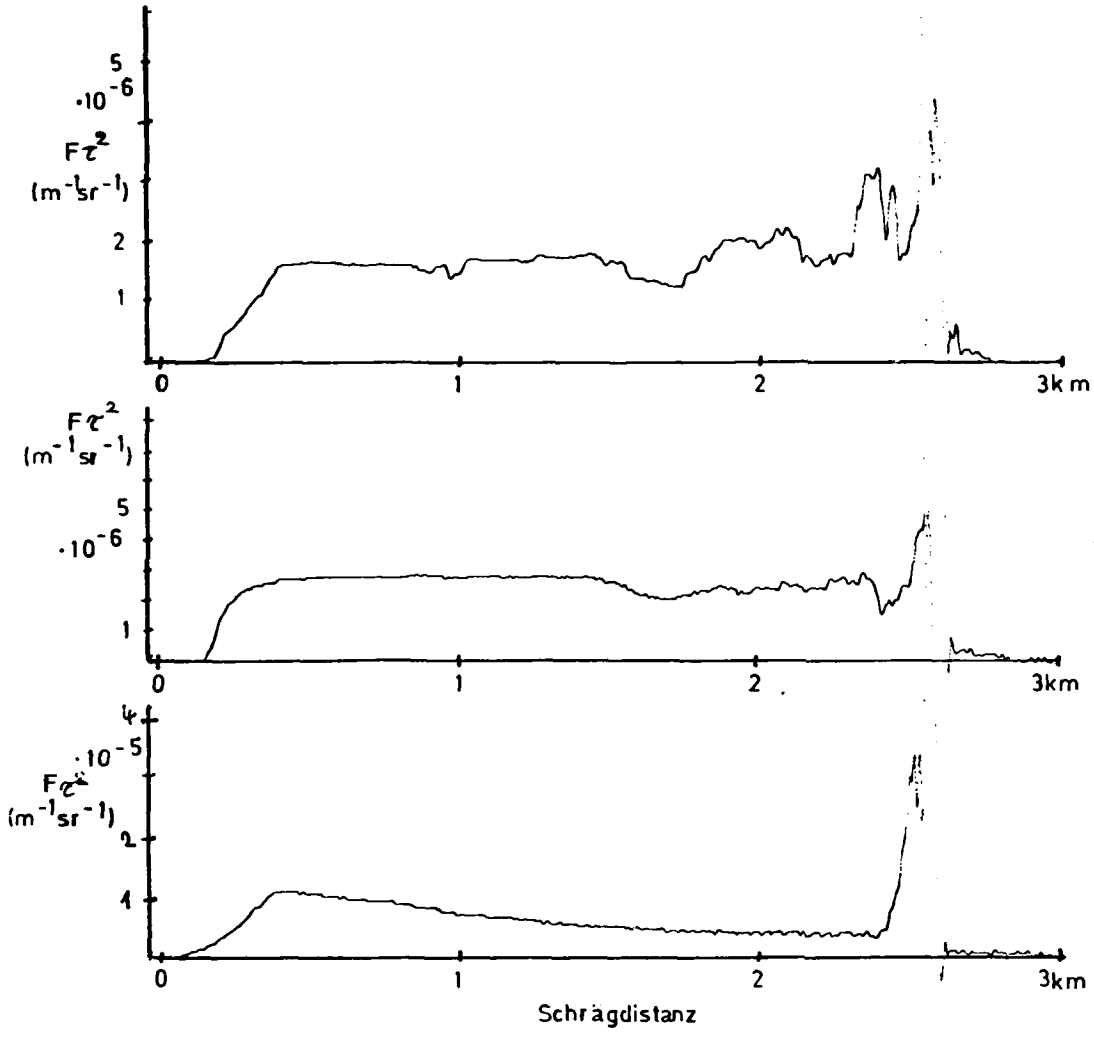

Datum:

19. Mai 1980

Uhrzeit:

14.56 MEZ

Fig. 65

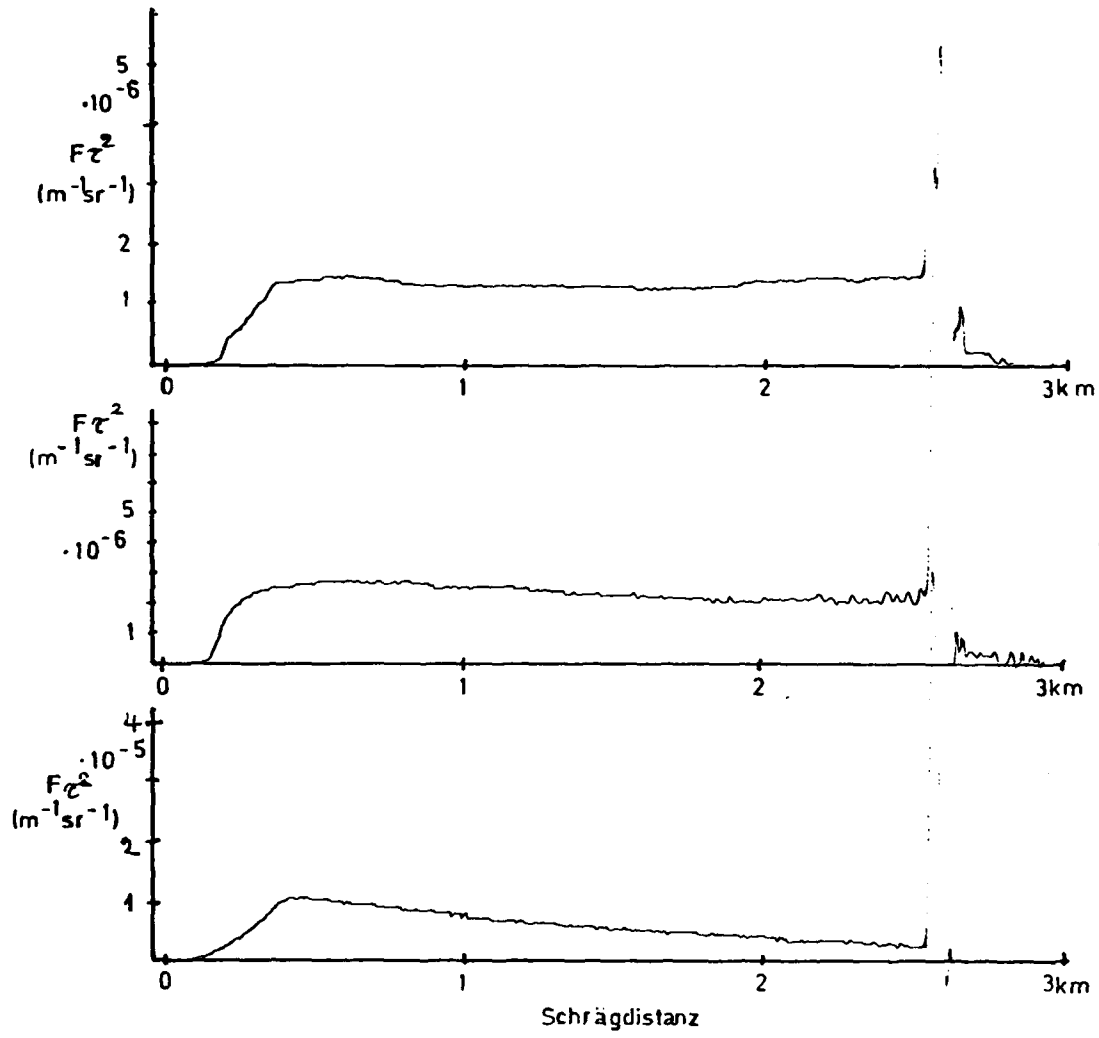

Datum:

19. Mai 1980

Uhrzeit:

15.30 MEZ

Fig. 66

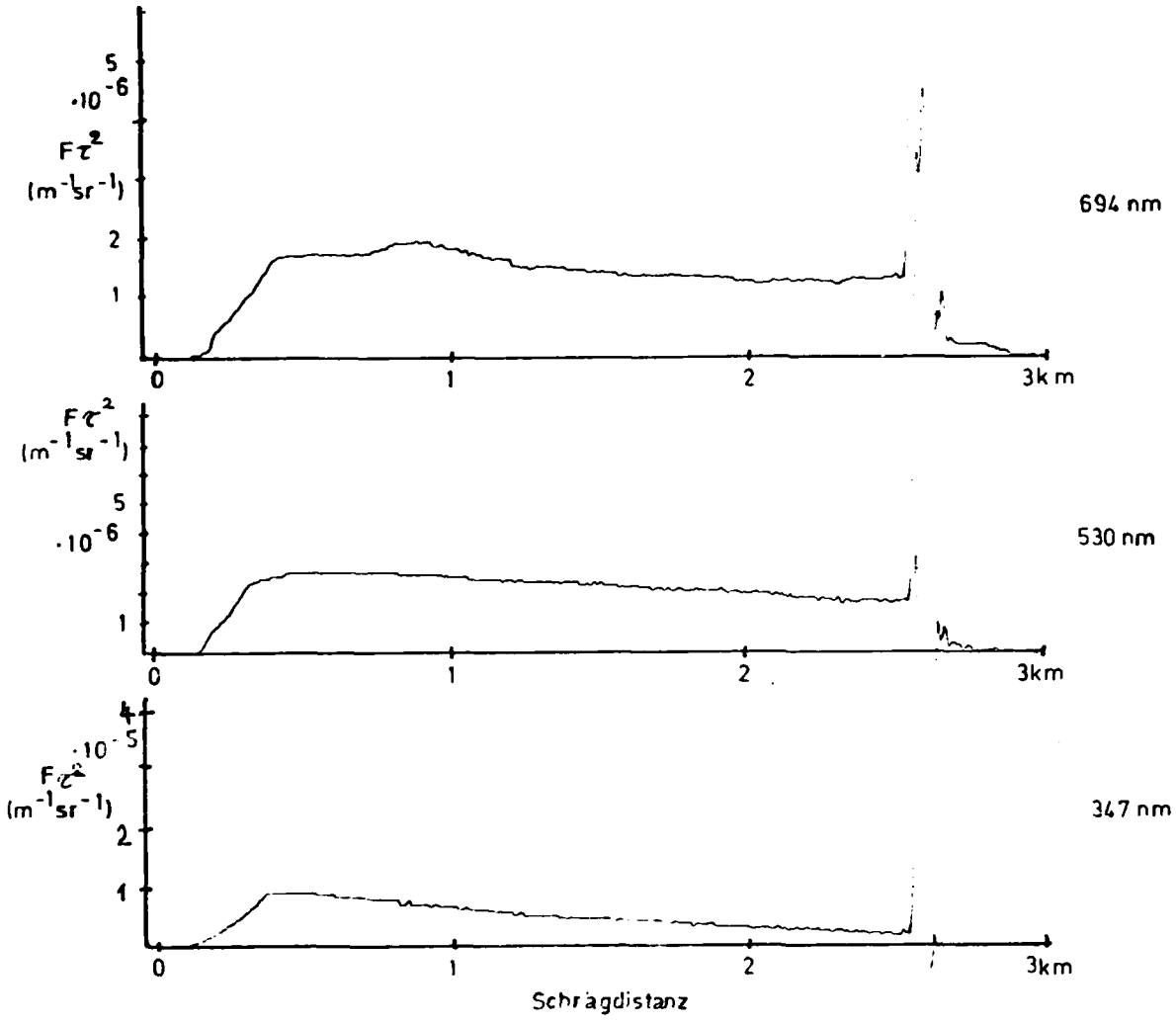

Datum:

19. Mai 1980

Uhrzeit:

1000 MEZ

Fig. 67

Fig. 68

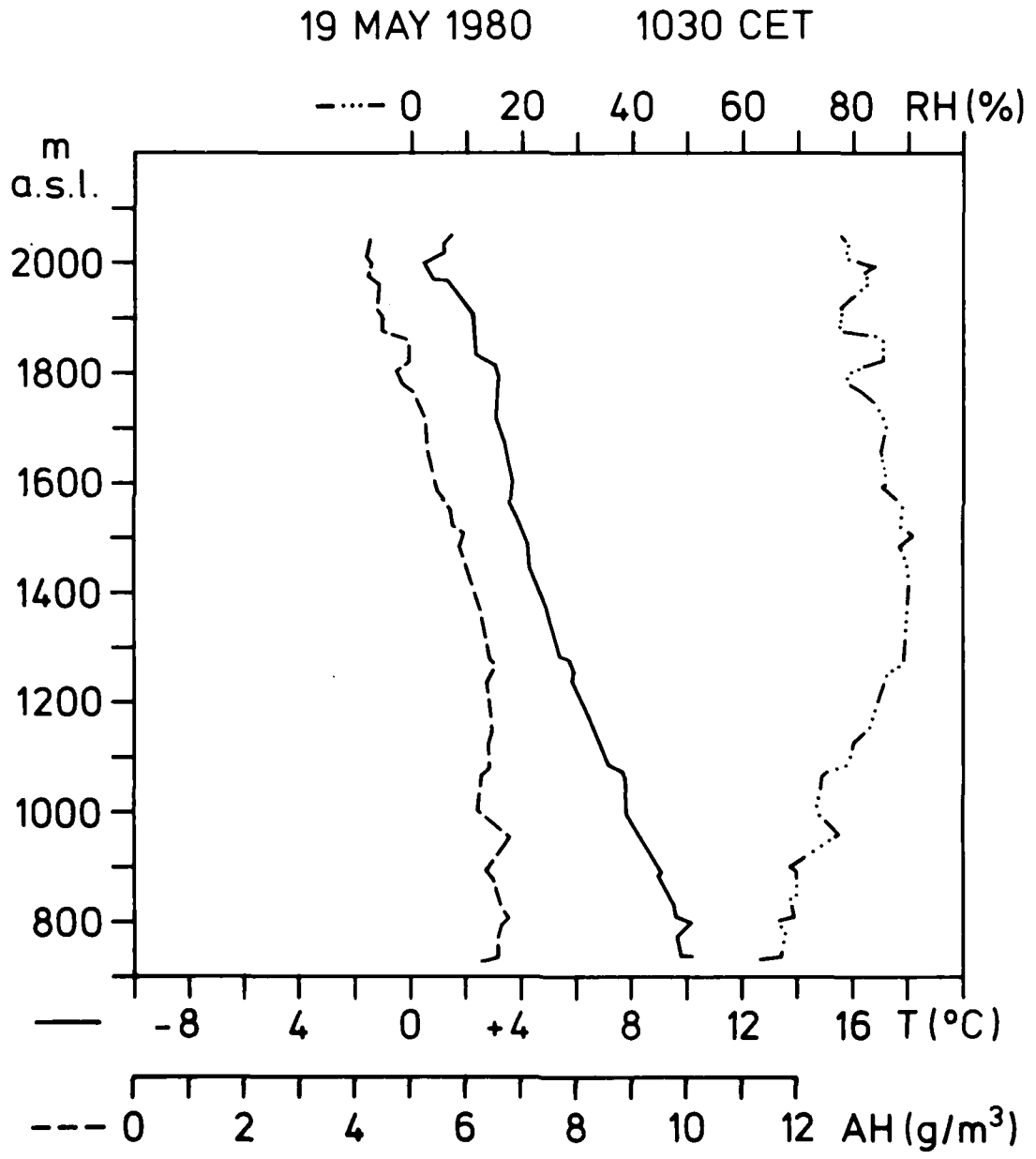
19 MAY 1980 1030 CET
0 20 40 60 80 RH (%)
m a.s.l.
2000
1800
1600
1400
1200
1000
800
-8 4 0 +4 8 12 16 T (°C)
0 2 4 6 8 10 12 AH (g/m³)

Fig. 69

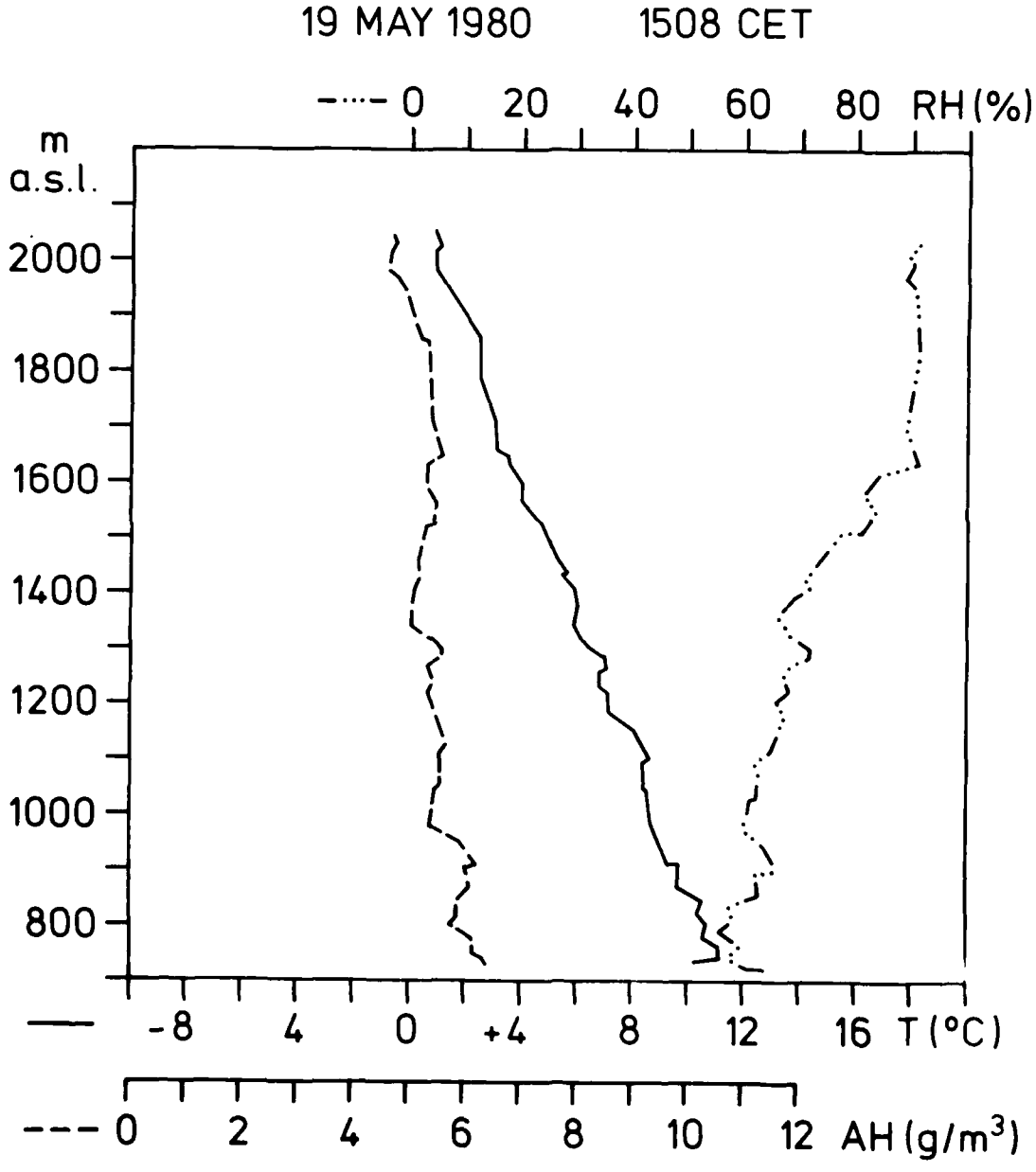
19 MAY 1980 1508 CET
0 20 40 60 80 RH (%)
m a.s.l.
2000
1800
1600
1400
1200
1000
800
-8 4 0 +4 8 12 16 T (°C)
0 2 4 6 8 10 12 AH (g/m³)

Fig. 70

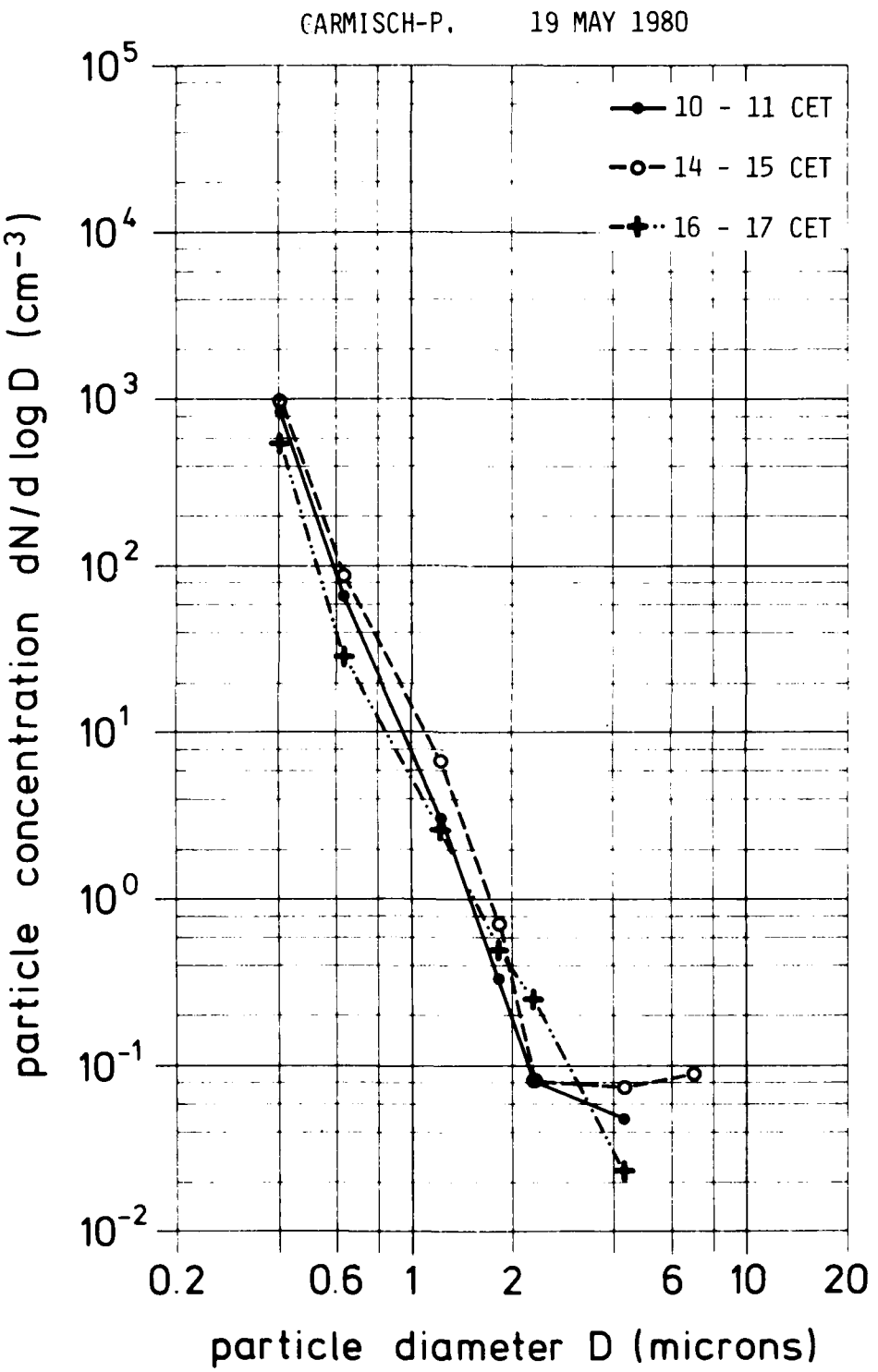
CARMISCH-P. 19 MAY 1980
10 - 11 CET
14 - 15 CET
16 - 17 CET
particle concentration dN/d log D (cm⁻³)
10⁵
10⁴
10³
10²
10¹
10⁰
10⁻¹
10⁻²
0.2
0.6
1
2
6
10
20
particle diameter D (microns)

Fig. 71

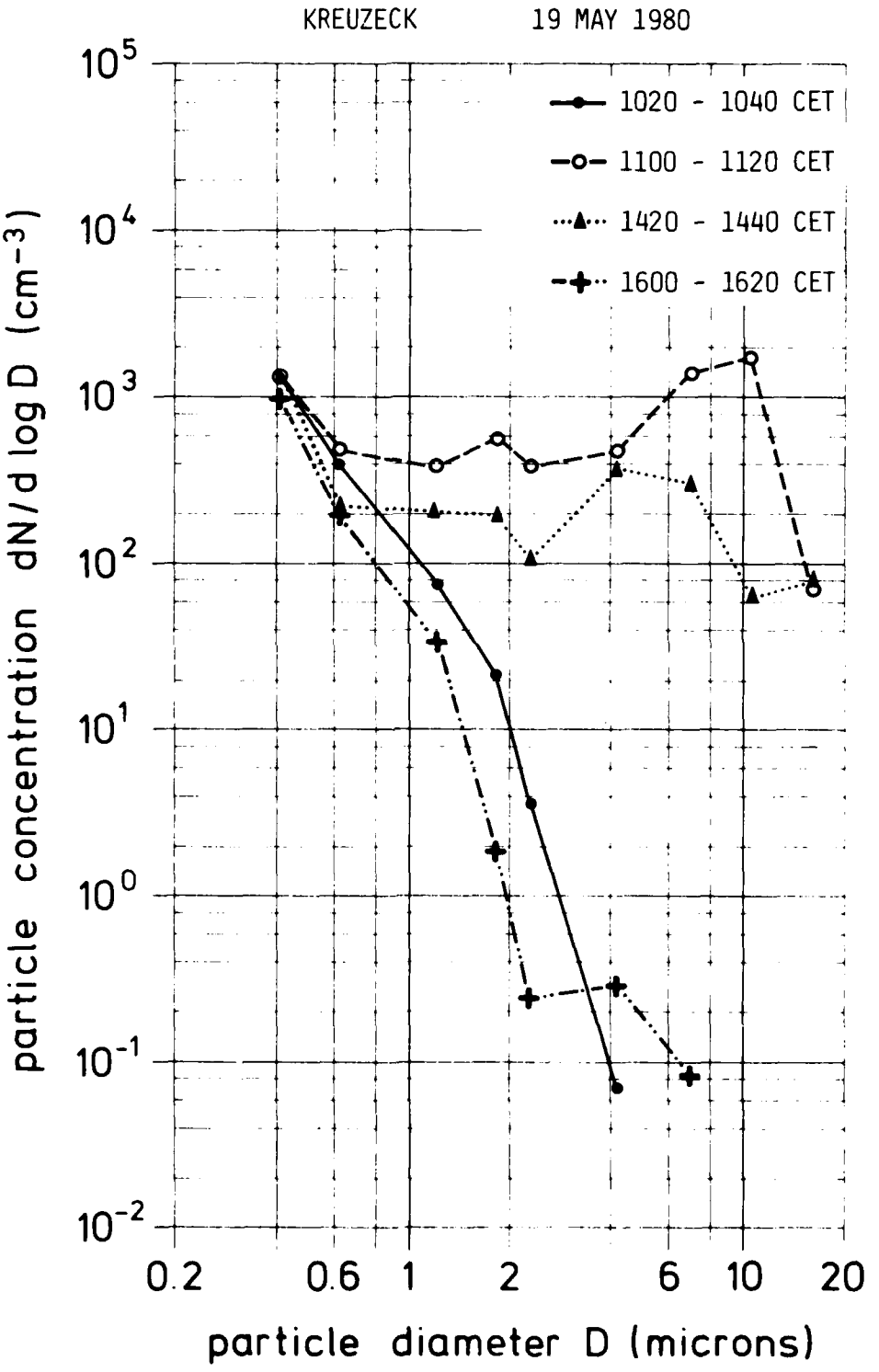
KREUZECK 19 MAY 1980
1020 - 1040 CET
1100 - 1120 CET
1420 - 1440 CET
1600 - 1620 CET
particle concentration dN/d log D (cm⁻³)
10⁵
10⁴
10³
10²
10¹
10⁰
10⁻¹
10⁻²
0.2
0.6
1
2
6
10
20
particle diameter D (microns)

Fig. 72

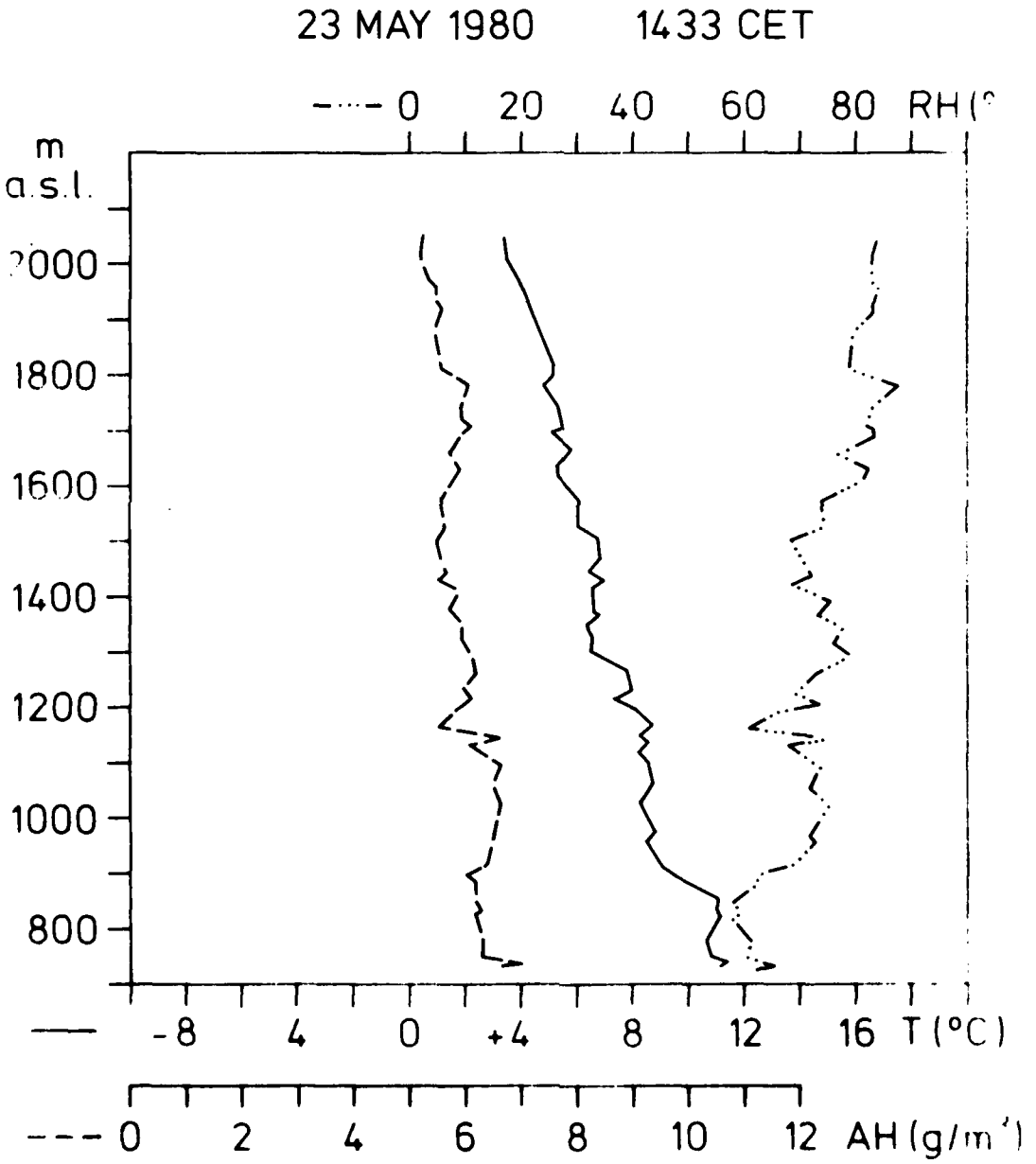
23 MAY 1980 1433 CET
0 20 40 60 80 RH (%)
m a.s.l.
2000
1800
1600
1400
1200
1000
800
-8 4 0 +4 8 12 16 T (°C)
0 2 4 6 8 10 12 AH (g/m³)

Fig. 73

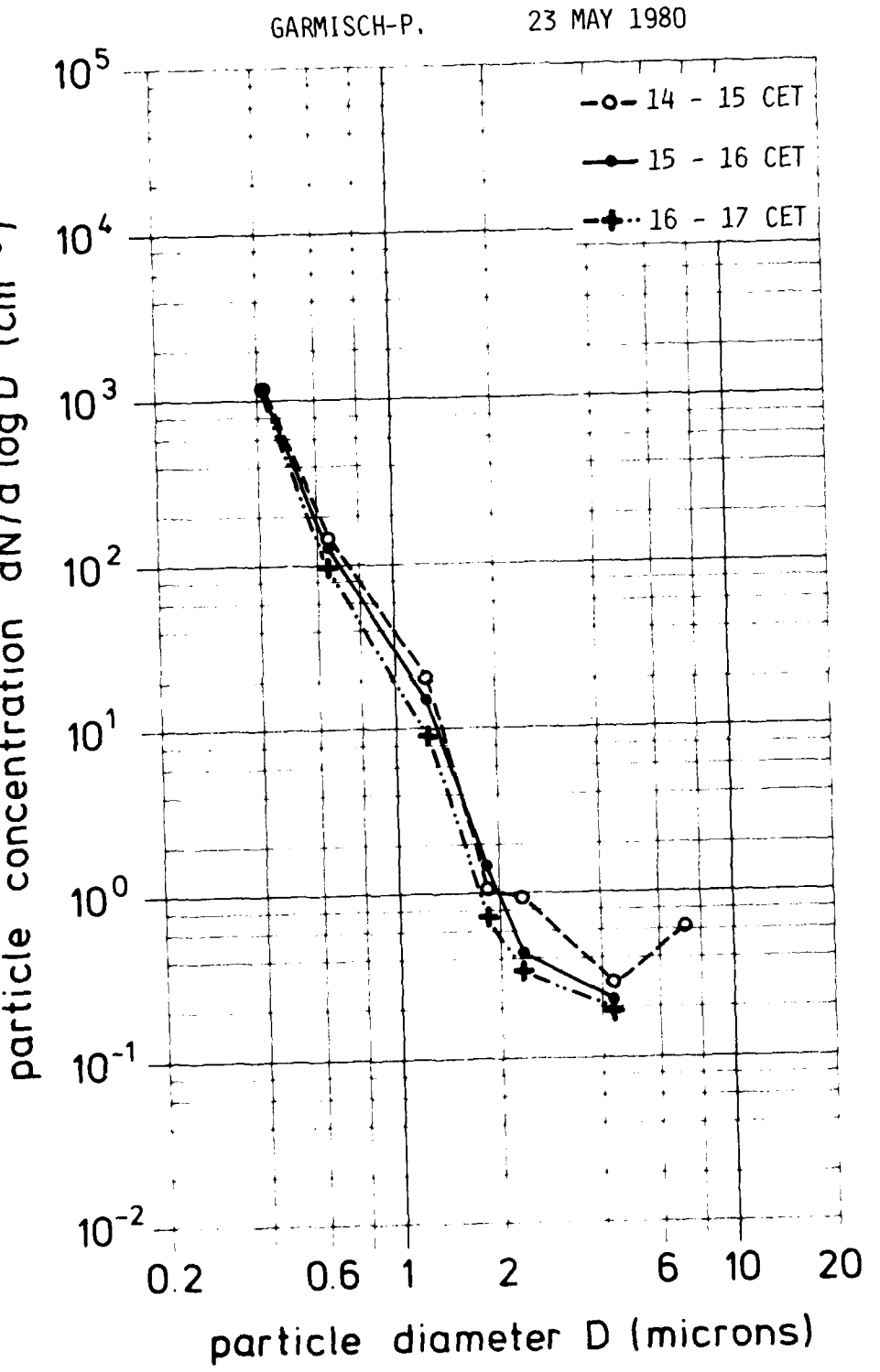
GARMISCH-P. 23 MAY 1980
14 - 15 CET
15 - 16 CET
16 - 17 CET
particle concentration dN/d log D (cm⁻³)
10⁵
10⁴
10³
10²
10¹
10⁰
10⁻¹
10⁻²
0.2
0.6
1
2
6
10
20
particle diameter D (microns)

Fig. 74

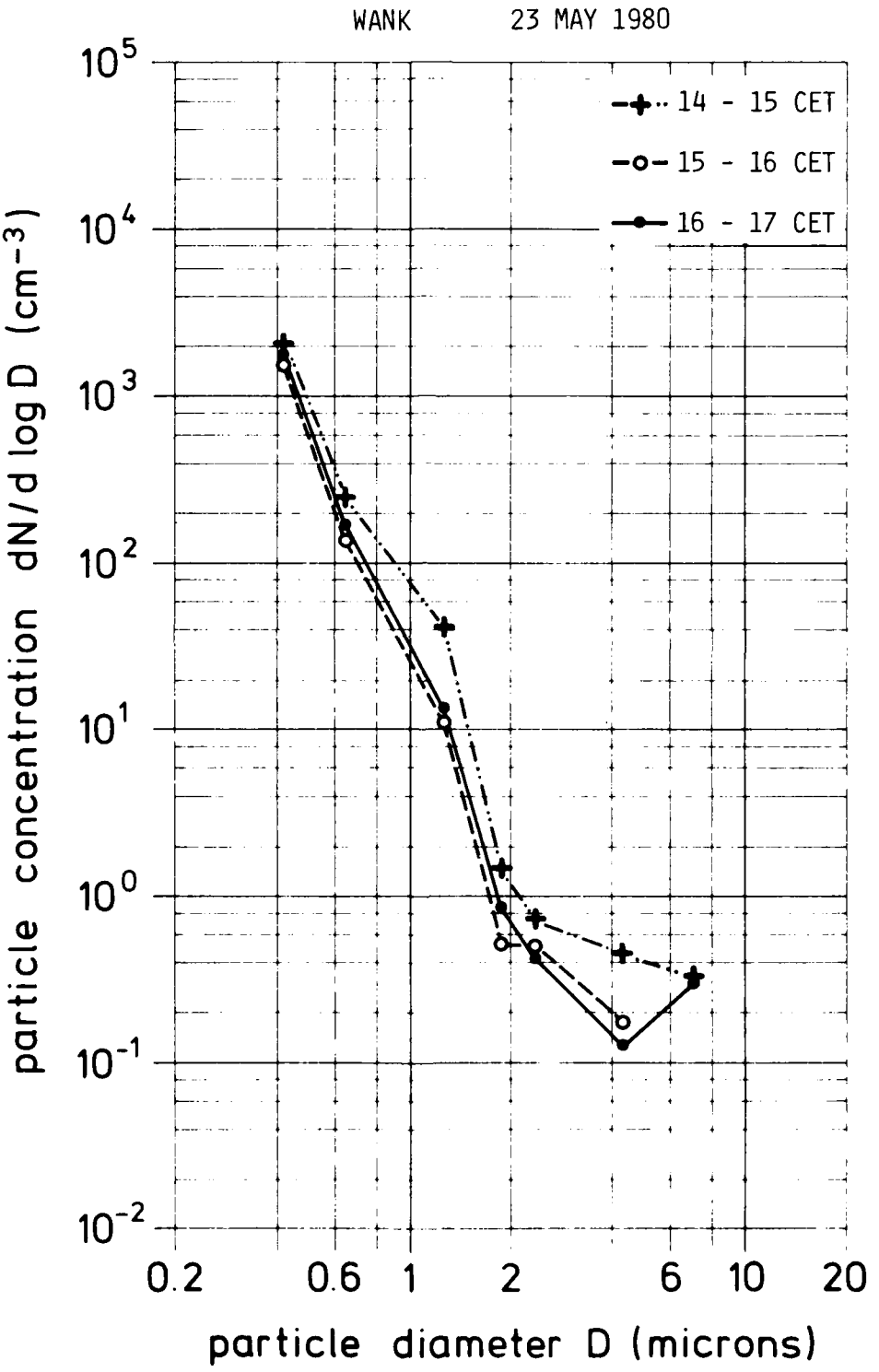
WANK 23 MAY 1980
14 - 15 CET
15 - 16 CET
16 - 17 CET
particle concentration dN/d log D (cm⁻³)
10⁵
10⁴
10³
10²
10¹
10⁰
10⁻¹
10⁻²
0.2
0.6
1
2
6
10
20
particle diameter D (microns)

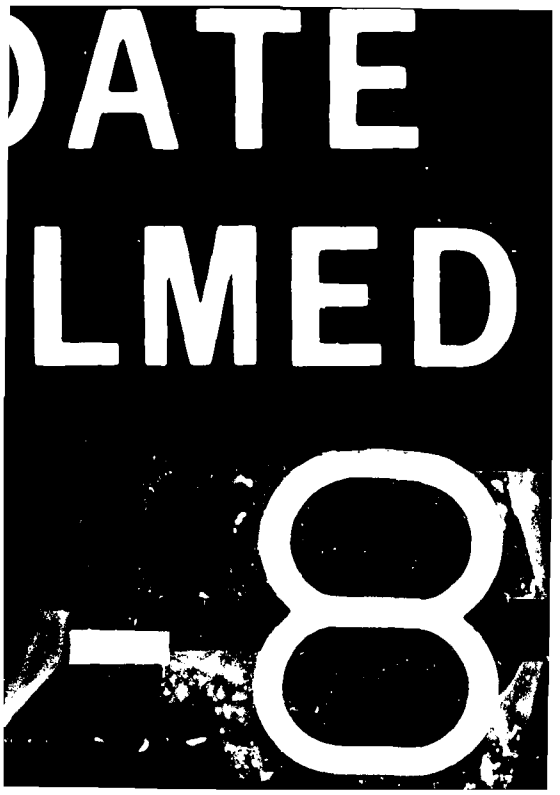
DATE
LMED
8